

Survey of data assimilation methods for convective-scale numerical weather prediction at operational centres

Nils Gustafsson¹ | Tijana Janjić² | Christoph Schraff³ | Daniel Leuenberger⁴ |
Martin Weissmann⁵ | Hendrik Reich⁵ | Pierre Brousseau⁶ | Thibaut Montmerle⁶ | Eric Wattrelot⁶ |
Antonín Bučánek⁷ | Máté Mile⁸ | Rafiq Hamdi⁹ | Magnus Lindskog¹ | Jan Barkmeijer¹⁰ |
Mats Dahlbom¹¹ | Bruce Macpherson¹² | Sue Ballard¹² | Gordon Inverarity¹² |
Jacob Carley¹³ | Curtis Alexander¹⁴ | David Dowell¹⁴ | Shun Liu¹³ | Yasutaka Ikuta¹⁵ |
Tadashi Fujita¹⁵

¹Swedish Meteorological and Hydrological Institute, Norrköping, Sweden

²Hans Ertel Centre for Weather Research, Deutscher Wetterdienst, München, Germany

³Deutscher Wetterdienst, Offenbach, Germany

⁴Federal Office of Meteorology and Climatology, MeteoSwiss, Zürich, Switzerland

⁵Hans Ertel Centre for Weather Research, Ludwig-Maximilians-Universität München, Munich, Germany

⁶Centre National de Recherches Météorologiques (Météo-France/CNRS), Toulouse, France

⁷Czech Hydrometeorological Institute, Praha, Czech Republic

⁸Hungarian Meteorological Service, Budapest, Hungary

⁹Royal Meteorological Institute of Belgium, Brussels, Belgium

¹⁰Royal Meteorological Institute of Netherlands, De Bilt, Netherlands

¹¹Danish Meteorological Institute, Copenhagen, Denmark

¹²Met Office, Exeter, UK

¹³NOAA/NCEP/EMC and IM Systems Group, College Park, Maryland

¹⁴NOAA/ESRL, Boulder, Colorado

¹⁵Japan Meteorological Agency, Tokyo, Japan

Correspondence

Nils Gustafsson, SMHI, Folkborgsvägen 17, 60176 Norrköping, Sweden.

Email: nils.gustafsson@smhi.se

Data assimilation (DA) methods for convective-scale numerical weather prediction at operational centres are surveyed. The operational methods include variational methods (3D-Var and 4D-Var), ensemble methods (LETKF) and hybrids between variational and ensemble methods (3D-EnVar and 4D-EnVar). At several operational centres, other assimilation algorithms, like latent heat nudging, are additionally applied to improve the model initial state, with emphasis on convective scales. It is demonstrated that the quality of forecasts based on initial data from convective-scale DA is significantly better than the quality of forecasts from simple downscaling of larger-scale initial data. However, the duration of positive impact depends on the weather situation, the size of the computational domain and the data that are assimilated. Furthermore it is shown that more advanced methods applied at convective scales provide improvements over simpler methods. This motivates continued research and development in convective-scale DA.

Challenges in research and development for improvements of convective-scale DA are also reviewed and discussed. The difficulty of handling the wide range of spatial and temporal scales makes development of multi-scale assimilation methods and space–time covariance localization techniques important. Improved utilization of observations is also important. In order to extract more information from existing observing systems of convective-scale phenomena (e.g. weather radar data and satellite image data), it is necessary to provide improved statistical descriptions of the observation errors associated with these observations.

KEYWORDS

convective-scale, data assimilation, numerical weather prediction

This article is published with the permission of the Controller of HMSO and the Queen's Printer for Scotland.

This is an open access article under the terms of the Creative Commons Attribution License, which permits use, distribution and reproduction in any medium, provided the original work is properly cited.

© 2017 The Authors and Crown Copyright, Met Office. *Quarterly Journal of the Royal Meteorological Society* published by John Wiley & Sons Ltd on behalf of the Royal Meteorological Society.

[The copyright line for this article was changed on 18 July 2018 after original publication]

1 | INTRODUCTION

Development of data assimilation (DA) methods for global numerical weather prediction (NWP) models started with simple horizontal interpolation methods (Eliassen, 1954) which gradually developed to become three-dimensional and to also include multivariate relationships (Lorenc, 1981). Variational methods were introduced to utilize the model dynamics in the DA process (Le Dimet and Talagrand, 1986) and four-dimensional variational DA is now applied operationally (Rabier *et al.*, 2000). In order to take into account flow-dependence of forecast errors in the DA process, various forms of Ensemble Kalman Filters (EnKF; Evensen, 1994) have become competitive with variational techniques for atmospheric DA. More recently, hybrids between variational and ensemble DA techniques have been proposed (Lorenc, 2003; Liu *et al.*, 2008) and are becoming mainstream in DA for global NWP at operational centres (review by Bannister, 2017).

The DA problem for convective-scale NWP differs from the global problem in several respects. The higher model resolution demands dense observations at a suitable temporal and spatial resolution. Given that convective systems are often a primary forecast aspect, these observations should ideally be related to convection: either of their environmental conditions or of the convective systems themselves. There is a wide variety of observations available that are not yet exploited in regional DA systems:

1. only a very small fraction of available satellite observations is currently used, in particular for cloud-affected observations;
2. the costs of many ground-based remote-sensing instruments have reduced significantly, which allows the installation of new sensor networks, and
3. useful information could be extracted from various observations made for other purposes (e.g. car or mobile phone sensors, output of wind and solar power production, visibility sensors, etc.).

However, little knowledge exists on where the community should put its emphasis regarding the refinement of observational networks and the development of suitable observation operators and assimilation methods. A few recent studies have exploited ensemble information to estimate the contribution of various observations to the reduction of analysis error (Brousseau *et al.*, 2014) or forecast sensitivity to observations (Sommer and Weissmann, 2016).

One may ask which atmospheric variables would be most efficient for assimilation at convective scales. Considering the geostrophic adjustment process, we may hypothesize that wind field information becomes relatively more important than mass field information. Simulation and sensitivity experiments with convective-scale models may provide us with more details on the relative importance of different meteorological variables as initial conditions. Fabry and Sun (2010)

investigated the sensitivity of the Weather Research and Forecasting (WRF) model to spatially coherent perturbations of different model variables for initialization of convective storms. They concluded that the state of the model atmosphere after a few hours of model integration, measured through an energy norm, was mostly sensitive to the initial vertical profiles of moisture, wind and temperature in the lower and middle troposphere. Vertical profiles of cloud and precipitation particles were of less importance, partly due to their lower predictability.

The question of spatial scale is of crucial importance for DA. For convective-scale DA we may need to know both the synoptic scales forcing the mesoscale phenomena and also information on the convective scales that we want to predict. A complicating factor is the difficulty of recovering all the scales resolved over a regional model domain using only observations from inside the domain. As will be discussed here, there are many open questions and many suggested solutions with regard to the handling of synoptic and meso scales in convective-scale DA.

Also associated with the spatial scale is the growing importance of nonlinearity, moist physical processes and unbalanced flows at convective scales (Pagé *et al.*, 2007). With nonlinearity comes flow dependence, since the structures of the convective-scale phenomena are dependent on the actual state of the large-scale forcing. The moist physical processes, for example latent heating, trigger unbalanced adjustment processes. This means that adjustment processes and associated unbalanced flow structures have to be taken into account during the DA. The tools which we have developed for synoptic-scale DA, for example linear balances and static background-error constraints, are no longer appropriate. Steps that have been taken to introduce flow dependence in synoptic-scale DA will certainly be even more important for convective-scale DA. It is an open question, however, to what extent these techniques will be completely satisfactory for convective-scale DA, or whether fully nonlinear DA techniques like particle filters (van Leeuwen, 2009) will be required, or if modifications to hybrid and ensemble methods to deal with non-Gaussianity, as suggested in Hodyss (2011), Janjić *et al.* (2014) and Bishop (2016), would be sufficient.

This manuscript provides a survey of DA methods for convective-scale NWP. As atmospheric DA for convective scales is in a quite early stage of development, the reader may notice that we do not all fully agree on fundamental principles for convective-scale DA – questions related to spatial scales and imbalance, for example. By making these questions and disagreements visible through this article, we will be able to take further steps to a joint understanding as a starting point for further developments.

Section 2 of this article describes operational DA methods for convective scales and section 3 discusses the impact of these methods for operational NWP. Challenges in research for development of convective-scale DA methods are discussed in section 4 and a summary and some concluding

TABLE 1 List of acronyms

Acronym	Description
3D-Var	Three-dimensional Variational DA
3DEnVar	Three-dimensional Ensemble Variational DA
4D-Var	Four-dimensional Variational DA
4DEnVar	Four-dimensional Ensemble Variational DA
AD	ADjoint
AEARP	Assimilation d'Ensemble ARPege
ALADIN	Aire Limitée Adaptation dynamique Développement InterNational
	– Limited-Area Model (LAM) and LAM consortium
ALARO	Physical parametrization package for ALADIN
AROME	Applications de la Recherche l'Opérationnel à MésO-Echelle
	– Convective-scale Limited-Area Model
ARPEGE	Action de Recherche Petite Echelle Grande Echelle – Global Model
ASUCA	JMA high-resolution model
BSS	Brier Scill Score
CONUS-NAM	CONtiguous United States nest of North American Mesoscale system
	– convective-scale forecasting system
COSMO	COnsortium for Small scale MOdeling
CRPS	Continuous Ranked Probability Score
DA	Data Assimilation
DF	Digital Filter
DFI	DF Initialization
DPCG	Double Preconditioned Conjugate Gradient
DWD	Deutscher WetterDienst
ECMWF	European Centre for Medium-range Weather Forecasts
EDA	Ensemble Data Assimilation
EKF	Extended Kalman Filter
EnKF	Ensemble Kalman Filter
EOF	Empirical Orthogonal Functions
EPS	Ensemble Prediction System
ERA	ECMWF Re-Analysis projects
ETKF	Ensemble Transform Kalman Filter
EUMETNET	EUropean METEorological services NETwork
FGAT	First Guess at Appropriate Time
FSS	Fractions Skill Score
GFS	Global Forecasting System, the global model of NCEP
GSM	Global Spectral Model at JMA
HARMONIE	HIRLAM ALADIN Research on Mesoscale Operational NWP In Europe
	– convective-scale forecasting system
HE-VI	Horizontally Explicit Vertically Implicit time-stepping
HIRLAM	HIgh-Resolution Limited-Area Modelling – LAM model and LAM consortium
HRRR	High-Resolution Rapid Refresh system – convective-scale forecasting system
IAU	Incremental Analysis Update
ICON	ICOsahedral Non-hydrostatic (atmospheric model)
IFS	Integrated Forecast System
IPW	Integrated Precipitable Water
JAXA	Japan Aerospace eXploration Agency
JMA	Japan Meteorological Agency
JMA-NHM	JMA Non-Hydrostatic Model
JNoVA	JMA Non-hydrostatic model-based Variational DA system

TABLE 1 List of acronyms (continued)

Acronym	Description
KENDA	Kilometre-scale ENsemble DA
LA	Local Analysis – JMA convective-scale DA system
LAM	Limited Area Model
LBC	Lateral Boundary Condition
LETKF	Local Ensemble Transform Kalman Filter
LFM	Local Forecast Model – JMA convective-scale forecast model
LHN	Latent Heat Nudging
MA	Mesoscale Analysis – JMA mesoscale assimilation system
MSM	MesoScale Model – JMA mesoscale model
MY2.5	Mellor–Yamada 2.5 turbulence parametrization
MYJ	Mellor–Yamada–Janjić planetary boundary-layer scheme
NAM	North American Mesoscale system
NDP	Nowcasting Demonstration Project
NCEP	National Centers for Environmental Prediction
NICT	National Institute of Information and Communications Technology (Japan)
NMC	National Meteorological Center (USA)
NOAA	National Oceanic and Atmospheric Administration (USA)
NWP	Numerical Weather Prediction
OI	Optimal Interpolation
QC	Quality Control
RAP	RApid Refresh mesoscale analysis and prediction system
RC LACE	Regional Cooperation for Limited-Area modelling in Central Europe
RGB	Red, Green, Blue colour table
RMSE	Root Mean Square Error
RRTMG	Rapid Radiative Transfer Model for General circulation model applications
RTPP	Relaxation-To-Prior Perturbations
RUC	Rapid Update Cycle/ing
SPPT	Stochastic Perturbations of Physical Tendencies
SURFEX	SURFace EXternalisée – a surface parametrization package
TERRA	COSMO surface parametrization scheme
TKE	Turbulent Kinetic Energy
TL	Tangent Linear
UKV	The UK Variable-resolution model (Met Office)
VarBC	Variational Bias Correction
VWC	Volume Water Content
WoF	Warn-on-Forecast – NOAA development project
WMO	World Meteorological Organization
WRF	Weather Research and Forecasting model

remarks are provided in section 5. A list of acronyms used is provided in Table 1 and a glossary of observations and instruments is contained in Table 2. In general, only the acronym will be used in the text.

2 | DESCRIPTION OF OPERATIONAL METHODS

Data assimilation systems for convective-scale NWP are presented and discussed here for the following organizations:

1. Météo-France, the national weather service of France.

TABLE 2 Glossary of observations and instruments

Name	Description
ACARS	Aircraft Communications Addressing and Reporting System
AIREP	AIRcraft REPorts
AIRS	Atmospheric InfraRed Sounder (satellite instrument)
AMDAR	Aircraft Meteorological Data Relay
AMeDAS	Automated Meteorological Data Acquisition System
AMSR	Advanced Microwave Scanning Radiometer (satellite instrument)
AMSU	Advanced Microwave Sounding Unit (satellite instrument)
AMV	Atmospheric Motion Vector
Aqua	Multi-national scientific research satellite
ARAMIS	Application Radar Á la Météorologie Infra-Synoptique
ASCAT	Advanced SCATterometer (satellite instrument)
ATMS	Advanced Technology Microwave Sounder (satellite instrument)
ATOVS	Advanced TIROS Operational Vertical Sounder (system of sounding instruments on NOAA TIROS series of satellites)
BALTRAD	BALTex RADar (Radar network in the Baltic Sea area)
BUFR	Binary Universal Form for the Representation of meteorological data
BUOY	Reporting format for buoy measurements
CRIS	CROss-track Infrared Sounder (satellite instrument)
CSR	Clear-Sky Radiance
DMSP	Defense Meteorological Satellite Program
DPOL	Dual POLarimetric (radar)
GCOM	Global Change Observation Mission (JAXA satellite)
GeoCloud	Cloud fraction profiles based on satellite cloud top information
GMI	Global Microwave Imager (satellite instrument)
GNSS	Global Navigation Satellite System
GOES	Geostationary Operational Environmental Satellite
GPM	Global Precipitation Measurement
GPM/DPR	Global Precipitation Measurement/Dual-frequency Precipitation Radar
GPS	Global Positioning System
GPS-RO	GPS Radio Occultation
HDF5	Hierarchical Data Format
Himawari	Japan meteorological satellite
HIRS	High-resolution InfraRed Sounder (satellite instrument)
IASI	Infrared Atmospheric Sounding Interferometer (satellite instrument)
IR	InfraRed
MDCARS	Meteorological Data Collection And Reporting System
MESONET	MESO-scale surface station NETwork
METAR	Format for reporting weather information (aviation)
METOP	European meteorological polar orbiting satellites
MHS	Microwave Humidity Sounder (satellite instrument)
Mode-S EHS	Mode-S EnHanced Surveillance winds – winds obtained from air traffic control systems
MRAR	Mode-S Meteorological Routine Air Report
MSG	Meteosat Second Generation – European operational meteorological geostationary satellite
MUAC	Maastricht Upper Air Control
MW	MicroWave
NPP	The SUOMI National Polar-orbiting Partnership
ODIM	OPERA Data Information Model

TABLE 2 Continued

Name	Description
OPERA	Operational Program for the Exchange of weather RADar information
PILOT	Balloon wind profile observations
PIREP	Pilot weather REPort
RASS	Radio Acoustic Sounding System
RTTOV	Radiative Transfer for TOVS (software package)
SAF	Satellite Application Facility
SEVIRI	Spinning Enhanced Visible and InfraRed Imager (satellite instrument)
SHIP	Format for marine (ship) observations
SSMIS	Special Sensor Microwave Imager/Sounder (satellite instrument)
SUOMI	Satellite named after the scientist Verner Suomi
SYNOP	Format for SYNOptic land surface observations
TEMP	Format for radiosonde TEMPerature, humidity and wind profiles
TIROS	Television InfraRed Observation Satellite programme
TOVS	TIROS Operational Vertical Sounder
WPR	Wind Profiling Radar
ZTD	Zenith Total Delay

2. The ALADIN and RC LACE consortia with participation of the weather services of Algeria, Austria, Belgium, Bulgaria, Czech Republic, Croatia, France, Hungary, Morocco, Poland, Portugal, Romania, Slovakia, Slovenia, Turkey and Tunisia.
3. The HIRLAM consortium with participation of the weather services of Denmark, Estonia, Finland, France, Iceland, Ireland, Latvia, Lithuania, the Netherlands, Norway, Spain and Sweden.
4. The Met Office, the national weather service of the UK.
5. The COSMO consortium with participation of the weather services of Germany, Italy and Switzerland.
6. NOAA, the National Oceanic and Atmospheric Administration of the USA.
7. JMA, the Japan Meteorological Agency.

An overview of the operational DA and forecasting systems of these organizations is provided in Tables 3–6. Table 3 describes the forecast models, Table 4 the core assimilation methods, Table 5 the operational cycling of DA at the different centres and Table 6 the observing systems used.

2.1 | Formulation of the different DA methods

In order to describe and discuss the assimilation techniques, we will here provide a brief description of their mathematical formulations. The notations follow Lorenc (2013) and Bannister (2017).

2.1.1 | Incremental 3D-Var and incremental 4D-Var

Let \mathbf{x} denote the model state of dimension n . The following cost function J is minimized with respect to the assimilation

TABLE 3 Main characteristics of the AROME-France, HARMONIE-AROME, ALADIN, COSMO, UKV, CONUS NAM, HRRR, MSM and LFM models

Model/Centre	Geometry	Physics	Dynamics	Coupling	References
AROME-France/ Météo-France	Spectral, 2D Fourier Linear grid 1.3 km 90 hybrid levels 1500 × 1400 points	AROME	Non-hydrostatic; Semi-implicit; Semi-Lagrangian	Davies relaxation; ARPEGE synchron.	Seity <i>et al.</i> (2011)
HARMONIE- AROME/HIRLAM	Spectral, 2D Fourier Linear grid 2.5 km 65 hybrid levels	Adapted AROME	Non-hydrostatic; Semi-implicit; Semi-Lagrangian	Davies relaxation; ECMWF forecasts (6 hr lag)	Bengtsson <i>et al.</i> (2017)
ALADIN/ ALADIN and RC LACE	Spectral, 2D Fourier Linear grid 2.5 km 90 hybrid levels	ALARO-1 or AROME	Hydrostatic or non-hydrostatic; Semi-implicit; Semi-Lagrangian;	Davies relaxation; ARPEGE synchr. or ECMWF (6 hr lag)	Szintai <i>et al.</i> (2015)
COSMO/ DWD and MeteoSwiss	Arakawa C DWD: 2.8 km 50 hybrid levels 421 × 461 points MeteoSwiss: 2.2 km 60 hybrid levels 582 × 390 points	1-moment 5-category cloud microphysics; Shallow convection; Prognostic TKE modified MY2.5; Radiation of Ritter and Geleyn; Surface scheme TERRA	Non-hydrostatic; Time-splitting 3D extension of Bott (1989)	ICON ensemble (0 hr lag); MeteoSwiss: ECMWF ensemble (IFS high res. 6 hr lag ensemble mean, IFS ensemble for perturbations 30–36 hr lag)	Baldauf (2010) Baldauf <i>et al.</i> (2011) Wicker and Skamarock (2002) Raschendorfer (2001) Ritter and Geleyn (1992) Tiedtke (1989)
UKV/ Met Office	Finite difference, C-grid Rotated lat–long, 1.5 km inner area, variable resolution 70 hybrid levels 950 × 1025 points		Non-hydrostatic; Semi-implicit; Semi-Lagrangian	Davies relaxation; Global forecasts 3 or 6 hr lag	Tang <i>et al.</i> (2013)

TABLE 3 Continued

Model/Centre	Geometry	Physics	Dynamics	Coupling	References
CONUS-NAM/ NOAA	Arakawa B grid 3 km Finite difference 60 hybrid levels 1827 × 1467 points	1-moment with varying rimed ice microphysics; Convection-permitting MYJ turbulence; RRTMG short/long-wave; Noah land surface	Non-hydrostatic; Fully compressible; Forward-backward for fast waves; Implicit for vert. prop. sound waves; Adams–Bashforth horiz. advection; Crank–Nicolson vert. advection	Parent 12 km NAM domain (uses NOAA GFS forecasts with 6 hr lag)	Janjić (2003) and Janjić and Gall (2012) Janji (2001) Iacono <i>et al.</i> (2008), Mlawer <i>et al.</i> (1997) Ek <i>et al.</i> (2003)
HRRR/ NOAA	Arakawa C grid 3 km Finite difference 51 sigma levels 1800 × 1060 points	1- and 2-moment 5-category Thompson microphysics; Convection-permitting MYNN boundary layer; RRTMG short/long-wave; RUC land surface	Non-hydrostatic; Eulerian mass-coordinate; Finite difference 5th-order positive-definite horizontal/vertical advection; 3rd-order Runge–Kutta time-splitting	Parent 13 km RAP domain (uses NOAA GFS forecasts with 9 hr lag)	Benjamin <i>et al.</i> (2004; 2016)
MSM/ JMA	Finite volume method Arakawa-C grid 5 km 76 hybrid-Z levels 817 × 661 points	Physics Library	Non-hydrostatic; Fully compressible; HE-VI conservative split-explicit; Finite diff. advection with flux limiter	Rayleigh damping; GSM forecasts (3 or 6 hr lag)	Ishida <i>et al.</i> (2009) and Ishida <i>et al.</i> (2010) Hara <i>et al.</i> (2012) Aranami <i>et al.</i> (2015)
LFM/JMA	As MSM but 2 km grid 58 levels 1531 × 1301 points	As MSM	As MSM	Rayleigh damping; MSM forecasts (3–5 hr lag)	As MSM

TABLE 4 Overview of core data assimilation methods applied operationally

Group/Centre	Method	Control variables	Spatial filters	Estimation of B or Localization/inflation	Initialization	References
Météo-France HIRLAM/ALADIN and RC LACE	Incremental 3D-Var (ALADIN 3D-Var)	ζ +unbalanced η , T , $\ln(p_s)$, q in spectral and vertical EOF space	$\mathbf{U} = \mathbf{B}^{-1/2}$ Statistical balance op. Spectral (hor.); EOF (vert.)	EDA or NMC		Brousseau <i>et al.</i> (2011) Berre (2000)
COSMO/DWD and MeteoSwiss	LETKF	p , T , u , v , w , specific contents of water vapour, cloud water, cloud ice	$\mathbf{U} = \mathbf{U}_h \mathbf{U}_p \mathbf{U}_v$	RTPP; Adaptive multiplicative cov. infl.; Adapt. horiz. localiz. vert. localiz. with 0.075–0.5 in $\ln(p)$	Hydrostatic balancing of increments	Schraff <i>et al.</i> (2016)
Met Office	Incremental 3D-Var and 4D-Var	ψ , Φ , unbalanced p , μ , \log_{10} (aerosol)	$\mathbf{U} = \mathbf{U}_p \mathbf{U}_a \mathbf{U}_h \mathbf{U}_v$	Lagged NMC	IAU J_{c-DFI} (4D-Var)	Ingleby <i>et al.</i> (2013)
CONUS NAM/NOAA	Incremental hybrid 3D-EnVar and cloud analysis non-variational	ψ +unbalanced Φ , T , p_s and normalized q cloud analysis: q_1 , q_c , q_s , T_{tend}	$y = \mathbf{B}^{-1}x$ Statistical balance op. Recursive filters	NMC with global EnKF members 25% static + 75% ensemble	DFI imposed radar-derived latent heating	Wu <i>et al.</i> (2017) Hu <i>et al.</i> (2006)
HRRR/NOAA	Incremental hybrid 3D-EnVar and non-variational cloud analysis	ψ +unbalanced Φ , T , p_s and normalized q cloud analysis: q_1 , q_c , q_r , q_s , q_g , T	$y = \mathbf{B}^{-1}x$ Statistical balance op. Recursive filters	NMC with global EnKF members 25% static + 75% ensemble	Directly imposed radar-derived latent heating	Benjamin <i>et al.</i> (2004) Benjamin <i>et al.</i> (2016) Hu <i>et al.</i> (2017)
MA/JMA	Incremental 4D-Var	u , v , θ , p_s , q/q_{sat}^b	Hydrostatic BALance op.; Sqrt of vert. cov. V ; Sqrt of hor. corr by CHOLesky dec.; $\mathbf{U} = \text{BAL} \times V^{1/2} \times \text{CHOL}$	NMC	J_{c-DFI}	Honda <i>et al.</i> (2005)
LA/JMA	3D-Var	u , v , θ , p_s , T_g , q/q_{sat} , VWC_g	Hydrostatic BALance op.; Vert. coord. transf. T ; Sqrt of vert. covar. V ; Sqrt of hor. corr. by Recurs. Filter; $\mathbf{U} = \text{BAL} \times V^{1/2} \times \text{RF}$	NMC	Cycling for 3 hr in each run	JMA (2016) Aranami <i>et al.</i> (2015)

The following symbols are used in the control variable transforms: u , v , w the zonal, meridional and vertical three-dimensional wind field components; ζ vorticity; ψ streamfunction; η divergence; Φ velocity potential; T temperature; θ potential temperature; p pressure; p_s surface pressure; q specific humidity; q_{sat}^b background saturation specific humidity; q_c cloud liquid water; q_i cloud ice; q_s cloud condensate; q_r rain water; q_g snow water; T_g ground temperature; T_{tend} temperature tendency; VWC_g ground volume water content; μ transformed humidity; **B** background-error covariance; **B** background-error covariance; **U** total control vector transform; \mathbf{U}_p parameter (from uncorrelated control variables to model variables) transform; \mathbf{U}_a adaptive grid transform; \mathbf{U}_h horizontal transform and \mathbf{U}_v vertical transform.

TABLE 5 Overview of operational data assimilation cycling

Group/centre	Method	Resol. of incem. (km)	DA cycle/ window (h)	Coupling to large-scale DA	LBCs during DA	Latent heat nudging	References
Météo-France	AL-ADIN 3D-Var	1.3	1		ARPEGE 0 hr lag	No	Brousseau <i>et al.</i> (2016)
HIRLAM	AL-ADIN 3D-Var	2.5	3 or 6	Spectral blending of background with LBCs	ECMWF 3–6 hr lag	No	Yang (2005)
AL-ADIN and RC LACE	AL-ADIN 3D-Var or BlendVar	2.5	3 or 6	BlendVar(section 2.2.5)	ARPEGE 0 hr lag or ECMWF 6 hr lag	No	Böläni <i>et al.</i> (2015) Mile <i>et al.</i> (2015)
COSMO/DWD	KENDA/LETKF	2.8	1		ICON ensemble (20 km); 0 hr lag	Yes	Schraff <i>et al.</i> (2016)
COSMO/ MeteoSwiss	KENDA/LETKF	2.2	1		ECMWF ensemble	Yes	
Met Office	Incem. 3D-Var	3.3	3		Met Office global 3–6 hr lag	Yes	
Met Office	Incem. 4D-Var	4.5	1		Met Office global 3–8 hr lag	Yes	
CONUS NAM/ NOAA	Incem. hybrid 3D-EnVar and non-variational cloud analysis	9.0	1 Free forecast every 6 hr	Restart from 6 hr forecast from global DA system at $t-6$ h; Global ensemble for 3D-EnVar covariances	Parent domain model (12 km)	Yes (via DFI)	
HRRR/NOAA	Incem. hybrid 3D-EnVar and non-variational cloud analysis	12.0	1 Free forecast every 1 hr	Restart from parent domain model (13 km) $t-1$ h; Global ensemble for 3D-EnVar covariances	Parent domain model (13 km)	Yes	
MA/JMA	Incremental 4D-Var	15.0	3		GSM 3–6 hr lag	No	
LA/JMA	3D-Var	5.0	1 / cycling from $t-3$ hr	Restart from MSM; $t-3$ hr as background	MSM 3–5 hr lag	No	

The notation $t-nh$ is explained in the text.
bg=background

TABLE 6 Overview of assimilated observation types

Centre	Data cut-off (min)	Ground-based			Satellites	Other	Bias correction
		Conventional	Radar	GPS			
Météo-France	45–105	TEMP, PILOT, BUOY, SYNOP, SHIP, AIREP, ACARS, AMDAR, MESONET	Doppler winds Reflectivities	ZTD	SEVIRI, ATOVS, IASI, AIRS, CRIS, ATMS, SSMIS, MHS, GMI, AMV, Scatterom. winds		VarBC partly shared with global system
HIRLAM	90–240	TEMP, PILOT, BUOY, SYNOP, SHIP, AIREP, Modes-S EHS and AMDAR	Multi-national reflectivities	ZTD	TOVS, IASI, Scatterom. winds, ATMS, GPS-RO, AMV		VarBC sat. and GPS
ALADIN and RC LACE	90–240	SYNOP, TEMP, PILOT, SHIP, AIREP			SEVIRI, TOVS, IASI, HIRS, AMV, Scatterom. winds		VarBC sat.
COSMO/DWD and MeteoSwiss	90–240 DWD:15	SYNOP, TEMP, PILOT, SHIP, AIREP	Surface precipitation rates by LHN in all ensemble members				
Met Office	45–75	SYNOP, SHIP, TEMP, PILOT, METAR, BUOY, AIREP, AMDAR	Doppler winds, surface rain rate	ZTD	AMV, Scatterom. winds, AMSU-B, IASI, CRIS, AIRS, ATMS, SEVIRI	Roadside sensors WPR GeoCloud	VarBC sat.
CONUS-NAM/NOAA	80	TEMP, PILOT, BUOY, SYNOP, SHIP, METAR, MESONET, PIREP, AMDAR, MDCARS/ACARS	Doppler winds Reflectivities WPR	IPW	GOES 15, METOP A/B, SUOMI NPP, Aqua, NOAA 19/18/15, GPS bending angle, Scatterom. winds, AMV	RASS, Lightning	VarBC in parent model
HRRR/NOAA	30	TEMP, PILOT, BUOY, SYNOP, SHIP, AIREP, MESONET, PIREP, AMDAR, MDCARS/ACARS	Reflectivities WPR	IPW	GPS bending angle, GOES (cloud prod.), Scatterom. winds, AMV	RASS, Lightning	
MA/JMA	50	SYNOP, METAR, SHIP, BUOY, TEMP, PILOT, AIREP, AMDAR	Radial velocities, reflectivities, Radar-rain gauge precip.	IPW	Radiance from MW/IR sounder/imager, AMV, GNSS RO refract., Scatterom. winds, Precip. from MW imager	WPR	VarBC in global system
LA/JMA	30	SYNOP, AMeDAS, SHIP, BUOY, TEMP, PILOT, AIREP, AMDAR	Radial velocities, reflectivities	IPW	Radiance from MW/IR sounder/imager, AMV, Soil moisture from MW imager/scatterom.	WPR	VarBC in global system

increment $\delta\mathbf{x} = \mathbf{x} - \mathbf{x}^b$ in incremental 4D-Var:

$$J = J^b + J^o = \frac{1}{2} \delta\mathbf{x}^T \mathbf{B}^{-1} \delta\mathbf{x} + \frac{1}{2} \sum_{k=0}^K (\mathbf{H}_k \mathbf{M}_k \delta\mathbf{x} - \mathbf{d}_k)^T \mathbf{R}_k^{-1} (\mathbf{H}_k \mathbf{M}_k \delta\mathbf{x} - \mathbf{d}_k), \quad (1)$$

where \mathbf{x}^b is the model background state valid at time t_0 , \mathbf{B} is the background-error covariance matrix and the subscript k denotes time $t_k = t_0 + k\Delta T$ within the assimilation window from time t_0 to time t_K for regular time interval ΔT , $\mathbf{d}_k = \mathbf{y}_k - \mathcal{H}_k(\mathcal{M}_k(\mathbf{x}^b))$ are the innovations, with \mathbf{y}_k being the vector of observations at time t_k , $\mathcal{M}_k(\cdot)$ denotes integration of the nonlinear model from time t_0 until time t_k and \mathbf{M}_k denotes the corresponding TL model integration, linearized around the background trajectory $\mathcal{M}_k(\mathbf{x}^b)$. \mathbf{R}_k is the observation-error covariance matrix, $\mathcal{H}_k(\cdot)$ is the nonlinear observation operator, and \mathbf{H}_k is the corresponding TL observation operator, linearized around $\mathcal{M}_k(\mathbf{x}^b)$, all valid at time t_k .

In the basic 3D-Var and 4D-Var formulations used in operations at convective scales, the covariance matrix \mathbf{B} is static and not dependent on the forecast errors ‘‘of the day.’’ Due to its large dimension, the inverse \mathbf{B}^{-1} cannot be obtained directly by matrix inversion techniques. Therefore we introduce a pre-conditioning matrix \mathbf{U} such that $\mathbf{B} = \mathbf{U}\mathbf{U}^T$, $\delta\mathbf{x} = \mathbf{U}\chi$ and χ is the assimilation control variable. With this choice $J^b = \chi^T \chi / 2$. The transformation matrix \mathbf{U} may be given as a series of simpler transform operators that define the background-error covariance model. The order in which these operators are carried out is important (Bannister, 2008). In the HARMONIE-AROME formulation (see below), balance operator transforms are carried out in spectral space, which makes these balance operators scale-dependent. Compared to what is usually done at global scales, an additional multivariate relationship may be used for specific humidity following Berre (2000), which is of great interest at convective scales where the coupling between humidity and divergence, for example, can be important.

The minimization of the cost function J is done iteratively by calculation of the gradient $\nabla_{\chi} J$ with respect to the control vector χ and application of, for example, conjugate gradient minimization. The spatial resolution of the assimilation increment can be reduced, making 4D-Var computationally more tractable.

Standard *incremental 3D-Var* is obtained from Equation (1) by referring all observations to the start of the assimilation window t_0 and 3D-Var FGAT by making the TL model an identity operator $\mathbf{M}_k = \mathbf{I}$ and, preferably, referring the assimilation increment to the middle of the assimilation window.

2.1.2 | Multi-incremental 4D-Var

The nonlinearities of the forecast model and the observation operators may be better treated by iterative relinearizations in an outer loop by splitting the minimization into a series ($\tau = 1, \dots, N_{\tau}$) of quadratic sub-problems to determine $\delta\mathbf{x}^{\tau}$, with the total increment $\delta\mathbf{x} = \sum_{\tau=1}^{N_{\tau}} \delta\mathbf{x}^{\tau}$. The cost-function for

each subproblem τ is given by (Courtier *et al.*, 1994)

$$J_{\tau} = J_{\tau}^b + J_{\tau}^o = \frac{1}{2} \{ \delta\mathbf{x}^{\tau} - (\mathbf{x}^b - \mathbf{x}^{\tau}) \}^T \mathbf{B}^{-1} \{ \delta\mathbf{x}^{\tau} - (\mathbf{x}^b - \mathbf{x}^{\tau}) \} + \frac{1}{2} \sum_{k=0}^K (\mathbf{H}_k^{\tau} \mathbf{M}_k^{\tau} \delta\mathbf{x}^{\tau} - \mathbf{d}_k^{\tau})^T \mathbf{R}_k^{-1} (\mathbf{H}_k^{\tau} \mathbf{M}_k^{\tau} \delta\mathbf{x}^{\tau} - \mathbf{d}_k^{\tau}), \quad (2)$$

where $\mathbf{d}_k^{\tau} = \mathbf{y}_k - \mathcal{H}_k(\mathcal{M}_k(\mathbf{x}^{\tau}))$, \mathbf{M}_k^{τ} is the TL forecast model linearized around the guess trajectory $\mathcal{M}_k(\mathbf{x}^{\tau})$ and \mathbf{H}_k^{τ} is the TL observation operator also linearized around $\mathcal{M}_k(\mathbf{x}^{\tau})$. The initial guess $\mathbf{x}^1 = \mathbf{x}^b$ is typically used and, starting from $\tau = 1$, Equation (2) is then minimized to find $\delta\mathbf{x}^{\tau}$, after which the guess state is updated with $\mathbf{x}^{\tau+1} = \mathbf{x}^{\tau} + \delta\mathbf{x}^{\tau}$. The spatial resolution of the increment may differ between different outer-loop iterations.

2.1.3 | The hybrid 3D-EnVar and the hybrid 4D-EnVar

The aim of hybrid variational ensemble DA methods is to combine the robustness and full-rank covariance matrix of variational methods with the flow-dependence of ensemble methods. For a simplest possible 3D-EnVar, we may follow Liu *et al.* (2008) and replace the static error covariance \mathbf{B} in (1) with a flow-dependent error covariance $\mathbf{P} = \mathbf{X}\mathbf{X}^T$ estimated from an ensemble of background model states. \mathbf{X} is a matrix whose columns are the normalized deviations of the ensemble background states from their mean $\bar{\mathbf{x}}^b$:

$$\mathbf{X} = \frac{1}{\sqrt{N_{\text{ens}} - 1}} \left(\mathbf{x}^{b,1} - \bar{\mathbf{x}}^b, \dots, \mathbf{x}^{b,N_{\text{ens}}} - \bar{\mathbf{x}}^b \right), \quad (3)$$

where N_{ens} is the number of ensemble members. We may apply \mathbf{X} for the pre-conditioning $\delta\mathbf{x} = \mathbf{X}\chi$. The control vector χ will have the dimension of the number of ensemble members and we can notice that the assimilation increment is just a linear combination of the ensemble perturbations.

Although flow-dependence has been achieved, this simple 3D-EnVar will suffer from two problems. Due to the limited number of ensemble members ($N_{\text{ens}} \sim 10 - 100$) small-amplitude covariances will be poorly represented, resulting in noisy assimilation increments. Furthermore, the spatial variations in a small ensemble may not describe all observed structures of importance. Standard remedies to these problems are to introduce covariance localization and to combine the ensemble covariance with a static full-rank covariance (hybridization). Localization in model space is generally carried out by a Schur product (element-by-element multiplication) of the ensemble covariance matrix \mathbf{P} with a localization matrix \mathbf{C} , $\mathbf{P}^{\text{loc}} = \mathbf{C}\mathbf{P}$, where the elements of the localization matrix force the covariances to become zero for grid separations larger than a pre-defined localization length-scale. Lorenc (2003) proposed that the covariance localization could be carried out through a Schur product between localized weights, included in an augmented control vector, and the ensemble background perturbations.

The mathematical equivalence of differently posed hybrid methods was proven by Wang *et al.* (2007) and a comprehensive review has been published by Bannister (2017). We will briefly describe the method suggested by Lorenc (2003), applied in several global (Clayton *et al.*, 2013; Kleist and Ide, 2015) and regional (Gustafsson and Bojarova, 2014) implementations.

For hybrid 4DEnVar, the increment $\delta\mathbf{x}(t_k)$ at time t_k within the assimilation window is formed as a linear combination of a variational (3D-Var FGAT) contribution $\delta\mathbf{x}_{\text{var}}$ and a time-varying ensemble contribution $\delta\mathbf{x}_{\text{ens}}(t_k)$:

$$\begin{aligned}\delta\mathbf{x}(t_k) &= \beta_{\text{var}}\delta\mathbf{x}_{\text{var}} + \beta_{\text{ens}}\delta\mathbf{x}_{\text{ens}}(t_k) \\ &= \beta_{\text{var}}\delta\mathbf{x}_{\text{var}} + \beta_{\text{ens}}\sum_{l=1}^{N_{\text{ens}}}\alpha_l\circ(\mathbf{X})_l(t_k),\end{aligned}\quad (4)$$

with $\beta_{\text{var}}^2 + \beta_{\text{ens}}^2 = 1$ (a larger value of β_{var} was used by Clayton *et al.*, 2013, as a form of covariance inflation) and using $(\mathbf{X})_l$ to denote column l of the matrix \mathbf{X} of scaled ensemble perturbations. The pre-conditioning for the variational contribution is done as for 3D-Var. The α_l vector can be considered as a localized weight field for the ensemble perturbation of member l . α_l will be a vector of the same dimension n as the model increment vector.

The cost function for 4DEnVar is given by

$$\begin{aligned}J^{\text{En-Var}} &= J^{\text{b}} + J^{\text{ens}} + J^{\text{o}} \\ &= \frac{1}{2}\delta\mathbf{x}_{\text{var}}^{\text{T}}\mathbf{B}^{-1}\delta\mathbf{x}_{\text{var}} + \frac{1}{2}\boldsymbol{\alpha}^{\text{T}}\mathbf{A}^{-1}\boldsymbol{\alpha} \\ &\quad + \frac{1}{2}\sum_{k=0}^K\{\mathbf{H}_k\delta\mathbf{x}(t_k) - \mathbf{d}_k\}^{\text{T}}\mathbf{R}_k^{-1}\{\mathbf{H}_k\delta\mathbf{x}(t_k) - \mathbf{d}_k\},\end{aligned}\quad (5)$$

where $\boldsymbol{\alpha}$ is a vector containing the α_l weighting factors for all ensemble members and \mathbf{A} is the localization correlation matrix. Pre-conditioning for J^{ens} is done by factorization of the \mathbf{A} matrix, often by Cholesky factorization. It should be noted that no TL and adjoint model integrations are needed for 4DEnVar, since the four-dimensional error covariances are estimated from the pre-calculated trajectories of the nonlinear ensemble members.

3DEnVar and 4DEnVar require that an ensemble of background model states is available. In several early applications of 3(4)DEnVar (Buehner, 2005; Buehner *et al.*, 2013; Kleist and Ide, 2015), the required ensemble is obtained from an existing EPS, possibly at lower model resolution. Gustafsson and Bojarova (2014) obtained an ensemble from running the full-resolution nonlinear model with an ETKF rescaling (Bishop *et al.*, 2001) of the background ensemble perturbations to represent analysis-error ensemble perturbations. It may be that a full-resolution ensemble is needed to fully benefit from ensemble DA at convective scales.

2.1.4 | A Local Ensemble Transform Kalman Filter (LETKF)

Dropping the k time index for observations, innovations, the observation-error covariance matrix, the observation operator

and its corresponding TL operator, the analysis step of the EnKF at a fixed time can be implemented by minimizing the cost function

$$J^{\text{LETKF}} = \frac{1}{2}\delta\mathbf{x}^{\text{T}}\mathbf{P}^{-1}\delta\mathbf{x} + \frac{1}{2}(\mathbf{d} - \mathbf{H}\delta\mathbf{x})^{\text{T}}\mathbf{R}^{-1}(\mathbf{d} - \mathbf{H}\delta\mathbf{x}),\quad (6)$$

where $\delta\mathbf{x} = \mathbf{x} - \mathbf{x}^{\text{b}}$ and $\mathbf{d} = \mathbf{y} - \mathbf{H}(\mathbf{x}^{\text{b}})$. However, the ensemble-derived background-error covariance matrix \mathbf{P} is not invertible, so the state variables are transformed into the space spanned by the ensemble (Bishop *et al.*, 2001; Zupanski, 2005; Hunt *et al.*, 2007), as is done for EnVar algorithms. The minimization is then carried out for the vector of weights \mathbf{w} , whose size is equal to the number of ensemble members N_{ens} . The analysis corresponding to the EnKF solution would then be $\mathbf{x}^{\text{a}} = \mathbf{x}^{\text{b}} + \mathbf{X}\mathbf{w}$, with \mathbf{X} and \mathbf{P} defined as in the previous section. Using the linear approximation $\mathbf{H}(\mathbf{x}^{\text{b}} + \mathbf{X}\mathbf{w}) \approx \mathbf{H}(\mathbf{x}^{\text{b}}) + \mathbf{Y}^{\text{b}}\mathbf{w}$, the cost function for \mathbf{w} in the ensemble space is then given by

$$\begin{aligned}J^{\text{LETKF}} &= \frac{1}{2}\mathbf{w}^{\text{T}}\mathbf{w} \\ &\quad + \frac{1}{2}\{\mathbf{y} - \mathbf{H}(\mathbf{x}^{\text{b}}) - \mathbf{Y}^{\text{b}}\mathbf{w}\}^{\text{T}}\mathbf{R}^{-1}\{\mathbf{y} - \mathbf{H}(\mathbf{x}^{\text{b}}) - \mathbf{Y}^{\text{b}}\mathbf{w}\},\end{aligned}\quad (7)$$

where

$$\mathbf{Y}^{\text{b}} = \frac{1}{\sqrt{N_{\text{ens}} - 1}}\left(\mathbf{y}^{\text{b},1} - \bar{\mathbf{y}}^{\text{b}}, \dots, \mathbf{y}^{\text{b},N_{\text{ens}}} - \bar{\mathbf{y}}^{\text{b}}\right)\quad (8)$$

is the ensemble background perturbation matrix in observation space (noting that $\bar{\mathbf{y}}^{\text{b}}$ is the mean of the observation space ensemble and $\mathbf{y}^{\text{b},l} = \mathbf{H}(\mathbf{x}^{\text{b},l})$ is obtained by applying the nonlinear observation operator to each ensemble member l).

For the minimum of J^{LETKF} and the analysis error covariance matrix \mathbf{P}^{a} , the Kalman filter equations in reduced rank would be used, resulting in the analysis for the deterministic run and the analysis ensemble perturbations from the mean given through

$$\mathbf{x}^{\text{a}} = \mathbf{x}^{\text{b}} + \mathbf{X}^{\text{a}}(\mathbf{Y}^{\text{a}})^{\text{T}}\mathbf{R}^{-1}\{\mathbf{y} - \mathbf{H}(\mathbf{x}^{\text{b}})\},\quad (9)$$

$$\mathbf{X}^{\text{a}} = \mathbf{X}\{\mathbf{I} + (\mathbf{Y}^{\text{b}})^{\text{T}}\mathbf{R}^{-1}\mathbf{Y}^{\text{b}}\}^{-1/2},\quad (10)$$

where $1/2$ denotes that a symmetric square root of the matrix is taken, $\mathbf{P}^{\text{a}} = \mathbf{X}^{\text{a}}(\mathbf{X}^{\text{a}})^{\text{T}}$ is the analysis-error covariance matrix and \mathbf{Y}^{a} is the ensemble analysis perturbation matrix in observation space. A more detailed description of the presented algorithm can be found in Schraff *et al.* (2016). Other LETKF implementations may differ in detail (e.g. Hunt *et al.*, 2007). Section 2.4 gives a description of domain localization with weighting of observations.

2.1.5 | Surface and soil assimilation

Since many convective-scale phenomena are forced from the lower boundary condition, surface and soil DA are important components of any convective-scale DA system. These components are of such importance that they could warrant a survey article by itself, but here we will give only a brief overview.

Surface assimilation techniques mainly use screen-level observations of relative humidity and temperature to infer realistic estimates about the soil variables (i.e. soil moisture and soil temperature) by optimally combining the screen-level observations with a short-range forecast. Satellite observations, for example ASCAT soil wetness data, have also started to be used operationally (Dharssi *et al.*, 2011). While OI has been the more commonly used technique for operational surface assimilation (Giard and Bazile, 2000; Drusch, 2007), the EKF has been gaining more attention and has, for example, replaced the old OI scheme for soil moisture analysis in the IFS system of the ECMWF (de Rosnay *et al.*, 2012). It is also used operationally at the DWD (Hess, 2001) and at the Met Office (Dharssi *et al.*, 2012). The main difference between OI and the EKF is that for OI the gain coefficients are static while the EKF uses dynamical gain coefficients. The main difference between the EKF and the ETKF, as described above, is that the error covariances of the EKF are estimated through model simulations with small enough perturbations to stay within linear regimes, while the ETKF uses perturbations of realistic magnitude calculated through an ensemble.

For the time being, the surface and soil assimilation is generally performed separately from the upper-air analysis. A unique feature of the JMA local NWP system is the inclusion of surface and soil variables among the control variables of the atmospheric DA (section 2.6).

2.2 | Météo-France and the HIRLAM and ALADIN consortia

Météo-France and the HIRLAM and ALADIN consortia use the same convective-scale DA system based on the spectral ALADIN variational DA scheme (Fischer *et al.*, 2005). The scheme was developed in the framework of the ARPEGE/IFS software (Courtier *et al.*, 1994) from which it has inherited most of its characteristics (in terms of incremental formulation, observation operators, minimization technique, data flow, etc.).

2.2.1 | Basic 3D-Var

In order to be informative across most model scales and particularly at the smaller ones, which is a major challenge in convective-scale DA, the analysis has to be performed at a horizontal resolution very close to that of the model. The system currently uses 3D-Var operationally to limit the numerical cost at these resolutions. To partially overcome the lack of the temporal dimension, this scheme is used in a forward intermittent cycle (1 or 3 h), which is more frequent than for global systems (usually with a 6 hr cycle). This allows us to take greater advantage of the high-frequency observations such as radar, radiances from geostationary satellites, the GNSS, Mode-S (section 3.2.2) or surface measurements. Each 3D-Var performs an analysis of the two wind components, temperature, specific humidity and surface pressure.

The other prognostic fields (such as TKE, non-hydrostatic fields or hydrometeors) are taken directly from the background. The scheme uses climatological background-error covariances that are modelled following the formalism proposed by Derber and Bouttier (1999) for global scales and adapted to regional and limited-area models by Berre (2000). This multivariate formulation, which uses the vorticity and the unbalanced divergence, temperature, specific humidity and surface pressure as control variables (Table 4) relies on assumptions of horizontal homogeneity, isotropy and non-separability. Cross-covariances between errors for the different variables are represented using scale-dependent statistical regressions, including a balance relationship for specific humidity.

2.2.2 | The Météo-France (AROME) DA cycling

AROME-France is the convective-scale NWP system which has been running operationally at Météo-France since the end of 2008 (Seity *et al.*, 2011), as a complement to the global model ARPEGE. Currently, and as described in Table 3, it uses a 1.3 km horizontal resolution and 90 vertical levels over a 1500 × 1400 grid point geographical domain and performs a 3D-Var analysis at these resolutions in a continuous DA cycle every hour (Brousseau *et al.*, 2016). The observation cut-off times range from 45 to 105 min depending on the analysis time. The DA scheme uses all observations within the assimilation time window that have been received before the observation cut-off time. Climatological background-error covariances are estimated from pre-computed AROME-France EDA training data at full resolution. Such covariances have been proven to be more representative of the smaller model scales than covariances obtained from forecasts downscaled from a global EDA, and consequently allow us to noticeably reduce the spin-up time (Brousseau *et al.*, 2016). As listed in Table 6, AROME-France uses the same observation types that are assimilated in the ARPEGE global model: conventional observations, radiances from ATOVS, IASI (Guidard *et al.*, 2011), AIRS, CRIS, ATMS, SSMIS, MHS and GMI on board polar-orbiting satellites, winds from AMVs and ASCAT, and ZTD measurements from GNSS satellites. Compared to the ARPEGE system, some of these observations are assimilated with different set-ups: a shorter thinning distance for aircraft and IASI measurements (respectively 25 and 90 km in AROME-France versus 50 and 125 km in ARPEGE), particular AMSU-A and IASI channel selections adapted to the lower AROME-France model top and a different GNSS station acceptance list. In addition to these observations, AROME-France also benefits from screen-level measurements (temperature and relative humidity at 2 m, and 10 m winds) and from reflectivities (Wattrelot *et al.*, 2014) and Doppler radial winds (Montmerle and Faccani, 2009) from the French radar network (section 2.2.3). Raw pixel values of SEVIRI radiances on board MSG have furthermore been preferred to the CSR

product, deduced from cloud-free pixels over segments of 16×16 pixel squares, which is usually considered to be global scale. As detailed in (Montmerle *et al.*, 2007), this allows the use of observations that are more representative of convective scales while enabling radiances from water vapour channels above low clouds, as defined by the SAF-NWP product, to be retained. Using *a posteriori* diagnostics, Brousseau *et al.* (2014) show that these high spatial density observations are the main information providers for analyzing the finest model scales. Variational bias correction (Auligné *et al.*, 2007), provided by the ARPEGE system for shared observations or estimated in the AROME-France system itself for its particular observations, is applied to satellite radiances and ZTD-GNSS.

AROME-France provides 36–42 hr range forecasts five times a day using Lateral Boundary Conditions (LBCs) synchronously from the global model ARPEGE: at synoptic times (0000, 0600, 1200 and 1800 UTC) the AROME forecast uses LBCs from the ARPEGE forecast initialized at the same analysis time (and the 0300 UTC AROME-France forecast uses LBCs from the 0000 UTC ARPEGE forecast). AROME-France long forecasts are thus launched with a delay reaching 90 min after the analysis time, which allows them to benefit from the next analysis of the hourly DA cycle provided this analysis was previously performed using a preliminary 1 hr range forecast as a background. Denoting the forecast n hours after the cycle time as $t + n$ hours, the forecast initialized with the analysis performed at $t + 0$ is updated with the $t + 1$ analysis during the model integration using the IAU (Bloom *et al.*, 1996). The idea is to perform the last updated forecast initialized at the main synoptic hours, compatible with operational needs and respecting operational delivery times. In this configuration, the IAU is not used for its filtering properties and it has been demonstrated that such forecasts and forecasts initialized 1 hr later perform equivalently (Brousseau *et al.*, 2016).

2.2.3 | Radar DA algorithms

High-resolution models are able to represent convective rainy patterns which can influence the development of new precipitating systems through cold pools or gust fronts: small scales cannot just adapt to large scales because of predictability limitations. Thus, mesoscale analysis can be essential, and often more important than lateral boundary conditions, for successful forecasts of heavy rain events (the convective case-study in section 3.3.1 is a perfect illustration). Since radial winds and reflectivities from Doppler radar are still the only observations that allow us to assess the three-dimensional structures of wind and humidity fields in precipitating areas, their contribution to the AROME-France mesoscale analysis is crucial. Volumes of Doppler radial winds were first assimilated in the AROME-France 3D-Var configuration (Montmerle and Faccani, 2009). In order to assimilate the radial wind, an *ad hoc* observation operator, mainly based on Lindskog *et al.*

(2004) and Caumont *et al.* (2006), has been developed. The broadening of the radar beam is taken into account through a representation of the main lobe by a Gaussian function. Furthermore, a specific Doppler wind preprocessing step is applied, consisting of the application of two successive nonlinear filters. These steps are essential as they allow us to remove noisy pixels whose de-aliasing has failed, particularly in highly turbulent areas where the Doppler power spectrum width is broadening. An observation quality check against the first guess is then applied. While Salonen *et al.* (2009) chose to apply a “superobbing” (spatial averaging of raw measurements) in order to reduce the representativeness errors, a thinning strategy is classically applied to the remaining filtered velocities to avoid the effects of the observation-error correlations, which are neglected in the observation-error covariance matrix.

As the radar reflectivity is a highly indirect observation of the NWP model variables, it is difficult to extract useful information about the main control variables from the observations. Moreover, with variational techniques, its assimilation raises a number of questions concerning several fundamental issues, such as:

1. the importance of accounting for relevant forecast errors in precipitating areas as shown by Montmerle and Berre (2010), in particular the multivariate relationships between errors of hydrometeors and the thermodynamic variables (Michel *et al.*, 2011) or the vertical motion (Pagé *et al.*, 2007);
2. the nonlinearity of the observation operator which can entail sub-optimalities during the minimization;
3. the “no-rain” issue, which occurs when there is no rain in the first guess but the observation is rainy;
4. or the opposite case (Wattrelot *et al.*, 2014, give more detailed explanations).

In that context, research into radar reflectivity assimilation has given some encouraging results in 3D-Var (Wang *et al.*, 2013a) and 4D-Var (Sun and Wang, 2013; Wang *et al.*, 2013b). Nevertheless, no operational applications have been performed yet, particularly because only warm microphysical processes are considered.

To circumvent these issues, an original 1D+3D-Var method to assimilate radar reflectivity, based on the first tests made in Caumont *et al.* (2010) using a research version of the non-hydrostatic mesoscale assimilation system, was implemented in the AROME system at Météo-France (Wattrelot *et al.*, 2014). The first step consists of a 1D-Bayesian inversion (based on a discretization of the formulation of Bayes’ theorem to get the best estimate of relative humidity profiles of the model state) that uses accurate simulations of the equivalent reflectivity factor of the model counterpart at the observation location, and in its vicinity. Thus, assuming that the errors of the observations and simulated observations are Gaussian and uncorrelated, a column of relative humidity pseudo-observations (\mathbf{y}_{po}^{HU}) corresponding to each

observed column of reflectivity \mathbf{y}_Z can be computed as a linear combination of relative humidity columns from the model background state in the vicinity of the observation (\mathbf{x}_i^{HU}) weighted by a function of the difference between observed and simulated reflectivities:

$$\mathbf{y}_{\text{po}}^{\text{HU}} = \sum_i \mathbf{x}_i^{\text{HU}} \frac{\exp\{-J_{\text{po}}(\mathbf{x}_i)\}}{\sum_j \exp\{-J_{\text{po}}(\mathbf{x}_j)\}} \quad (11)$$

with

$$J_{\text{po}}(\mathbf{x}) = \frac{1}{2} \{\mathbf{y}_Z - H_Z(\mathbf{x})\}^T \mathbf{R}_Z^{-1} \{\mathbf{y}_Z - H_Z(\mathbf{x})\}, \quad (12)$$

where $H_Z(\mathbf{x})$ is the simulated reflectivity and \mathbf{R}_Z is the observation-error covariance matrix. Equation 11 can be interpreted as one particle filter formulation, in which “neighbouring” vertical columns in the first-guess field are treated as prior ensemble members. Following sensitivity studies, the vicinity of the observation has been chosen to be a moving window of 13×13 columns spread uniformly within a $200 \text{ km} \times 200 \text{ km}$ square centred on the observation location. The assumptions for the reflectivity observation operator H_Z , largely discussed in Wattrelot *et al.* (2014), were chosen in order to provide a good compromise between a realistic simulation (which takes into account cold processes and an accurate modelling of the radar beam) and the need to adapt to the massively parallel code AROME. Once retrieved, the humidity profiles enter a screening procedure where a specific quality check is done to control *a posteriori* the convergence of the 1D Bayesian inversion. As for the radial velocities, horizontal spatial thinning is used to reduce the representativeness errors.

The assimilation of radar reflectivities alone gave a positive impact on quantitative precipitation forecasts. Adding Doppler radial winds also improved the quality of the low-level winds. This is due to the complementary nature of the two observation types and the multivariate balance operators used to model \mathbf{B} (Berre, 2000).

Using these techniques, the radial velocities and the reflectivities observed by the national ARAMIS radar network have been operationally assimilated in AROME-France since the beginning of the operational suite in 2008 and 2010, respectively. Their impact in the system has subsequently increased with the adoption of hourly DA cycling in 2015. The 1D+3D-Var technique to assimilate reflectivities has since been successfully tested in HARMONIE-AROME (see below) and is used operationally by JMA, as described in section 2.6.

2.2.4 | HARMONIE-AROME DA

The configuration of the AROME DA and forecasting system as run by the countries in the HIRLAM consortium is usually referred to as HARMONIE-AROME. The adaptation of the AROME physics for HARMONIE has been described by Bengtsson *et al.* (2017). The DA part consists of surface DA and upper-air variational DA. There are some differences

in each local implementation of the HARMONIE system, in particular concerning observation usage for upper-air DA.

The baseline background-error statistics have been obtained by downscaling forecasts from the ECMWF ensemble DA system and applying the HARMONIE configuration of the AROME forecast model. Statistics have also been derived by using ensemble DA within the HARMONIE-AROME system itself. Observation usage for the baseline upper-air DA is restricted to conventional types of *in situ* measurements and ATOVS AMSU-A and AMSU-B/MHS radiance measurements from polar-orbiting satellites. Systematic errors are frequently present in many of the satellite-based measurements and are handled through adaptive variational bias correction (Auligné *et al.*, 2007).

In local pre-operational and operational HARMONIE implementations, the observation usage includes satellite radiances from the IASI and ATMS instruments, as well as ASCAT wind measurements. ZTD measurements from GNSS satellites are assimilated (Arriola *et al.*, 2016) as well as AMVs and Mode-S EHS winds obtained from air traffic control systems and GNSS radio-occultations. Last, but not least important, radar reflectivities, pre-processed to relative humidity profiles, are assimilated. These can be obtained for most European weather radars through the OPERA network (section 4.2.2). In research experiments Doppler radar radial winds have also been assimilated, aiming for operational implementation. Other observation types revealing encouraging results in DA experiments are radiances from the SEVIRI instrument on board the geostationary MSG satellites as well as assimilation of the cloud cover products obtained from the nowcasting SAF.

A crucial challenge for limited-area DA is how to best utilize information from the larger-scale host model in nested DA. ECMWF operational forecasts, with a 6 hr lag, provide the LBCs. In the baseline HARMONIE-AROME, upper-air DA system spectral mixing of large-scale host model information with smaller-scale HARMONIE-AROME model data is applied in a step prior to upper-air DA (Müller *et al.*, 2017). The characteristic scale of the spectral mixing is dependent on a rather empirically selected vertically dependent mixing wave number. An alternative, more attractive, approach is to incorporate the host model information in the cost function through a large-scale error constraint (Guidard and Fischer, 2008; Dahlgren and Gustafsson, 2012) which has been applied for reanalysis purposes, but further refinements are needed.

2.2.5 | ALADIN/LACE data assimilation

Member countries of the ALADIN consortium have taken part in the implementation of limited-area variational DA tools (Fischer *et al.*, 2005; Bölöni, 2006). The use of upper-air observations in the operational suites varies across the 16 ALADIN member countries depending on the local

availabilities of the different types of observation. A closer cooperation of Central European ALADIN countries formed into the RC LACE consortium (Austria, Croatia, the Czech Republic, Hungary, Romania, Slovakia and Slovenia). Due to the strengthened partnership of RC LACE countries, nowadays more than ten operational DA systems exist employing increased numbers of national observations in NWP analyses over LACE domains. Since configurations vary (e.g. resolution, use of observations) within RC LACE, we denote only general properties in Tables 3–6. In many of those DA systems, the so-called RUC (Benjamin *et al.*, 2004) method further extends the capabilities of applied 3D-Var (Mile *et al.*, 2015). The Slovenian 3D-Var three hourly RUC is a good example of such a system, where the efficiency of the increased analysis frequency is magnified by the operational use of MRAR observations (Strajnar, 2012; Strajnar *et al.*, 2015).

The idea of combining large scales analyzed by a host global model with a high-resolution LAM background or analysis has received great attention (Yang, 2005; Brožková *et al.*, 2006; Guidard *et al.*, 2006; Guidard and Fischer, 2008; Wang *et al.*, 2014). Within RC LACE the DF idea led to development of the DF blending method (Brožková *et al.*, 2001) which came into operational use in 2001. DF blending can be seen as a pseudo-assimilation method since it incrementally adds large scales from a global model analysis to a high-resolution ALADIN background. This gives initial conditions that are clearly better than pure dynamical adaptation of the global model analysis, as small scales are better captured in ALADIN than in the global model analysis. DF blending is implemented in spectral space and consists of several steps:

1. first global and LAM spectra are truncated to a cut-off wavelength given by an empirical formula (Derková and Belluš, 2007);
2. this is followed by filtering with a non-recursive Dolph–Chebyshev digital filter (Lynch *et al.*, 1997);
3. at the end the ALADIN background is incremented with the difference between the filtered models' spectra interpolated back to high resolution.

As an extension to DF blending, Šíroká *et al.* (2001) proposed a method called BlendVar in which a 3D-Var assimilation is performed after DF blending. Since DF blending is preserving aspects of a global analysis, it is expected that it will provide a better start for 3D-Var than the ALADIN background itself. Guidard *et al.* (2006) used BlendVar to assimilate observations from Intensive Observing Period 14 of the Mesoscale Alpine Programme with a positive impact on precipitation forecasts. Encouraged by the findings of Guidard *et al.*, the BlendVar method was operationally implemented within RC LACE in the Czech Republic in 2015.

2.3 | Met Office 3D-Var

The Met Office's variational DA is designed so that it can be used for both global and limited-area grid-point models, in either 3D-Var or 4D-Var mode (Lorenz *et al.*, 2000; Rawlins *et al.*, 2007). The global model system uses 4D-Var with a 6 hr cycle. Although an hourly 4D-Var system at convective scale went operational in July 2017 (section 4.3.2 gives an outline), we choose to describe here the cheaper 3D-Var system with a 3 hr cycle, which has featured in various earlier Met Office operational models since 1999. The 3D-Var system uses FGAT and initialization is performed by the IAU scheme to introduce analysis increments gradually as a tendency forcing term over a 2 hr window centred on the nominal analysis time. The observation cut-off is $t + 75$ min.

Forecast-error covariances in the UKV model are currently specified climatologically through the so-called NMC method (Parrish and Derber, 1992) although a flow-dependent hybrid system is now implemented in the global model (Clayton *et al.*, 2013). They are computed from forecast differences between different runs of the model driven by the same lateral boundary conditions – the so-called “lagged” NMC method (Šíroká *et al.*, 2003). The input forecast fields are valid at $t + 6$ and $t + 3$ hr on successive cycles. When calibrating the latest covariances, the horizontal control variable transform is applied to each model level, providing a spectral representation as a function of total horizontal wavebands, and the vertical transform subsequently computes a full vertical covariance matrix for each waveband (Berre, 2000; Gustafsson *et al.*, 2001; Brousseau *et al.*, 2011). This approach allows horizontal correlations to vary with height and vertical correlations to vary with horizontal length-scale. In the UK model, the vertical structure functions are modified by the introduction of a vertically adaptive grid (Piccolo and Cullen, 2011; 2012), which deforms grid points vertically in regions of large static stability prior to applying the parameter transform. This helps ensure that the climatological covariance correlations are appropriately applied around temperature inversions in particular. Limited-area analyses use the same humidity control variable as the global system (Ingleby *et al.*, 2013).

The operational UKV model grid has an inner area of fixed 1.5 km grid spacing and an outer region with 4 km×4 km grid boxes at the corners and 1.5 km×4 km in the remainder of the outer domain. There are 70 vertical levels of a hybrid-height coordinate, which is terrain-following at the surface and locally horizontal at the top of the domain, reaching 40 km above the surface (Tang *et al.*, 2013). The analysis grid, however, is of fixed 3.3 km grid spacing across the whole model domain. At the boundaries, the unbalanced pressure, humidity and logarithm of aerosol control variables are constrained to be zero. The streamfunction is zero and the velocity potential has zero normal gradient at the boundaries, consistent with the vector wind having zero normal components at the boundaries. In practice, numerical discretization of partial

derivatives and grid staggering means that the increments are not identically zero at the boundaries after being transformed back to model variables. This approach relies on a good quality large-scale forecast; it assumes that the large-scale forcing cannot be improved using the observations inside the limited domain, most of which will have been available to the driving model.

In terms of observation usage, the UKV model assimilates a number of extra sources of high-resolution information not present in the global system. For example, screen-level temperature and humidity data from roadside sensors are a valuable supplement to the SYNOP network. High-resolution AMVs from MSG are also available. A radar-based precipitation rate analysis is assimilated via the technique of LHN (Jones and Macpherson, 1997; Macpherson, 2001) as well as Doppler radial wind data from UK weather radars (Simonin *et al.*, 2014). A novel feature is the variational assimilation of visibility observations (Clark *et al.*, 2008). The visibility observation operator is a highly nonlinear function of humidity, aerosol content and temperature.

Cloud fraction data are also assimilated directly in 3D-Var (Renshaw and Francis, 2011). There are two kinds of cloud data, which are assimilated independently. The first, known as GeoCloud profiles, are based only on satellite cloud-top information, and consist of a cloud fraction profile with zeros above the cloud top, one or more layers of non-zero cloud fraction representing the observed cloud layer, and missing data beneath. The number of layers of cloud inserted is height dependent, and drawn from a UKV model climatology of cloud thickness. The second category is cloud from surface reports, which are also inserted with a thickness derived from model climatology.

2.4 | DWD and the COSMO consortium – KENDA (LETKF)

The DWD and its partners have recently developed the KENDA system (Schraff *et al.*, 2016) for the COSMO model (Baldauf *et al.*, 2011), which is a non-hydrostatic convection-permitting model, whose main specifications are given in Table 3. The DA algorithm used in KENDA is based on an LETKF (section 2.1.4) applied in a 1 hr cycle with each analysis step assimilating conventional data from 59 to 0 min prior to the analysis time (Table 6). The LETKF is combined with LHN (Stephan *et al.*, 2008) of every ensemble member towards radar-estimated surface precipitation (Tables 4 and 6).

To sample the background-error covariance, a 40-member ensemble is currently used. Each member consists of the prognostic variables for the three-dimensional wind components, temperature, pressure perturbation, specific humidity, cloud water and ice. The prognostic variables of TKE, rain, snow, and graupel are excluded from the analysis update. When used at DWD, each ensemble member is driven by LBCs from one member of the ICON (Zängl *et al.*, 2015) LETKF

ensemble which has a resolution of 40 km globally and 20 km over Europe. At MeteoSwiss, the LBCs are derived from the deterministic ECMWF high-resolution forecasts with a 6 hr lag plus ensemble perturbations from the ECMWF ensemble with 30–36 hr lag in order to ensure a large enough spread.

In KENDA, domain localization with a weighting of the observations is used to calculate the analysis separately at every grid point within the model domain using observations within a horizontal radius from the analysis point (e.g. Hunt *et al.*, 2007; Janjić *et al.*, 2011). Within certain limits, the horizontal radius is chosen adaptively in such a way that a fixed number of observations is always assimilated in the vicinity of an analysis grid point (Periáñez *et al.*, 2014). This results in a half-length-scale of the Gaspari and Cohn covariance function (Gaspari and Cohn, 1999) of around 100 km (Lange and Janjić, 2016) for assimilation of conventional data given in Table 6 when the number of observations is chosen to be 100 (2.5 times the number of ensemble members). In the vertical, the localization is height dependent and varies in the range of 0.075–0.5 in logarithm of pressure.

The background-error covariance derived from the ensemble does not adequately represent the uncertainty of the background field due to both sampling and model error. Several mechanisms are introduced to alleviate the effects of underestimated ensemble covariances. In KENDA, the methods of background covariance inflation, adaptive covariance localization, RTPP and random surface perturbations are used.

The RTPP scheme (Zhang *et al.*, 2004) relaxes the analysis ensemble perturbations towards the background ensemble perturbations at every grid point of the model. As shown in Zhang *et al.* (2004), this technique is beneficial when the initial background is not accurate. Depending on the spread of LBCs, it can inflate or deflate the ensemble (Schraff *et al.*, 2016). Furthermore, the variance of the analysis is artificially increased only where observations are present (Zhang *et al.*, 2004; Whitaker and Hamill, 2012). Multiplicative inflation (Anderson and Anderson, 1999) in KENDA is adaptive with a multiplicative covariance inflation factor applied separately for every coarse analysis grid point (Li *et al.*, 2009). Whitaker *et al.* (2004) and Whitaker *et al.* (2008) report that multiplicative inflation generates either too much spread in regions less constrained by the observations or too little spread in areas with high observational coverage. The need for so many different techniques is a result of each method resolving only certain aspects of model and sampling errors. For example, since localization does not affect the variances themselves, the combination of multiplicative inflation and the RTPP scheme is usually used to deal with the sampling problem (Whitaker and Hamill, 2012). Random perturbations of soil moisture content with two horizontal correlation length-scales of 10 and 100 km are applied after each analysis update to partly account for the uncertainty in the soil conditions. These perturbations turned out to increase the low-level temperature and humidity spread, resulting in a larger weight being given to the observations and an improvement in analysis

and forecast skill (Schraff *et al.*, 2016). The effect of the soil moisture perturbations is particularly noticeable in summer conditions. Soil moisture perturbations and SPPT (Buizza *et al.*, 1999; Bouttier *et al.*, 2012) were able to increase the temperature (humidity) spread by 62% (31%) near the surface and 6% (5%) at 700 hPa in a one-month summer experiment and to slightly reduce the root-mean-square error (RMSE). This illustrates the sensitivity of the LETKF to model error and the need to account for it. To further account for this, additive covariance inflation based on random samples of the climatological atmospheric background-error covariances from the global EnVar DA system for ICON has been added recently to the operational KENDA system at DWD. However, this has not yet been used in the tests with KENDA shown in section 3.

Rapid updates in high-resolution models often lead to problems with balance and noise. It has been found that computing the upper-air pressure analysis increments using hydrostatic balancing of analysis increments (Rhodin *et al.*, 2013) reduces the noise that projects onto surface pressure tendencies, and it is the only balancing method currently applied (apart from a saturation adjustment).

Finally, the observation-error covariance matrix is assumed to be diagonal for all observation types and the Desroziers method (Desroziers *et al.*, 2005) is used to tune the observation-error variances in KENDA. The inclusion of additional observation types in KENDA is currently ongoing. For example, in research experiments Doppler radar reflectivity (Bick *et al.*, 2016) has also been assimilated using a newly developed observation operator (Zeng *et al.*, 2016), as well as the Meteosat SEVIRI-derived cloud information (Schomburg *et al.*, 2015), SEVIRI radiances (Harnisch *et al.*, 2016) and Mode-S EHS data (Lange and Janjić, 2016).

2.5 | NOAA

The NOAA NCEP provides high-resolution, convection-permitting forecasts for the USA with two analysis and forecast systems: the 3 km CONUS-NAM (Rogers *et al.*, 2017) and the HRRR (Benjamin *et al.*, 2016).

The CONUS-NAM nest features an hourly DA cycle and issues free forecasts out to 60 hr four times per day (0000, 0600, 1200, and 1800 UTC). The LBCs for the CONUS nest come from the 12 km North American parent domain. The CONUS-NAM nest provides support for users in need of convective-scale information (severe weather, heavy rainfall, renewable energy, and winter weather events) out to time ranges of about 2.5 days.

The HRRR is a 3 km, hourly updating convection-permitting implementation of the Advanced WRF model, run operationally at NCEP since September 2014. The HRRR produces forecasts every hour out to 18 hr over a domain covering the entire CONUS, using initial and lateral boundary fields from the hourly update 13 km RAP (Benjamin *et al.*, 2016). The HRRR has many applications for users who need frequently updated numerical weather guidance on

time-scales of hours to a day, for severe weather, aviation and renewable energy applications.

Both systems employ a hybrid 3DEnVar technique (section 2.1.3; Table 4) which is used for the assimilation of a wide variety of conventional and satellite observations (Table 6). The implementation of hybrid 3DEnVar in each system does not involve running a system-specific ensemble, but rather makes passive use of the EnKF members associated with the NCEP global model's DA. This approach has led to immediate significant improvements in forecast skill (Wu *et al.*, 2017) while research efforts continue toward constructing an appropriate convection-permitting ensemble suitable for DA covering the large CONUS domain.

The CONUS-NAM nest begins its DA cycle 6 hr prior to the advertised cycle time. The first-guess atmospheric state provided at the start of the assimilation window is specified by a 6 hr forecast from NCEP's global DA system. However, the model land states are maintained from the previous cycle (i.e. the global model land states are not used). Following a hybrid 3DEnVar analysis is a 1 hr forecast issued to provide the background for the next analysis time. After each hybrid 3DEnVar analysis, except for the very first analysis using a global background, a non-variational cloud and precipitation hydrometeor analysis is applied to specify clouds and precipitation in more statically stable regions. For the initialization of each of the forecasts during the cycling procedure, a radar-reflectivity-derived latent heating tendency is applied during the forward part of the model digital filter initialization to introduce observed deep convection into the model. This hourly forecast/analysis process continues for a 6 hr period until the advertised cycle time is met and a 60 hr forecast is issued.

In the HRRR, each cycle begins 1 hr prior to free-forecast initialization via interpolation of initial conditions from its coarser 13 km parent domain. The representation of small scales is then enhanced during this 1 hr period through sub-hourly radar reflectivity DA with a latent-heating method. At the end of this 1 hr period, a hybrid 3DEnVar analysis is performed which is then followed by a non-variational cloud and precipitation hydrometeor analysis, similar to the one described for the CONUS-NAM nest. Following the cloud analysis, an 18 hr forecast is issued.

2.5.1 | Cloud analysis and radar-derived latent heating

As has been noted, both the CONUS-NAM nest and HRRR systems depend upon the use of a cloud analysis technique along with the application of radar-derived latent heating tendencies to effectively introduce cloud and convective-scale information.

The cloud and precipitation analysis scheme (Hu *et al.*, 2006) is applied to specify clouds and precipitation in more statically stable regions using a combination of METAR ceilometers and GOES cloud-top pressures along with background saturation (or subsaturation) to improve retention

of the cloud features. Radar reflectivity observations, in traditionally stratiform precipitation areas, are used to retrieve and specify rain and snow hydrometeors.

Three-dimensional radar reflectivity information is further assimilated through a latent-heating method (Benjamin *et al.*, 2016). A heating rate is computed from reflectivity as follows:

$$LH(i, j, k) = \left(\frac{p_0}{p}\right)^{R_d/c_p} \left(\frac{(L_v + L_f)f[Z_e]}{c_p t}\right), \quad (13)$$

where LH is the latent heating rate (K s^{-1}), p is pressure (hPa), $p_0 = 10^3$ hPa is the surface pressure, L_v is the latent heat of vaporization (J kg^{-1}), L_f is the latent heat of fusion (J kg^{-1}), R_d is the dry gas constant ($\text{J kg}^{-1}\text{K}^{-1}$), c_p is the specific heat of dry air at a constant pressure ($\text{J kg}^{-1}\text{K}^{-1}$), $f[Z_e]$ is the reflectivity factor converted to rain/snow condensate (kg kg^{-1}), and t is the time period of condensate formation (s).

During a short period of forward model integration, the temperature tendency from the model's microphysics scheme is replaced with this reflectivity-based temperature tendency (i.e. LH). Essentially, observation-based forcing is introduced into the model where precipitation is occurring, and a response in the model's dynamic, thermodynamic, and microphysical fields develops during the forward integration. This computationally inexpensive approach promotes mesoscale circulations and/or convective-scale structures in regions of ongoing observed precipitation while suppressing development of these features in regions of radar coverage where precipitation is not observed (≤ 0 dBZ), by setting the microphysical temperature tendency to zero.

Several tunable parameters control the strength, location and duration of the specified latent heating. The strength of the specified heating is modulated through a time-scale over which reflectivity-producing precipitation condensates are assumed to have formed with typical values ranging from 10 min for the CONUS-NAM nest to 20 min for the HRRR (t in Equation (13)). A shorter (longer) assumed time period forces a stronger (weaker) latent heating rate. The locations of latent heating specification are controlled through an observed reflectivity threshold, below which the model's microphysical tendencies are permitted to evolve freely, as is done in regions with no radar coverage. A reflectivity threshold of 28 dBZ has been chosen for the CONUS-NAM nest and HRRR to target precipitating regions mostly associated with relatively deep (above 200 hPa) moist convection. In the CONUS-NAM nest, latent heat specification during a 20 min model integration is combined with a DFI that reduces noise in the subsequent forecast (Benjamin *et al.*, 2004; 2016). As mentioned previously, the HRRR is initialized with a full hour of latent heating using a time-varying temperature tendency based on sub-hourly radar data, without DFI. Figure 1 demonstrates the positive impact of this radar-reflectivity-derived latent heating initialization technique in the CONUS-NAM nest via statistically significant improvement in FSS (Roberts and Lean, 2008) for composite radar reflectivity ≥ 30 dBZ for the first 5 hr of the forecast.

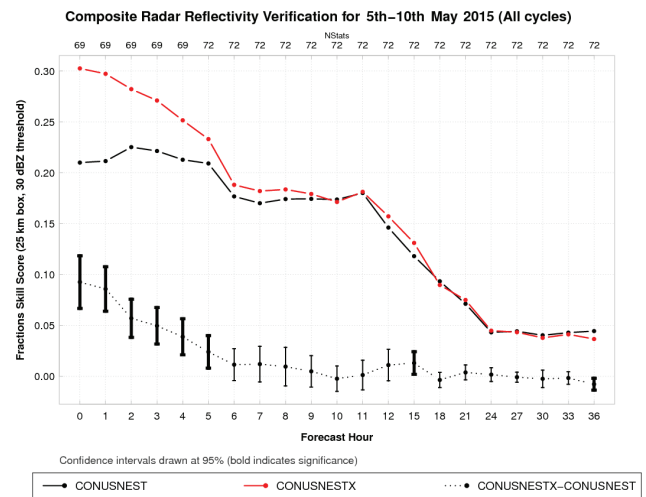


FIGURE 1 Fractions skill score (FSS) verification with a 25 km box size for forecast composite radar reflectivity ≥ 30 dBZ as a function of forecast hour covering 0000, 0600, 1200, 1800 UTC forecast initialization cycles over a 5-day period for 5–10 May 2015. Red lines (CONUS NESTX (experiment), i.e. the operational configuration) depict the forecast with radar-reflectivity-derived latent heating applied during the model digital filter initialization. Black lines (CONUS NEST) depict the forecast without the radar enhancement applied during the model digital filter initialization. The black dotted line is the difference in FSS between the two experiments and shows standard median error confidence intervals. Bold confidence intervals indicate significance at the 95% level (i.e. the confidence intervals do not encompass zero)

Furthermore, lightning flash density and cloud-growth observations provide convective-scale information beyond regions of radar coverage (e.g. oceans). In the initialization of the operational CONUS-NAM nest and HRRR, lightning flash density is converted into a proxy reflectivity field (Liu *et al.*, 2017) which is combined with the radar reflectivity field; the combined reflectivity field is assimilated through the latent-heating method described previously. In experimental HRRR versions, observations of rapidly growing deep clouds are assimilated in a similar manner.

2.5.2 | Radar data QC

Since May 2005 NCEP has had real-time access to level-II radar data from the Doppler weather radar network of the USA. Using these real-time Doppler radar data in operational DA requires that the data be processed reliably and efficiently through rigorous data QC methods. Such methods have been developed and implemented in the radar data processing system at NCEP (Liu *et al.*, 2016). The radar data QC for processing real-time radar data consists of six major components:

1. detect and remove non-meteorological echoes (Jiang *et al.*, 2013; Tang *et al.*, 2014);
2. correct or remove aliased radial velocities (Xu *et al.*, 2011);
3. remove unqualified returns when the radar antenna is aimed at the sun;
4. calculate QC statistical parameters;

5. identify and remove contamination from migrating birds with a Bayesian method (Liu *et al.*, 2005; Zhang *et al.*, 2005b) and dual polarization-based QC; and
6. statistically remove noisy and other bad-quality data as indicated by QC parameters falling outside the range of significant probability.

The radar data processing system has been implemented in operations for more than eight years and has been proven to be efficient and effective (Liu *et al.*, 2016). Following QC, these Doppler radial velocities are assimilated into the CONUS-NAM nest system.

NCEP also employs a radar reflectivity mosaic algorithm based upon procedures developed at the National Severe Storms Laboratory. The QC methods are used to generate hourly and sub-hourly three-dimensional reflectivity mosaics and two-dimensional derived products (Zhang *et al.*, 2005a) which are then used in the CONUS-NAM nest and HRRR DA systems through the aforementioned cloud analysis and radar-derived latent heating techniques.

2.6 | Japan Meteorological Agency – Operational limited-area DA systems

JMA operates two limited-area NWP systems, called Meso-scale and Local NWP systems, aiming to enhance disaster prevention and aviation forecasting.

The Meso-scale NWP system runs MSM forecasts every 3 hr out to 39 h (Table 3). The MSM domain covers Japan and its surrounding area at a horizontal grid spacing of 5 km with 817×661 horizontal grid points. MSM uses 76 vertical layers reaching a height of 21.8 km. The forecast model of MSM is the non-hydrostatic model ASUCA (Ishida *et al.*, 2009; 2010; Hara *et al.*, 2012; Aranami *et al.*, 2015). LBCs for MSM are obtained from the Global Spectral Model (GSM; JMA, 2016) forecasts, with a lag of 3 hr for 0300, 0900, 1500 and 2100 UTC or 6 hr for 0000, 0600, 1200 and 1800 UTC runs.

The MSM forecast is initialized using 4D-Var (section 2.1.1) in the MA (Tables 4 and 5), which is based on JNoVA. MA uses an incremental approach. After calculation of innovation vectors at a resolution of 5 km, variational optimization of analysis increments runs with a larger horizontal grid spacing of 15 km using 38 vertical layers. MA 4D-Var does not use the TL model in forward time integrations. Its forward model is the nonlinear version of the JMA-NHM (Saito *et al.*, 2006; 2007), but with simplified physics schemes. Thus, the trajectory over the 3 hr assimilation window is updated in each optimization iteration, approximately 30 times a run, using the nonlinear forward model at a horizontal grid spacing of 15 km. The adjoint model consists of the adjoint of the linearized dynamical core and a limited set of physics schemes (large-scale condensation, planetary boundary layer and surface flux schemes, etc.). The optimized analysis increment thus obtained is added to the high-resolution first guess, and a 3 hr forecast over the

assimilation window runs at a resolution of 5 km to generate the initial condition of the MSM. Each MA run uses the result from the previous evolved MA analysis as the first guess, forming a 4D-Var DA cycle.

Control variables of the MA 4D-Var are the eastward and northward wind components u and v , respectively, potential temperature θ , surface pressure p_s and scaled specific humidity q/q_{sat}^b , where q_{sat}^b is saturation specific humidity of the background state. The background error is taken to be homogeneous over the domain, and its profiles are estimated by the NMC method (Parrish and Derber, 1992), taking the difference between 6 and 12 hr MSM forecasts valid at the same time, taking two samples a day from the first ten days of each month over a historical one-year period of operational MSM forecasts. Vertical correlation between θ and p_s background errors is taken into account, but other variables are assumed to be independent. Hydrostatic balance is also assumed. The diagnosed level of geostrophic balance was small in the sampled training data. Digital filter initialization is applied as a weak constraint (Gauthier and Thépaut, 2001), using a penalty term to produce a more balanced analysis.

The observation cut-off time is 50 min past the nominal MSM analysis time t . Observations from $t - 3.5$ hr until $t + 0.5$ hr are assimilated, apart from observations which were assimilated in the previous assimilation cycle. Observations are collected in hourly batches when computing the cost function. Besides conventional observations, MA utilizes various satellite and remote-sensing data (Table 6). JMA operates Doppler radars and wind profiler networks over Japan, and MA uses radial velocity, reflectivity and wind observational data from these systems, which are important sources of information on detailed atmospheric situations that could cause severe weather events. Relative humidity pseudo-observations are generated from reflectivity data of both ground-based and satellite radars, and are used as inputs to 4D-Var (section 4.2.4). Variational bias-correction coefficients from the latest global analysis are applied to satellite radiances. GNSS radio occultation and ground-based GNSS data are assimilated as refractivity and total precipitable water data, respectively. Precipitation rates from radar/rain-gauge composites and satellite microwave imagers are also assimilated.

The Local NWP system runs the LFM, which has an even higher horizontal resolution of 2 km, and 58 vertical layers reaching up to a height of approximately 20.2 km (Table 3). LFM uses ASUCA as its forecast model to provide 9 hr forecasts every hour over the domain covering Japan and its surrounding area with 1531×1301 grid points. MSM forecasts, lagged 3, 4 or 5 hr depending on the LFM initial time, are used as LBCs for LFM.

The higher resolution of LFM makes it possible to resolve more detailed structures of atmospheric states, taking into account small-scale terrain effects and other atmospheric forcings, which can lead to localized severe weather

events. LFM rapidly updates the forecast, promptly reflecting observational information newly received from one hour to the next. An efficient DA system is required in order to realize the high-resolution and high-frequency operation of this system. To this end, LA applies a 3D-Var scheme (section 2.1.1) to initiate LFM forecasts (Tables 4 and 5). LA uses ASUCA-3DVar, which is a 3D-Var version of ASUCA-Var, the variational assimilation system based on the ASUCA forecast model (Aranami *et al.*, 2015; JMA, 2016).

In each hourly operation, LA iterates 3D-Var analyses and 1 hr forecasts in turn over 3 h, starting from 3 hr before the LFM initial time. This 3D-Var cycle runs at a resolution of 5 km, with 48 vertical layers. Each LA operation uses a zero, 1 or 2 hr MSM forecast, initiated using MA 4D-Var, as the first guess at the beginning of the cycle.

The control variables of LA 3D-Var include ground and underground temperature (T_g) and volume water content (VWC_g) in addition to those of MA. This extension of the control variables aids assimilation of surface temperature and satellite soil moisture observations. Background-error profiles of the LA control variables are also estimated using the NMC method. Different vertical background-error covariances are applied for vertical columns on land or over sea. A vertical coordinate transform is also used to moderate terrain-following profiles exceeding given altitudes.

For the hourly LA runs with nominal analysis time t , the observation cutoff time is $t+0.5$ h. In each LA run, observations from $t-3.5$ to $t+0.5$ h, including delayed data not received in time for the previous LA run, are assimilated in 3D-Var assimilation cycles for $t-3$, $t-2$, $t-1$ and t h. Assimilated observations include conventional, remote-sensing and satellite data as in MSM (Table 6). Land surface temperature and wind observations from the automated surface station network over Japan (AMeDAS) are used ahead of other analysis systems at lower resolutions at JMA, reflecting detailed atmospheric conditions of local environments near the surface. Satellite radiance and soil moisture data, both with variational bias correction, were introduced in January 2017 (section 4.2.4).

3 | IMPACT OF DA AND OBSERVATIONS AT CONVECTIVE SCALES

3.1 | Impact of DA

Now that operational global models are approaching 10 km resolution, it is natural to ask how we can benefit from convective-scale DA. A related issue is the impact of the quality of the LBCs. A few examples will be given in this section. The general problems for DA over a small model domain are first illustrated by applying the HARMONIE-AROME system over Iran (section 3.1.1). Then the benefit from applying convective-scale DA, versus downscaling of large-scale initial data, for precipitation forecasting is illustrated for both the KENDA and the AROME-France systems (section 3.1.2).

Furthermore, the impact of using more advanced DA algorithms is illustrated in section 3.1.3.

3.1.1 | Downscaling versus convective-scale DA and the importance of LBCs – HARMONIE over Iran

Figure 2 shows standard deviations of the differences between the forecasts and the observations for 500 hPa temperature and 2 m temperature from three experiments in a small model domain over Iran. Experiment ERA-NODA is a simple downscaling from ECMWF re-analyses (ERA) to HARMONIE with LBCs also derived from ERA analyses, ERA-DA uses HARMONIE 3D-Var DA with LBCs derived from ERA analyses. Finally, OPER-DA is an experiment with HARMONIE 3D-Var DA with LBCs derived from operational ECMWF forecasts (6 hr lag). The experiment OPER-DA was selected to be a typical scenario for applying convective-scale NWP at a small weather service. The model domain consisted of 600×500 horizontal grid points, a 2.5 km horizontal resolution and 65 vertical levels. The period of the experiments was 1–15 December 2013.

The experiment ERA-NODA should be interpreted as a simulation rather than a forecast experiment and results in rather flat verification scores as a function of forecast length (Figure 2). Introducing DA (experiment ERA-DA) with the same analysis LBCs gives improved verification scores for the first 12–24 hr for 500 hPa temperature and 2 m temperature. This is due to the finer resolution of the HARMONIE 3D-Var assimilation but also to the *assimilation cycling* of the HARMONIE model state. The effect of the assimilation cycling is more pronounced for the 2 m temperature due to the high-resolution model state adjustment to the complex orography in the Iran area. The time series of 2 m temperature verification scores (not shown) indicated a gradually improving impact of DA over the period, most likely an effect of the HARMONIE soil and surface DA (with slower time-scales). Comparing the ERA-DA and OPER-DA experiments, we can see that the LBCs influence the forecast quality quite quickly over the small model domain, particularly in the free atmosphere.

3.1.2 | Downscaling versus convective-scale DA – KENDA and AROME-France

Figure 3 compares the impact on deterministic precipitation forecasts of initial conditions taken from KENDA or interpolated from the ICON-EU model. The deterministic ICON-EU model has a horizontal resolution of 7 km and is based on the operational 3DVar analysis of the ICON system. The FSS is plotted corresponding to 30 km × 30 km regions for 0.1 and 1.0 mm h⁻¹ over the period from 26 May to 9 June 2016, which had frequent local severe weather conditions. The scores were averaged over all 0000, 0600, 1200, and 1800 UTC forecast runs and show improved precipitation forecasts up to lead times of 18 hr if initial conditions are taken from KENDA analyses.

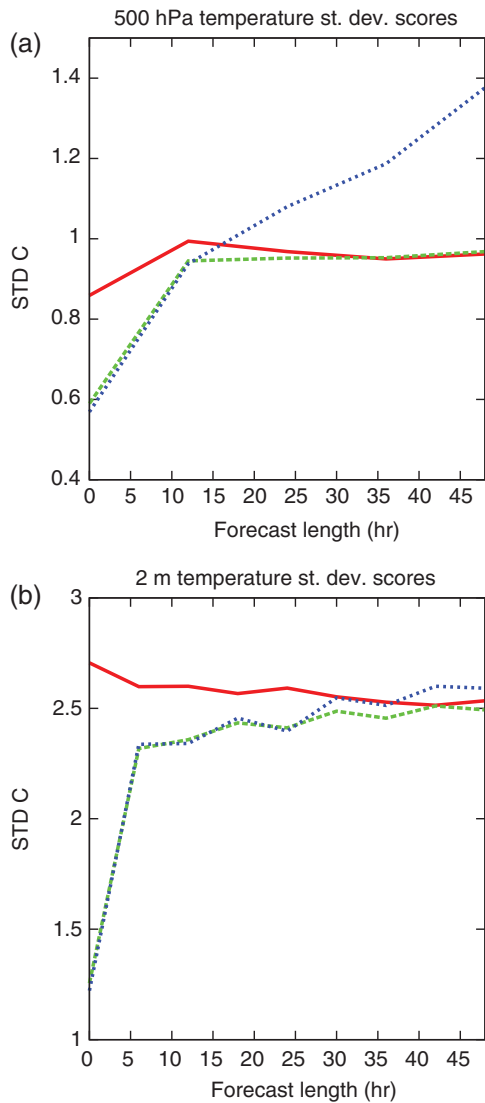


FIGURE 2 Standard deviation forecast scores for verification of (a) 500 hPa temperature against radiosonde observations and (b) 2 m temperature against SYNOP stations. The HARMONIE forecasting system was applied to a small model domain over Iran. ERA-NODA (red solid line) represents downscaling (no DA) from ERA re-analysis data with ERA data also on the lateral boundaries. ERA-DA (green dashed line) represents DA with ERA analyses on the lateral boundaries. OPER-DA (blue dotted line) represents DA with 6 hr lagged ECMWF forecasts on the lateral boundaries

Similar results are obtained when comparing operational AROME-France forecasts using convective-scale DA and AROME-France forecasts starting from initial conditions interpolated from the global ARPEGE system. The latter uses a stretched horizontal grid reaching a peak 7 km resolution over France and performs 4D-Var analyses with two outer loop iterations (using 130 and 50 km resolutions in turn) in a 6 hr cycle (section 2.1.2). Operational and down-scaled AROME-France forecasts use the same LBCs from the ARPEGE model and the same surface initial conditions from the operational AROME-France surface DA cycle. Figure 4 displays Brier Skill Scores for 6 h cumulative rainfall forecasts computed from 30 hr forecasts produced by these two

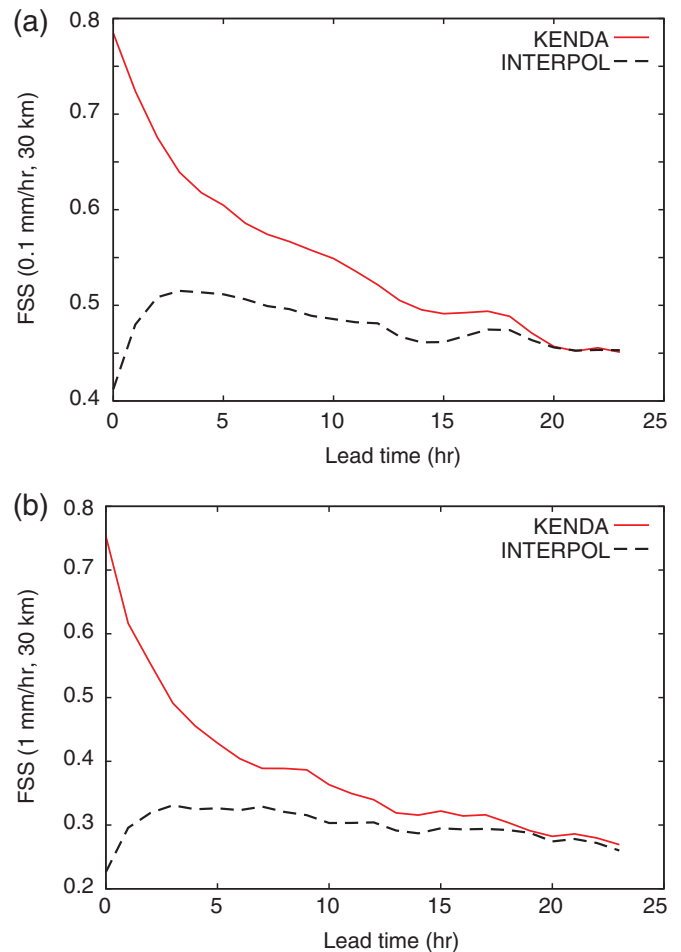


FIGURE 3 The FSS (Fractions Skill Score) corresponding to areas of 30 km \times 30 km for (a) 0.1 and (b) 1.0 mm h⁻¹ 1 hr precipitation verified against radar-derived precipitation as a function of forecast lead time for a convective two-week period from 26 May to 9 June 2016. The red solid line denotes forecasts started from KENDA, and the black line forecasts started from interpolated ICON-EU coarser-scale analyses. Note the effect of spin-up time in the first 4 hr for forecasts started from interpolated ICON-EU coarse-scale analysis

configurations over the seven-month convective time period from 1 May to 1 November 2016. The evolution of the score difference as a function of forecast range clearly indicates that the initial conditions provided by the convective-scale DA, which are representative of convective-scale phenomena and adapted to the model resolution and to the accurate topography description, significantly improve the forecast performance during the first 12 hr for all precipitation thresholds. Smaller improvements also exist at longer forecast ranges for the higher thresholds which are likely to be linked to convective activity. However, they are not statistically significant as the LBC signal dominates with increasing forecast range in both cases. An illustration of expected improvement for a strongly convective event is given in section 3.3.1. During winter periods, when precipitation is mainly driven by the synoptic circulation correctly analyzed by global DA systems, it is more difficult to demonstrate the improvement provided by convective-scale DA.

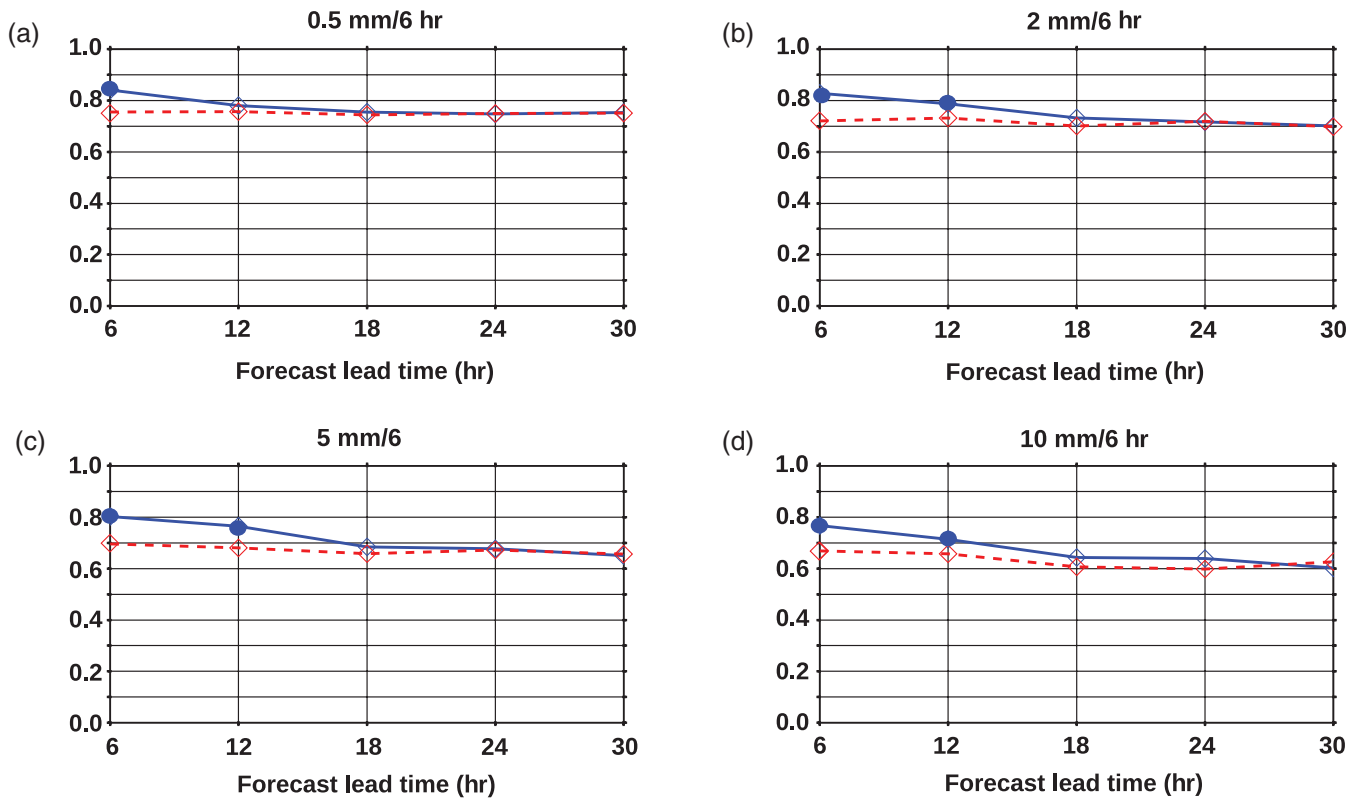


FIGURE 4 Regional Brier Skill Score, calculated against 2050 automatic rain gauges over the French territory for 6 hr cumulative rainfall. The score is computed for threshold exceedances of (a) 0.5, (b) 2, (c) 5 and (d) 10 mm and estimated using a neighbourhood of radius 50 km. Red dotted line: AROME-France forecasts started from ARPEGE initial conditions. Solid blue line: operational AROME-France forecasts with convective-scale DA. The blue dots indicate the forecast ranges where BSS differences are statistically significant (95%) using a bootstrap test. Higher scores reflect improved forecast skill (Amodei and Stein, 2009)

3.1.3 | Influence of DA methods – KENDA initial conditions versus nudging combined with multi-model perturbations

Due to the strong nonlinearities and stochastic properties of convection, the forecast for convective scales should be probabilistic. To illustrate this, we compare the ensemble prediction from the COSMO-DE model configuration (Baldauf *et al.*, 2011) using KENDA initial conditions with the operational ensemble prediction system COSMO-DE-EPS of DWD (Gebhardt *et al.*, 2011). The initial conditions of the latter system are based on deterministic nudging analyses using perturbations derived from four different operational global model systems. The comparison covers a one-month convective summer period from 26 May to 25 June 2016. Precipitation verification is shown in Figure 5 with the Brier Score components for resolution and reliability at the 1 mm h^{-1} threshold as a function of lead time for the 1200 UTC runs. Forecasts using KENDA initial conditions maintain an advantage lasting up to a day for both resolution and reliability.

In terms of CRPS, large improvements can be seen in Figure 6 for 2 m temperature, 2 m relative humidity and 10 m wind up to one day. The CRPS decreases (improves) by 7–15% in the first 6 hr and to about 5% later. This is primarily a result of the strong increase of spread in KENDA for 2 m temperature and 2 m relative humidity, and moderate increase of spread in 10 m wind speed, compared to the EPS (not shown). Furthermore, there is also a decrease of the

RMSE of up to 10%, particularly during the early stages of the forecast. On the other hand, there is an increase in the night-time warm bias and dry bias measured in terms of relative humidity, which results in an increased RMSE at night for lead times beyond 6 hr (not shown).

3.2 | Impact of observations

Radar data have been used for DA in a few National Meteorological Services for several years using different techniques, such as 1D+3D-Var, 4D-Var and nudging (Caumont *et al.*, 2010; Wang *et al.*, 2013b; Simonin *et al.*, 2014). The development of convection-resolving models highlights the need for high-resolution observations which are relevant to the weather situations that the models aim to describe. The second source of high-resolution observations that have become available in recent years is Mode-S EHS. Both of these datasets will now be discussed.

3.2.1 | Internationally collected radar data

In preparation for the OPERA redistribution of quality-controlled radar volume data over Europe (section 4.2.2 gives more details), Ridal and Dahlbom (2017) demonstrated the possibility of using a multi-country set of radar data, in this case over a domain covering nine countries surrounding Denmark. In this framework, the HIRLAM consortium

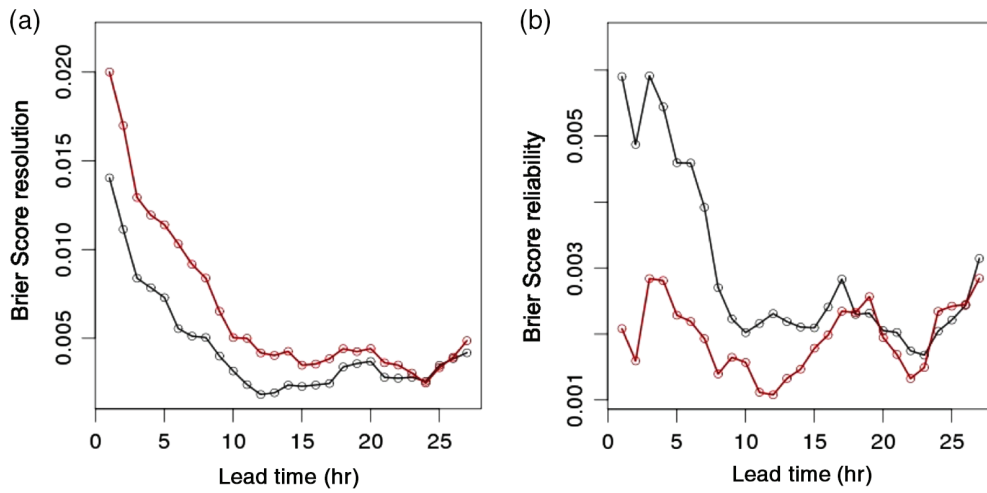


FIGURE 5 (a) Resolution and (b) reliability of hourly precipitation for a threshold of 1 mm h^{-1} as a function of forecast lead time, from 1200 UTC forecast runs for the period from 26 May to 25 June 2016. The red line denotes forecasts started from KENDA initial conditions, and the black line operational COSMO-DE-EPS forecasts

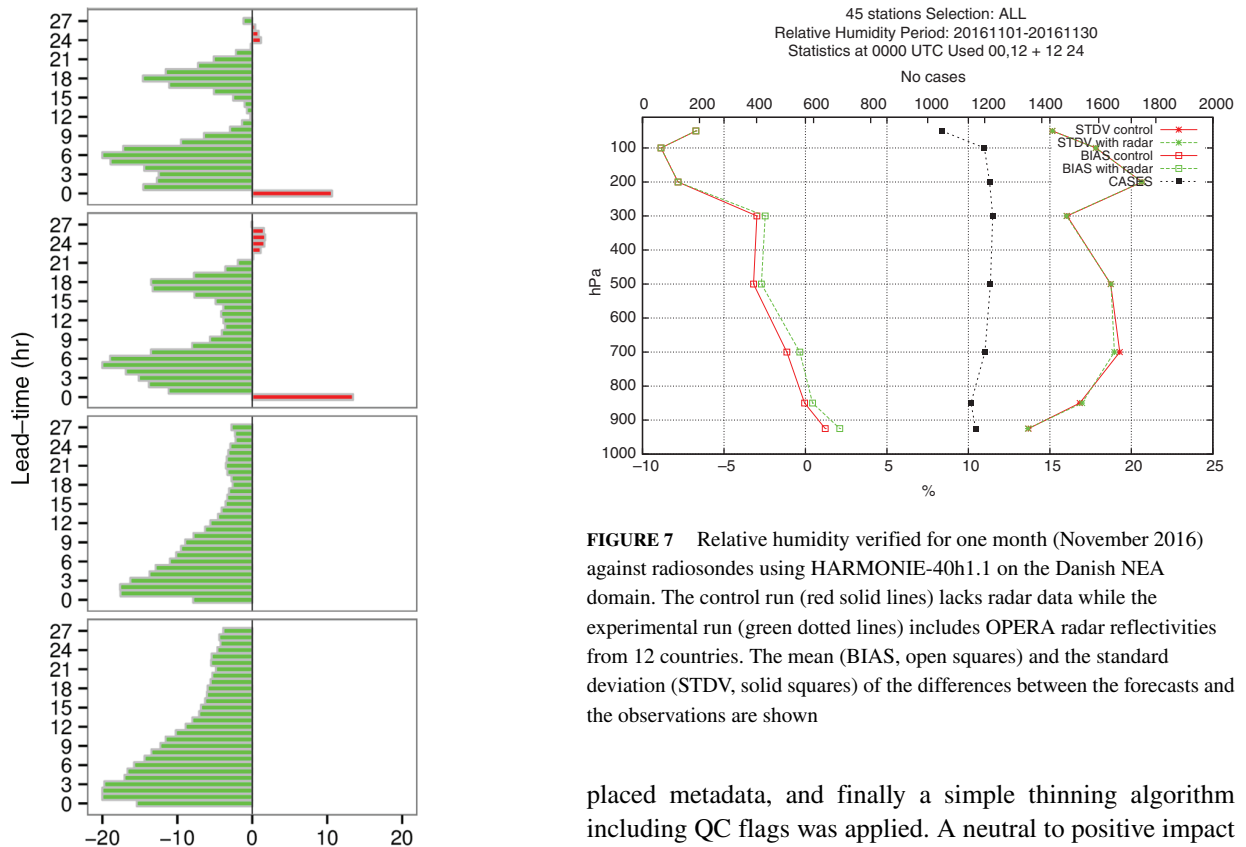


FIGURE 6 Change in CRPS (%) by using KENDA initial conditions against the operational COSMO-DE-EPS for surface variables (a) 2 m temperature, (b) 2 m relative humidity, (c) zonal and (d) meridional components of 10 m wind, for a lead time of 27 h, averaged over 0000 and 1200 UTC EPS forecasts for the period 26 May to 25 June 2016

FIGURE 7 Relative humidity verified for one month (November 2016) against radiosondes using HARMONIE-40h1.1 on the Danish NEA domain. The control run (red solid lines) lacks radar data while the experimental run (green dotted lines) includes OPERA radar reflectivities from 12 countries. The mean (BIAS, open squares) and the standard deviation (STDV, solid squares) of the differences between the forecasts and the observations are shown

developed a pre-processing scheme capable of handling radar volumes from multiple countries using OPERA’s ODIM HDF5 format. Quality control filters using the BALTRAD QC package were first imposed, then the HDF5 file structures were harmonized by correcting missing or incorrectly

placed metadata, and finally a simple thinning algorithm including QC flags was applied. A neutral to positive impact on the forecast skill scores was achieved with the thinning algorithm alone. Figure 7 shows one month of relative humidity verification against radiosonde observations from 45 stations for the Danish North European domain (NEA) using HARMONIE-40h1.1 with and without assimilation of radar reflectivity. Positive improvement can be seen for levels between 850 and 500 hPa in the form of a reduction in both bias and standard deviation. The impact on other parameters was more neutral in this verification.

These results show not only the feasibility of the data usage with regards to availability, timeliness and format convention, but also encouraging results in forecast verification. In

order to improve data usage, the thinning has recently been further developed using a super-obbing algorithm inspired by the work of Lindskog *et al.* (2004). OPERA's upcoming redistribution of quality-controlled volume files and radial wind data will make the European radar network fully usable for the NWP community.

3.2.2 | Mode-S EHS and the IMPACT experiment

Recently a method was developed to derive wind and temperature information from aircraft within the range of Mode-S EHS tracking and ranging radar (de Haan, 2011). By combining ground vector, air-speed, heading and Mach number as provided by each individual aircraft, temperature and wind information can be inferred. Using radar data from the air traffic control at Schiphol airport, de Haan and Stoffelen (2012) showed that Mode-S EHS wind information thus obtained is of a quality comparable to AMDAR wind observations, while Mode-S EHS temperature is of lower quality than available with AMDAR near the surface; at 10 km altitude the temperature quality is comparable. de Haan (2015) showed using triple collocation that the wind observation error is around $1\text{--}1.5\text{ m s}^{-1}$. The Mode-S EHS dataset is a high-resolution observation set both with respect to spatial and temporal density, as can be seen in Figure 8. The data are obtained from Maastricht upper air control (MUAC) covering Benelux and German air-space. The vertical extent of the data range from ground level to the upper flight levels at around 100 hPa.

The Mode-S EHS observation frequency depends on the scanning period of the radar, which can be between 4 and 20 s. At present the observations are made available in batches of 15 min duration with a 5 min latency. However, note that the coverage of low-level aircraft observations is limited to the locations and operating hours of airports. As a consequence, fewer observations are collected between midnight and the early morning hours. Apart from this, Mode-S EHS can be considered as an important observation set for constraining the atmospheric dynamics of high-resolution NWP models when describing small and rapidly moving weather phenomena, for example. Improvements in the 3 hr forecast when assimilating Mode-S EHS data have been shown by de Haan and Stoffelen (2012) and Lange and Janjić (2016). To investigate the impact on forecasting performance of several observation sets, including Mode-S EHS, the observation-impact experiment IMPACT was established.

For the period 15 November to 31 December 2013, several DA experiments have been performed with the HARMONIE-AROME 3D-Var and also the more advanced 4D-Var (section 4.3.1).

The experiments were run using Mode-S EHS combined with conventional observations. The Mode-S EHS data were spatially thinned to 25 km and in the case of 3D-Var only data within 15 min of the analysis time were selected. Both 3D-Var and 4D-Var yielded a positive impact on forecasting performance for a comprehensive list of parameters, with 4D-Var

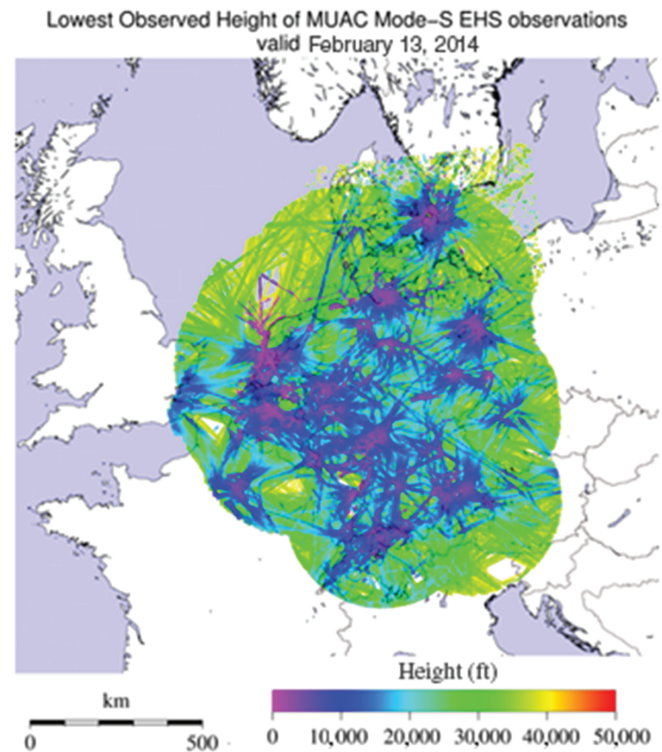


FIGURE 8 Illustration of Mode-S EHS data coverage in terms of the lowest observed height on 13 February 2014

generally leading. The impact in terms of standard deviation and bias is usually noticeable for at least 3–6 hr and longer for 4D-Var. Figure 9 shows the performance of 24 hr forecasts, verified against surface observations, during the IMPACT period for 2 m temperature over the Netherlands, in case of 3D-Var, 4D-Var and a 3D-Var without observations. In terms of standard deviation for the differences between the forecasts and the observations, 4D-Var is leading over 3D-Var, while the bias shows a reduction both for 3D-Var and 4D-Var for lead times up to 9 h. Inspection of the nonlinear evolution of the analysis increment reveals that the increment remains coherent for longer with 4D-Var. For wind profiles, the largest impact is around 400–600 hPa, where most of the Mode-S EHS data originate. However, there is a distinct drying out and warming of the lower troposphere with 4D-Var, as was also reported by Strajnar (2015). As a result, the negative temperature bias is reduced. For 1200 UTC specific humidity profiles, the drying turns out to be beneficial when compared to radiosonde profiles. The lowest standard deviation and near-zero bias for specific humidity are achieved with 4D-Var. For the 0000 UTC specific humidity profiles, 4D-Var again gives the lowest standard deviation below 700 hPa and similar performance to 3D-Var above 700 hPa. However, the already negative bias below 700 hPa becomes more pronounced for 4D-Var (up to -0.05 g/kg at 700–850 hPa). Overall 4D-Var performance using mainly wind observations is also encouraging for parameters associated with moist processes. In Figure 10 this is illustrated for the daily cycle of cloud cover

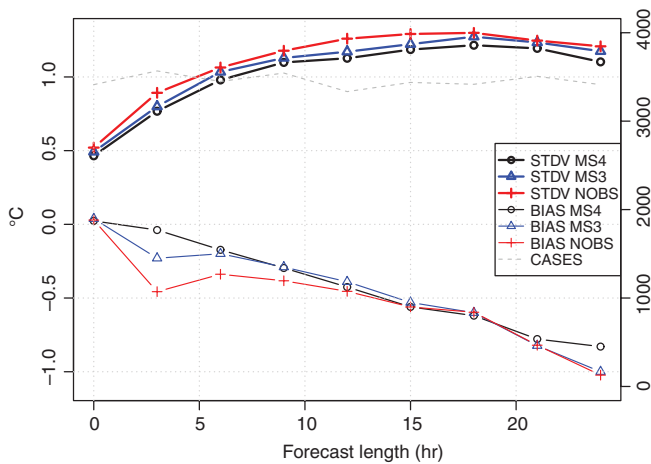


FIGURE 9 Temperature at 2 m standard deviation (top curves) and bias (bottom curves) for forecasts over the Netherlands, verified against surface observations during the IMPACT period, for 3D-Var (blue), 4D-Var (black) and 3D-Var without observations (red)

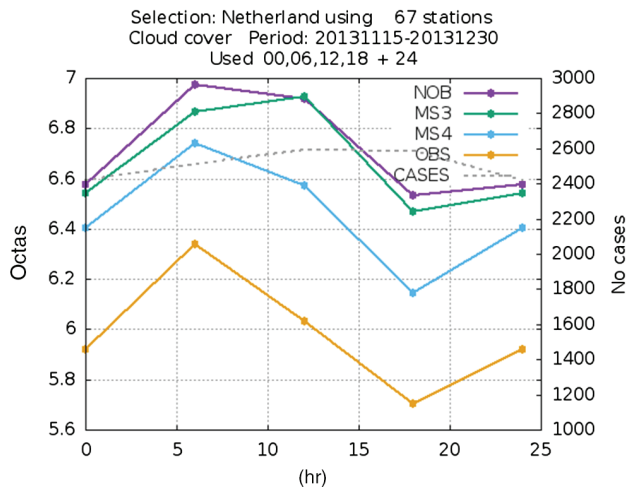


FIGURE 10 Daily cycle of total cloud cover given by 3D-Var without use of observations (purple) or with conventional observations and Mode-S EHS in 3D-Var (green) and 4D-Var (blue). The observed cloud cover is also given (orange)

given by 3D-Var and 4D-Var in comparison to a 3D-Var reference experiment without the use of observations. The superior performance of 4D-Var is also noticeable in the ability to forecast precipitation (Figure 11). For various choices of forecast lead time and thresholds, the FSS indicates that 4D-Var performs better. Here the FSS is shown for accumulated precipitation exceeding 0.3 mm over 3 hr and with a 12 hr lead time. Motivated by these positive results, it is envisaged that in the near future observations associated with humidity, such as radar and GNSS, will also be tested in HARMONIE 4D-Var.

3.3 | Case-studies

3.3.1 | Strong convective precipitation

On 3 October 2015, a strong southerly flow brought very unstable air from the Mediterranean Sea over the French

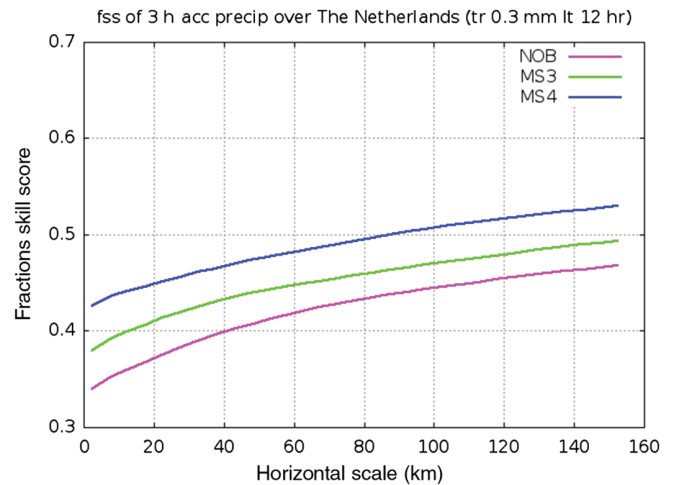


FIGURE 11 Fractions skill score as a function of horizontal scale for 3 hr accumulated precipitation with a forecast lead time of 12 hr and a threshold exceeding 0.3 mm. Results are shown for 3D-Var without observations (purple), 3D-Var (green) and 4D-Var (blue) using conventional observations and Mode-S EHS

Riviera, located on the southern flank of the Alps. As a result and as displayed in Figure 12a, heavy convective precipitation exceeding 100 mm h^{-1} occurred in the Cannes region between 1500 and 2100 UTC, which unfortunately caused twenty casualties and much damage in this urban area.

The 0000 UTC cycle AROME forecast starting from a dynamical adaptation of the operational ARPEGE analysis at global scales clearly failed to forecast this particularly localized convective event (Figure 12b). The operational AROME suite, which assimilates a comprehensive set of observations every hour (listed in Table 6), noticeably improved the forecast by creating precipitation in the right locations but underestimating the intensities (Figure 12c). The 0300 UTC cycle forecast clearly benefits from data which were successively assimilated in the three intermediate assimilation cycles, especially conventional data, radar observations and SEVIRI radiances in clear air (Figure 12d). The simulated intensities are indeed much more realistic while the main precipitating structure is still accurately located.

3.3.2 | Frontal rainband over the Netherlands

In section 3.2.2 the impact of Mode-S EHS on general scores was considered, thereby taking into account the entire testing period. The improvement on forecast performance as a result of assimilating Mode-S EHS data can be complemented with case-studies. An example of this is presented in Figure 13, which shows the improvement to the forecast wind speed and direction with a lead time of 12 hr due to the assimilation of Mode-S EHS in addition to conventional observations during the passage of an intense rain band. The addition of Mode-S EHS indeed allows us to improve the predicted arrival time and orientation of the rain band (de Bruijn *et al.*, 2016, give more details).

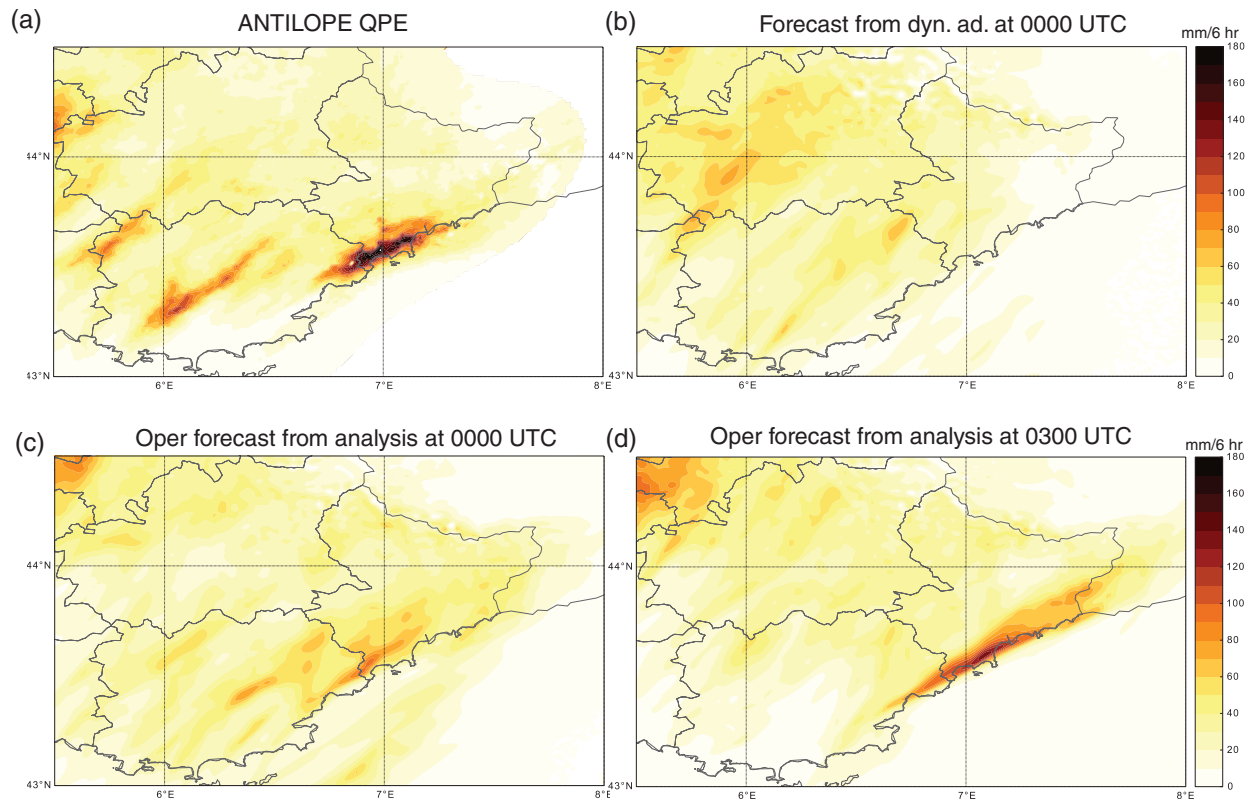


FIGURE 12 Accumulated rainfall (mm h^{-1}) over southeast France between 1500 and 2100 UTC on 3 October 2015 deduced from (a) ANTILOPE quantitative precipitation estimation computed by blending radar and rain-gauge data, (b) the AROME forecast starting from an interpolated large-scale ARPEGE analysis at 0000 UTC, and the operational AROME forecast starting from the (c) 0000 UTC and (d) 0300 UTC assimilation cycles

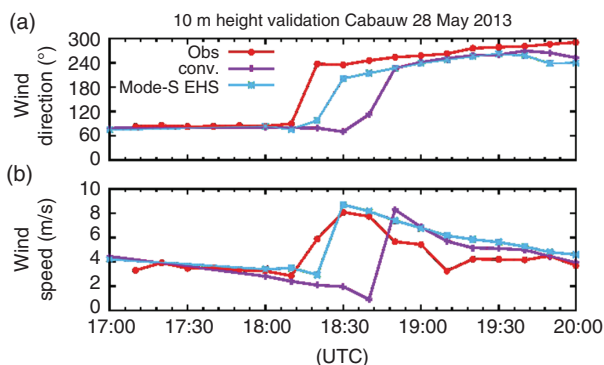


FIGURE 13 Time series on 28 May 2013 of 12 hr HARMONIE-AROME forecasts of (a) wind direction (degrees) and (b) wind speed (m s^{-1}) at 10 m for Cabauw (The Netherlands), using conventional data (purple lines) and additional Mode-S EHS data (blue lines). The observed values are depicted by red lines

4 | CHALLENGES

4.1 | What observations do we ideally need at convective scales, in particular cloud-related observations?

Convective-scale models explicitly represent convection and generally experience a rapid evolution of weather systems. Furthermore, they can exhibit low predictability for the convective systems that are of principal interest (Lilly, 1990; Hohenegger and Schär, 2007; Keil *et al.*, 2014). Overcoming these challenges requires the assimilation of spatially

dense and temporally frequent observations, either of the prevailing environmental conditions related to convection in some way, or of the convection itself. The relative importance of larger-scale environmental conditions versus fine-scale details of convective systems is an ongoing field of research as there is a shortage of basic studies on fundamental aspects of atmospheric predictability on these scales. However, better knowledge of these fundamental issues would be important for deciding which initial condition variables are most important on which scales. A comprehensive overview of our current knowledge on what is and what should be observed for high-resolution NWP, as well as the different existing instruments providing such information, is given by Montmerle (2016). Mode-S aircraft observations (section 3.2.2) are promising, but well-constrained initial conditions will additionally require better use of various remote-sensing observations. In recent years, GNSS total delay observations have been added in several regional DA systems (Macpherson *et al.*, 2008; Bennit and Jupp, 2012; Arriola *et al.*, 2016) and show benefits for constraining the humidity field which is only poorly observed by conventional observations. Radar is another valuable data source for convective-scale models, which, as discussed in section 2.2.3, allows us to analyze thermodynamically coherent structures within precipitating systems. Moreover, progress with algorithms is under way to further improve the assimilation of high-density radar

data (section 4.2.1) and also dual-polarimetric radar data (section 4.2.3).

Therefore it seems crucial to facilitate better use of satellite observations in convective-scale modelling systems. In this respect, regional models mostly lag far behind global modelling systems and only a very small fraction of the available observations is assimilated. Geostationary satellites today provide observations with a spatial resolution similar to the model grid (kilometres) and a time resolution of 15 min or less. The assimilation of cloud-affected and cloud-related observations is particularly promising. Introducing all-sky satellite observations in global modelling systems has been one of the major advances in recent years. The potential is even greater for convective-scale models as clouds exhibit the first area-wide observable aspect of convective systems. This is also reflected in the fact that observation-based now-casting systems rely heavily on geostationary satellite observations, in particular for the identification of convective systems through the cloud signal and the evolution of brightness temperature that indicates the evolution of the cloud-top height. The three major challenges for the improved use of cloud-affected satellite observations are (i) improved assimilation concepts for cloud-affected observations, (ii) improved model representation (parametrization) of cloud particles and (iii) improved observation operators.

The first challenge is related to the nonlinearity associated with clouds and the non-Gaussianity of observation departures. Recent developments showed that the non-Gaussianity of cloud-affected infrared observations can be mitigated through the use of cloud-dependent error models (Harnisch *et al.*, 2016), following the work of Geer and Bauer (2011) for microwave channels. Nonlinearity still poses a severe challenge, but this may be mitigated through the use of different control variables in DA.

The second and third challenges can lead to systematic deviations of observations and model equivalents such as simulated brightness temperatures that are very sensitive to model and operator assumptions on particle size distribution, particle shape and sub-grid cloud cover. In consequence, errors of simulated cloud-affected observations are typically much larger than for clear-sky conditions and more work is required to minimize systematic deviations. Another aspect is that channels in the visible and near-infrared range are currently ignored in DA although they potentially provide a lot of information on clouds. This is partly due to the lack of suitable observation operators for these channels, but recent work demonstrated the feasibility of efficiently calculating realistic satellite images in the visible range (Kostka *et al.*, 2014; Scheck *et al.*, 2016). Figure 14 shows a synthetic satellite image over Germany in the visible range calculated from a short-term forecast by the regional model COSMO-DE and histograms of observed and simulated reflectances averaged over a one-month period. After accounting for the most important three-dimensional radiative transfer effect, the variation of reflectance with the inclination of cloud tops, the

distribution of simulated reflectances (green line) is fairly realistic. Further optimization of this operator is ongoing and it is planned to include the operator in the RTTOV model in the near future.

Besides satellite observations, there are also various promising ground-based remote-sensing instruments whose data could be assimilated in regional DA. Many countries already operate networks for the detection of lightning and ceilometers which detect cloud-base height and the height of the atmospheric boundary layer. Several other instruments (e.g. wind and humidity lidars) have recently significantly reduced in price, which may facilitate the installation of such networks in the near future. Furthermore, information from observations made for various other purposes could be used in DA. Many new mobile phones have sensors for pressure and temperature (Madaus and Mass, 2016), many countries operate roadside sensors for visibility and temperature or icing, many new cars have temperature and visibility sensors that transmit their observations to networks while wind and solar power generation are potentially useful sources of information. The challenges for assimilating such observations vary for each type. Information on lightning or boundary layer and cloud-base height is hard to use in DA, wind and water vapour lidars are limited by the cost of installation and maintenance, while obtaining information from energy companies in real time is a challenge for power generation observations. It is therefore essential to conduct further studies on those observations which are potentially most useful in order to prioritize efforts towards network installation and assimilation system development.

4.2 | Better use of satellite and radar data

4.2.1 | Treatment of correlated observation errors

With the development of high-resolution models, the efficient use of observations at high density in DA is becoming increasingly important. Indeed, under the assumption of uncorrelated observation errors, a large amount of data has to be discarded by horizontal spatial thinning to avoid degrading the forecast (Liu and Rabier, 2003). Recent theoretical studies on the impact of the specification of radar observation errors suggest that the positive effect of data thinning could be enhanced if it were possible, for such high-density observations, to neglect also the error correlations of the background (Jacques and Zawadzki, 2014; 2015). Another common method to counteract spatial or inter-channel observation-error correlations for satellite radiances is error inflation. But this method is sub-optimal as it artificially down-weights observations from these instruments (Weston *et al.*, 2014). Another disadvantage of this observation-error variance inflation method of dealing with correlated observation errors is that it removes small-scale information that is vital for convection-permitting models (Rainwater *et al.*, 2015). Hence, there is a requirement to increase the quantity of observations used in the assimilation system. Indeed, analysing smaller scales could

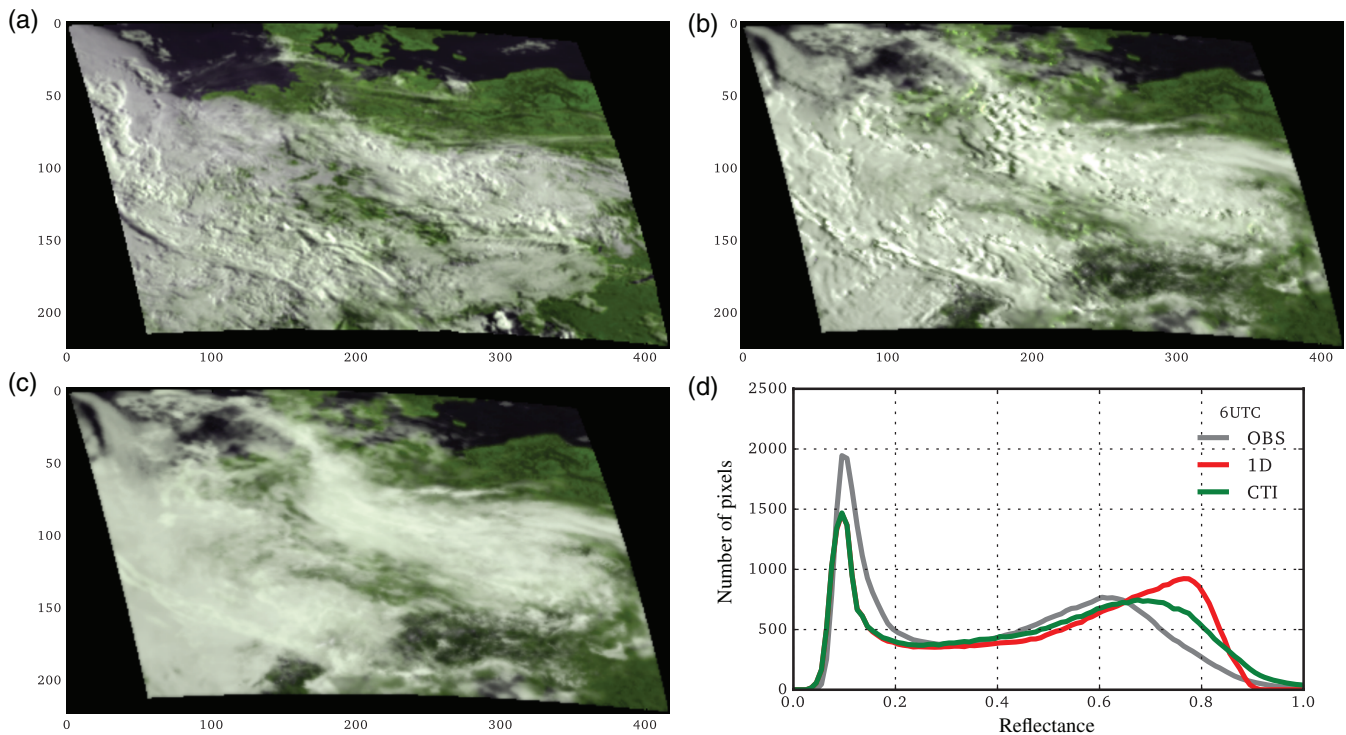


FIGURE 14 (a) SEVIRI observation of the COSMO-DE domain for 0600 UTC on 3 June 2016, and (c) synthetic image computed with the one-dimensional radiative transfer solver from the operational COSMO-DE forecast. (b) is as (c), but with an additional cloud-top inclination correction. To generate these RGB images, the $0.6\ \mu\text{m}$ reflectance was used for the red channel, the $0.8\ \mu\text{m}$ reflectance for the green channel and the mean value of the 0.6 and $0.8\ \mu\text{m}$ reflectances for the blue channel. (d) Average 0600 UTC reflectance histograms for SEVIRI observations (grey) and model equivalents with (green) and without (red) cloud-top inclination taken into account for the period 28 May to 30 June 2016 (L. Scheck, personal communication)

improve the predictability of the assimilation system (i.e. sections 2.2.3 and 2.5.1). As a consequence, there is a need to both reduce the data thinning and better specify the spatial and inter-channel correlated observation errors to enhance the spatial information extracted from satellite radiances or ground radar data.

In that context, the attempt to assimilate radar data (in particular Doppler radial wind) with a spatial horizontal density higher than 15 km in the 2.5 km convective AROME model was a failure. Nevertheless, positive impact was obtained with 8 km spatial density in the assimilation system using a higher horizontal resolution of 1.3 km (Wattrelot, 2016). This suggests that better representation of fine scales (in the 1.3 km horizontal resolution against 2.5 km) contributes to a clear reduction in the part of the observation-error correlations induced by the errors of “representation” (i.e. part of error of representation that occurs when the observations can resolve scales that the model cannot (Janjić *et al.*, 2017).

When the Met Office trialled Doppler radial winds in a 1.5 km model/1.5 km analysis grid hourly cycling 3D-Var system (Simonin *et al.*, 2014), positive benefit from the hourly data were found with much denser data (every 1.5–3 km depending on range). Therefore the impact of observations may depend on the observation pre-processing, design of the assimilation system, observation mix, assumed observation and background errors and the method for assessing benefit. In July 2011, when Doppler radial winds were

introduced operationally into the Met Office UK 3 hr cycling 3D-Var system with a 4 km model/4 km analysis grid and the subsequent variable resolution UKV system described in section 2.3 (1.5 km grid in the domain interior/3 km analysis grid over the whole domain), an 8 km and 6 km thinning was used, respectively. This was partly for cost reasons but also to make some allowance for horizontal correlation of the observation errors.

Estimates of spatial and inter-channel observation-error characteristics for clear-sky sounder radiances have been *a posteriori* diagnosed by Bormann and Bauer (2010), for cloudy microwave imager radiances (Bormann *et al.*, 2011) and by Stewart *et al.* (2014) for IASI inter-channel observation-error correlations. The inter-channel error correlations have been accounted for in the assimilation (Weston *et al.*, 2014; Bormann *et al.*, 2016; Campbell *et al.*, 2016) and shown to have positive benefit. The Met Office currently accounts for inter-channel radiance error correlations in the operational global and UK regional systems for AIRS (Aqua), IASI (METOP A and B) and CRIS (SUOMI) instruments.

The Hollingsworth and Lönnerberg (1986) method has historically been used to estimate observation-error variances but it is very difficult to clearly separate the FG departure correlations into a combination of a spatially correlated observation error and a spatially correlated FG error, especially at small separation distances. For radar data, estimates of such observation-error statistics have been first *a posteriori*

diagnosed in the Météo-France AROME assimilation system (Wattrelot *et al.*, 2012) and results indicate that the observation errors have a correlation length-scale of more than 10 km. These diagnostics are based on Desroziers *et al.* (2005) but also on methods that rely on an estimate of the background-error covariance matrix using a forecast ensemble as in Bormann and Bauer (2010). Similar results have been found by Waller *et al.* (2016b) for Doppler radial winds using the Met Office's UKV model and Desroziers *et al.* diagnostics. However, current methods for estimating observation-error covariances could be improved. New research and better methods will be needed in this area to accurately characterize observation-error correlations and thus better extract small-scale information from high-density observations.

Studies have also been performed for SEVIRI geostationary radiances (Waller *et al.*, 2016c) and AMVs (Cordoba *et al.*, 2017). These found long implied horizontal correlation length-scales. Currently the Met Office is trialling a system to allow for horizontally correlated Doppler radial winds.

Recent research advances at Météo-France to evaluate the quality of the methods used for calculating correlated observation errors have shown that the estimated correlated observation errors for Doppler radial winds could be underestimated for the smallest separation distance (Wattrelot *et al.*, 2016). This last work was based on using an additional diagnostic, the lag-innovation covariance described in Daley (1992) and Ménard (2016). The diagnosis based on the lag-innovation covariances suggests a longer observation-error length-scale and is consistent with theoretical insight in Waller *et al.* (2016a) which shows that the results are strongly dependent on specific underlying assumptions and very difficult to interpret if absolutely no information is known *a priori* on the nature of these statistics.

4.2.2 | International collection of radar data

Europe has a complex radar network, predominantly of C-Band type, with reasonable coverage, which contains a potential wealth of useful information for NWP (Figure 15). The EUMETNET program for radar data (OPERA) has established a unified file format, the OPERA Data Information Model (ODIM) using the HDF5 and BUFR formats, and a continent-wide collection and redistribution set-up (Huuskonen *et al.*, 2014). Each radar performs a full set of scans every 5–15 min and the national meteorological services broadcast this (either in single-scan or full-volume format) directly to OPERA. Although at present OPERA is only redistributing two-dimensional post-processed radar composites, these data will be available in a quality-controlled form for end-users in the near future. It will then be possible to use the reflectivity (volumes, scans or derived products) from most radars in Europe for the purpose of NWP. For example, the timeliness of the reflectivity volume data is approximately 15 min after the sampling time, which fulfils most needs. At the moment, there is no requirement for radial winds to be redistributed

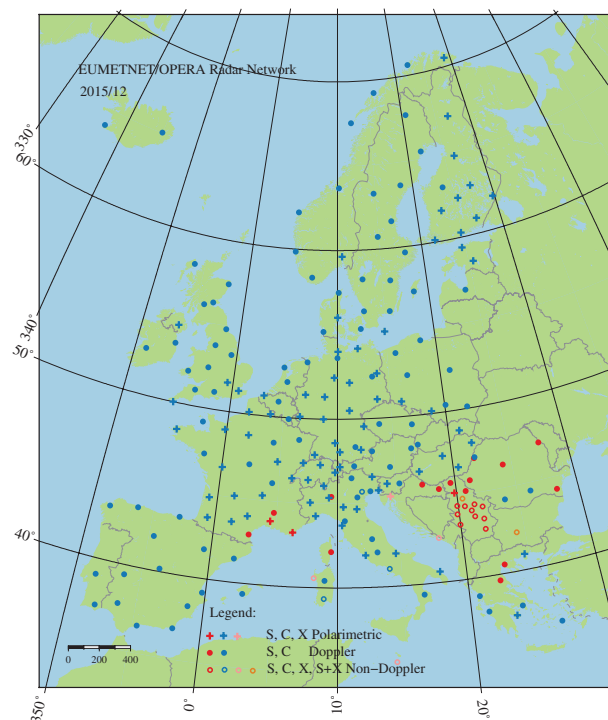


FIGURE 15 The European radar stations included in the OPERA program. S: S-band with wavelength 8–15 cm and frequency 2–4 GHz. C: C-band with wavelength 4–8 cm and frequency 4–8 GHz. X: X-band with wavelength 2.5–4 cm

but it is hoped this will be done in the very near future. It is important to report inconsistencies encountered and/or suggestions back to the OPERA user group so that products can be improved.

In the case of raw radar volume data used in DA, there are several challenges that need to be addressed for the data to be used beneficially. The presence of data contaminated by ground and sea clutter, external emitters and beam blockage needs to be flagged or compensated for. Furthermore, for the successful use of these data it is still necessary to perform quality checks to capture format issues that have to be addressed, such as wrongly labelled, missing and/or misplaced metadata in the ODIM files, and thus to harmonize the data so that all relevant information needed for the DA method is in place.

4.2.3 | Use of dual polarimetric radars

In addition to allowing for a better non-meteorological scatter detection and a much better correction of the attenuation of the signal, DPOL meteorological radars can provide microphysical information of sampled precipitation, such as the particle size distribution, as well as the shape and thermodynamical phase of hydrometeors. The assimilation of the main polarimetric variables, namely the differential reflectivity Z_{dr} , the specific differential phase K_{dp} or the cross-correlation coefficient ρ_{hv} , presents similar challenges to those encountered when assimilating radar reflectivity in the variational context (section 2.2.3). Moreover, the microphysics of the convection-permitting NWP model have to be

able to provide realistic simulations of model counterparts to these DPOL variables (Jung *et al.*, 2010). Fortunately, Augros *et al.* (2015) have shown that it is possible to obtain accurate K_{dp} estimates which are sufficiently consistent with the AROME model one-moment microphysics scheme.

The benefit of the assimilation of DPOL observations has been tested in an operational context, with the constraints of the AROME model and its 3D-Var assimilation system (Clotilde Augros, personal communication). The impact of DPOL observations on the precipitation forecast was found to be slightly positive for periods of intense convection. In particular, the assimilation of the specific differential phase K_{dp} alone, using the 1D+3D-Var assimilation method (Wattrelot *et al.*, 2014), has shown positive impact in regions of intense convection affected by partial beam blockage.

4.2.4 | JMA advances in assimilation of radar and satellite observations

JMA has been assimilating data from GPM/DPR, a space-borne radar developed by the JAXA and the NICT for the GPM core satellite, since March 2016 (Ikuta, 2016d). This improves the initial conditions around precipitating systems in ocean areas beyond the reach of ground-based radars. The DPR assimilation method is an indirect method which assimilates the relative humidity profile estimated from radar reflectivity. Assimilation of GPM/DPR improves water vapour in the initial conditions with the impact persisting to improve precipitation predictions.

JMA introduced a VarBC for LA, making it possible to reduce the negative impact of observation and observation operator bias in DA. As a result, JMA started assimilating satellite clear-sky radiance data in LA using RTTOV, with VarBC applied to the observation bias of these assimilated data from various satellites (NOAA-15, 18, 19/ATOVS, METOP-A, B/ATOVS, Aqua/AMSU-A, DMSP-F17, 18/SSMIS, GCOM-W/AMSR2, GPM-core/GMI and Himawari-8). These satellite data are already assimilated in MA, which currently applies the VarBC coefficients from a global analysis based on a different model, and development is in progress to renew MA VarBC in the near future. As a result of the satellite radiance assimilation in LA, the accuracy of temperature and water vapour profiles improved in LFM forecasts. In addition, assimilating satellite radiance data improved the forecast of precipitation resulting from cumulus convection in the winter, because its influence on the sea area was advected rapidly to the land area by the strong seasonal wind.

4.3 | Development of advanced methods

4.3.1 | HARMONIE-AROME 4D-Var developments

The successful application of 4D-Var for operational global (Rabier *et al.*, 2000) and regional high-resolution NWP (Gustafsson *et al.*, 2012) motivated the development of 4D-Var for the convective-scale HARMONIE-AROME

system. A first step was the construction of a framework for ALADIN 4D-Var (Soci *et al.*, 2006). A second step was adaptation of this 4D-Var to AROME and the external surface module SURFEX (Masson *et al.*, 2013). In order to improve the treatment of weak nonlinearities, this was followed by the introduction of a multi-incremental minimization with the possibility of using different horizontal resolutions in each outer loop iteration (section 2.1.2).

The HARMONIE-AROME nonlinear model used in full-resolution forecasting is non-hydrostatic, while the TL and AD models applied in the quadratic minimization are obtained by linearizing the hydrostatic version of the nonlinear model. Furthermore, the physics of the TL and AD models has so far been restricted to include simplified versions of vertical turbulence and surface friction only (Buizza, 1994; Janisková *et al.*, 1997). A challenge is to introduce simplified moist physics parametrizations, such that, for example, radar reflectivity data can be assimilated efficiently.

HARMONIE-AROME 4D-Var also includes a weak digital-filter constraint applied to the assimilation increment in each outer loop iteration to damp the amplification of high-frequency oscillations during the DA process. Such a weak digital-filter constraint has turned out to work efficiently for synoptic-scale DA windows with filters based on cut-off periods on the order of 6 hr (Gustafsson *et al.*, 2012). However, it is not clear how such a constraint should be applied optimally to assimilation windows with a length of a few hours.

The HARMONIE-AROME 4D-Var has been tested using a multi-incremental minimization with an assimilation cycle of 3 h, a 2 hr assimilation window with observations every 20 min (e.g. 2300–0100 UTC for nominal analysis time 0000 UTC with observations at 2300, 2320, 2340, 0000, 0020, 0040 and 0100 UTC), with two outer loop iterations and an assimilation increment resolution of 5 km with the HARMONIE-AROME model running with a horizontal grid resolution of 2.5 km. Longer overlapping assimilation windows may also be considered in order to determine more dynamically consistent initial states.

Comparing HARMONIE-AROME 3D-Var and 4D-Var experiments favours 4D-Var, both with regard to forecast verification scores and the ability of the forecast model to preserve the assimilated information over a longer forecast range (section 3.2.2). Due to the (multi-)incremental formulation of HARMONIE-AROME 4D-Var, the computing time is not excessive and operational implementation of HARMONIE-AROME 4D-Var is being considered.

4.3.2 | Met Office 4D-Var

A convective-scale, hourly cycling 4D-Var system was implemented operationally in July 2017 at the Met Office. The aim is to provide fresher NWP output based on the latest observations to improve post-processing products in the 0–6 hr forecast range and give improved warnings of severe weather in the 0–12 hr period. Development of this configuration was

motivated by a successful pilot study, the NDP, run for the London 2012 Olympic and Paralympic Games (Ballard *et al.*, 2016). The NDP configuration was an hourly cycling 4D-Var system covering southern England using a finite-difference forecast model with a 1.5 km grid spacing and was itself based in general terms on the coarser limited-area 4D-Var system run operationally over a North Atlantic and European domain. The operational version uses the same domain and grid described in section 2.3 for the forecast model. The analysis grid over which the linear perturbation forecast model is run is at fixed resolution. After some experimentation, a 4.5 km grid spacing has been chosen for reasons of economy and stability.

The assimilation cycle uses a time window of $t-30$ to $t+30$ min, with analysis increments added at the start of the window. Initialization is via a digital filter penalty term (Gauthier and Thépaut, 2001). The observation cut-off is $t+45$ min and the same observation types available to the 3-hourly 3D-Var system are assimilated. Most are assimilated at an hourly frequency, but Doppler radial winds are used every 10 min and SEVIRI radiances and wind profilers every 15 min. Surface rain rate from radar is still assimilated via LHN and with radar frames every 15 min. The shorter cut-off does mean that some lower-tropospheric radiosonde data arrive too late to be assimilated. However, the corresponding upper-tropospheric radiosonde data can be used, by virtue of the accurate treatment of balloon drift and assimilation of the data at their correct times and locations rather than at nominal times and launch locations. The upper-atmospheric data typically fall into the next hourly window after the one for which the lower data arrive too late. VarBC of satellite data is included, following its recent operational implementation in the global model.

At present, forecast error covariances for the hourly 4D-Var system are the same as those used in the 3-hourly 3D-Var assimilation. This is a temporary situation and new covariances will be derived from the hourly system itself and based on training data at earlier forecast lead times than the $t+6/t+3$ forecast differences used in the calculation of the covariances for 3-hourly 3D-Var.

4.3.3 | HARMONIE hybrid 3D-EnVar and 4D-EnVar

The success on synoptic scales of the HIRLAM Hybrid 3D-EnVar and 4D-EnVar (Gustafsson and Bojarova, 2014) combined with the ETKF-based ensemble rescaling algorithm for ensemble generation applied at full model resolution (Bojarova *et al.*, 2010) encouraged development of similar algorithms for the HARMONIE system at convective scales. The HARMONIE EnVar assimilation algorithm uses an augmented control vector space (section 2.1.3) and provides a straightforward multi-scale extension (Buehner and Shlyueva, 2015). One could expect that a consistent treatment of a wide range of scales is an essential feature of a successful convective-scale DA scheme. However, much development is still needed in order to extract the full

potential of a hybrid approach on convective scales. Experience with the HIRLAM 4D-EnVar scheme indicates the importance of a rich and dynamically mature ensemble to capture flow-dependence. At the same time, the methodologies for generating an ensemble capable of meaningfully sampling uncertainty on convective scales are generally still at an early stage of development. Recently the LETKF assimilation scheme has been implemented into the ECMWF IFS code environment and it has also been tested in the HARMONIE framework at convective scales with encouraging results (Pau Escriba, 2017; personal communication). Many scientific questions have not been answered yet. For example, we need to investigate whether a sufficiently large ensemble is affordable at full convective-scale model resolution on a domain large enough to allow the convective phenomena to develop. Alternatively, a compromise between the domain size, model resolution and ensemble size needs to be found.

4.3.4 | EnVars at Météo-France

Different flavours of EnVar (3D-EnVar and 4D-EnVar, hybrids) are currently being tested in order to make the DA algorithm more flow-dependent at the current operational resolution of 1.3 km. Their formulations follow the general idea described in section 2.1.3, except that the minimization is based on the DPCG algorithm (Derber and Rosati, 1989) with a **B**-preconditioning. As explained in Desroziers *et al.* (2014), this allows us to manipulate control vectors of the same size as the model state in the conjugate-gradient iterative descent algorithm in hybrid DA methods (i.e. without increasing the size of the control vector).

To provide the background perturbations, an EDA (Houtekamer *et al.*, 1996), which is planned to run operationally at the end of 2017, has been built for AROME, using explicit observation perturbations and explicitly perturbed LBCs from the operational global EDA (AEARP; Berre *et al.*, 2015). Vertically dependent optimal localization length-scales have been retrieved from its 25 members for the different control variables following Ménétrier *et al.* (2015). In the 4D-EnVar case, Lagrangian advection is furthermore applied to the localization using a filtered wind from the background, following work at global scales by Desroziers *et al.* (2016).

4.3.5 | Rapid update NWP for severe weather warnings at NOAA

NOAA's WoF project is developing high-resolution NWP for very short (0–3 h) lead times which can enhance the warning process for convective storm hazards (Stensrud *et al.*, 2009). While significant challenges exist in producing reliable probabilistic forecasts on convective time- and space-scales, an existing prototype system has demonstrated promising potential for this type of NWP to produce forecasts of convective storms and systems that evolve realistically (Wheatley *et al.*, 2015; Jones *et al.*, 2016). This prototype WoF

system, a 3 km, 36-member convection-permitting ensemble adjustment Kalman filter (Anderson *et al.*, 2009), was employed to assimilate Doppler radial wind velocity, reflectivity, and satellite liquid and ice water path retrievals with a 15 min interval. This system was demonstrated in real time during the spring seasons of 2015 and 2016 and was able to provide forecasts every 30 min which identified significant severe weather events from ensemble-based probability swaths with lead times of as much as 3 h. While several challenges remain, such as rapid observation processing/ingestion, computational efficiency, representation of model error, etc., these prototype results are encouraging.

4.3.6 | Development of a JMA DA system based on the new limited-area forecast model ASUCA

JMA is proceeding with a project to update the operational limited-area DA system to a new system based on ASUCA. The analysis/forecast cycle system based on ASUCA has already been used operationally in the LA system. Development of ASUCA 4D-Var is similarly under way. At the same time, JMA is investigating ensemble and variational hybrid DA as its next-generation DA system. The hybrid method adds flow dependence to the background error using the extended control variable method.

Ikuta (2016a) investigated the impact of assimilating observations with high temporal resolution using this hybrid 4D-Var. High temporal resolution observation data such as radar, wind profiler, satellite and aircraft data have been assimilated into an operational mesoscale 4D-Var system for many years at JMA. However, these observational data are thinned in time and assimilated at the nearest hour rather than the correct observation time because the observation time slot is fixed to 1 hr intervals. The new hybrid 4D-Var enables the assimilation of observational data at the correct observation times because observation time slots are not fixed. It has been confirmed that the appropriate treatment of the observation time is more effective with flow-dependent DA.

High-frequency observations such as radar reflectivity and satellite radiances are needed to provide detailed information about hydrometeors. In this regard, Ikuta (2016b) has developed a TL and AD model including a simplified six-class three-ice one-moment bulk cloud microphysics scheme. The scheme assumes that the growth of nonlinear perturbations during the 3 hr assimilation window can be approximated by the TL model. The AD model propagates the gradient of the cost function with respect to hydrometeors from observation times of reflectivity and brightness temperature back to the beginning of the assimilation window. In most cases, ice-phase information from observations is transformed into water vapour information through the backward integration with adjoint operators of the microphysics scheme. Ikuta (2016c) shows the impact of the assimilation of radar reflectivity data using the meso-scale hybrid 4D-Var DA system.

5 | DISCUSSION AND CONCLUDING REMARKS

DA methods for convective-scale NWP at operational centres are surveyed in this article. The basic operational methods include variational methods like 3D-Var and 4D-Var, ensemble methods like LETKF and hybrids between variational and ensemble methods. At several of the operational centres, additional assimilation algorithms, like LHN, are utilized to improve the model initial state, with emphasis on convective scales.

The development of operational DA methods for convective-scale NWP has followed the development of methods for global DA with a time lag of several years. Operational DA systems for convective-scale NWP at some centres are still based on 3D-Var, while their DA systems for global NWP have moved to more advanced methods like 4D-Var or 4D-EnVar. From a scientific point of view this is not satisfactory, since flow-dependence, which is introduced by the more advanced methods, becomes more important at convective scales. The reason is partly the difficulty of sharing huge investments into DA software between the global and convective-scale systems with higher priority being given to the global version. Convective-scale DA has certainly gained from the global inheritance, but it is possible that this wish to share development resources has also hampered the development of more-dedicated convective-scale methods.

To be successful, convective-scale DA requires access to observations with convective-scale resolution. Such observations exist and are used operationally, for example weather radar and satellite observations. Radar reflectivity observations are utilized operationally today, either via a 1D-Bayesian inversion to vertical moisture profiles or via LHN, but better optimized methods for direct assimilation of radar reflectivity data should also be investigated. In order to utilize radar and satellite data more efficiently for convective-scale DA, it is necessary to improve observation operators and also observation-error statistics. Some early attempts to derive models for spatial error correlations and satellite radiance inter-channel error correlations have been partly successful, at least for global DA, but these attempts have also shown that access to *a priori* information about the whole measurement process is needed.

Simultaneous assimilation of broadly distributed observations, such as rawinsonde data, alongside comparatively dense observations, such as Doppler radial wind velocity, presents practical challenges owing to these networks' abilities to resolve different scales. This is especially challenging when one considers that methods often employed for modelling background-error covariances assume decorrelation lengths associated with a fixed scale of motion, yet an analysis that reflects many scales of motion is desired, i.e. a multi-scale DA method is needed. To date, most efforts have addressed this challenge through multi-pass methods, where broadly distributed observations are assimilated first,

followed by a second pass of the analysis system using comparatively shorter decorrelation lengths to assimilate the high-resolution observations (Xie *et al.*, 2011; Gao *et al.*, 2013; Xu *et al.*, 2016). However such approaches require somewhat subjective characterization of broad- and fine-scale observations and neglect the fact that fine-scale observations do provide some information about the larger scales and, correspondingly, broad-scale observations do contain information pertinent to the finer scales. To address this challenge, Buehner and Shlyeva (2015) recently proposed a scale-dependent background-error covariance localization technique that avoids the need to split the observations and analysis into dense and broad scales, thus allowing for the use of all observations simultaneously. Future applications of this technique to radar DA at convection-permitting time- and spatial scales could prove to be quite interesting.

Ensemble methods and hybrids between ensemble and variational methods are under examination for convective-scale DA at operational centres. In order to counteract the effects of detrimental sampling errors due to the use of relatively small ensembles, covariance localization methods need to be applied. The reasons for this are twofold. One is that the sampling error produces noisy background-error covariance estimates, whose inclusion in the DA can make the analysis inaccurate (Hamill *et al.*, 2001). Secondly, the localization increases the rank of the ensemble-derived covariances, allowing for an analysis outside the space spanned by the unlocalized background ensemble only. However, localization can severely affect dynamical properties of the analysis. It has been shown that rigorous localization in global hydrostatic models can disturb geostrophic balance (Kepert, 2009; Greybush *et al.*, 2011) or conservation laws (Zeng and Janjić, 2016). Due to the multiple atmospheric scales that are present in the limited-area models, on the one hand the localization radius needs to be large enough not to disturb the known balances of the large-scale flow and in that way not endanger reliable environmental forecasts necessary for good convective-scale forecasts. On the other hand, the localization radius would need to be small to capture the convective cells when assimilating radar data, for example. Currently, the decision about how large the localization radius should be depends on the size of the ensemble. By applying their methodology based on the optimal linear filtering theory, Ménétrier *et al.* (2015) have indeed shown that localization lengths are inversely proportional to the size of the ensemble, and that its optimal values can be diagnosed directly from the ensemble.

To summarize, in order to make further progress in development of DA for convective-scale NWP at operational centres, we have identified the need to strengthen research efforts with regard to observation operators, models for observation-error statistics, multi-scale DA, generation of convective-scale ensembles and covariance localization. There is also need for more research on balances at convective scales and on practical ways to represent balances

as well as model error in advanced DA systems. We should also keep in mind that nonlinear effects and moist physical processes become more important when we include the convective scales in our DA and forecasting process. For this reason, it may become necessary to move towards nonlinear DA methods like particle filters, or hybrids between particle filters and those methods that we have discussed in this article.

ACKNOWLEDGEMENTS

Many thanks to colleagues at JMA, Météo-France, NOAA, Met Office, the participating weather services in the ALADIN, COSMO, HIRLAM and LACE consortia and the University of Tehran for stimulating discussions and material provided for this article.

T. Janjić and Martin Weissmann are grateful to the Hans-Ertel Centre for Weather Research (Weissmann *et al.*, 2014; Simmer *et al.*, 2016) for providing support for this study. This research network of universities, research institutes, and the Deutscher Wetterdienst is funded by the BMVI (Federal Ministry of Transport and Digital Infrastructure). T. Janjić would also like to acknowledge the support of the Transregional Collaborative Research Center SFB/TRR 165 *Waves to Weather* funded by the German Science Foundation (DFG).

The authors and KNMI thank MUAC-EUROCONTROL for kind provision of Mode-S EHS data.

REFERENCES

- Amodei, M. and Stein, J. (2009) Deterministic and fuzzy verification methods for a hierarchy of numerical models. *Meteorological Applications*, 16, 191–203. <https://doi.org/10.1002/met.101>.
- Anderson, J. and Anderson, S.-L. (1999) A Monte Carlo implementation of the nonlinear filtering problem to produce ensemble assimilations and forecasts. *Monthly Weather Review*, 124, 2741–2758. [https://doi.org/10.1175/1520-0493\(1999\)127<2741:AMCIOT>2.0.CO;2](https://doi.org/10.1175/1520-0493(1999)127<2741:AMCIOT>2.0.CO;2).
- Anderson, J.L., Hoar, T., Raeder, K., Liu, H., Collins, N., Torn, R. and Avellano, A. (2009) The data assimilation research testbed: a community facility. *Bulletin of the American Meteorological Society*, 90, 1283–1296. <https://doi.org/10.1175/2009BAMS2618.1>.
- Aranami, K., Hara, T., Ikuta, Y., Kawano, K., Matsubayashi, K., Kusabiraki, H. and Ishida, J. (2015) A new operational regional model for convection-permitting numerical weather prediction at JMA. *CAS/JSC WGNE Research Activities in Atmospheric and Oceanic Modelling*, 45, 0505–0506.
- Arriola, J.S., Lindskog, M., Thorsteinsson, S. and Bojarova, J. (2016) Variational bias correction of GNSS ZTD in the HARMONIE modeling system. *Journal of Applied Meteorology and Climatology*, 55, 1259–1276. <https://doi.org/10.1175/JAMC-D-15-0137.1>.
- Augros, C., Caumont, O., Ducrocq, V., Gaussiat, N. and Tabary, P. (2015) Comparisons between S-, C- and X-band polarimetric radar observations and convective-scale simulations of the HyMeX first special observing period. *Quarterly Journal of the Royal Meteorological Society*, 142, 347–362. <https://doi.org/10.1002/qj.2572>.
- Auligné, T., McNally, A.P. and Dee, D.P. (2007) Adaptive bias correction for satellite data in a numerical weather prediction system. *Quarterly Journal of the Royal Meteorological Society*, 133, 631–642. <https://doi.org/10.1002/qj.56>.
- Baldauf, M. (2010) Linear stability analysis of Runge–Kutta based partial time-splitting schemes for the Euler equations. *Monthly Weather Review*, 138, 4475–4496. <https://doi.org/10.1175/2010MWR3355.1>.

- Baldauf, M., Seifert, A., Foerstneri, J., Majewski, D., Raschendorfer, M. and Reinhardt, T. (2011) Operational convective-scale numerical weather prediction with the COSMO model: description and sensitivities. *Monthly Weather Review*, 139, 3887–3995. <https://doi.org/10.1175/MWR-D-10-05013.1>.
- Ballard, S.P., Li, Z., Simonin, D. and Caron, J.-F. (2016) Performance of 4D-Var NWP-based nowcasting of precipitation at the Met Office for summer 2012. *Quarterly Journal of the Royal Meteorological Society*, 142, 472–487. <https://doi.org/10.1002/qj.2665>.
- Bannister, R.N. (2008) A review of forecast-error covariance statistics in atmospheric variational data assimilation. II: modelling the forecast-error covariance statistics. *Quarterly Journal of the Royal Meteorological Society*, 134, 1971–1996. <https://doi.org/10.1002/qj.340>.
- Bannister, R.N. (2017) A review of operational methods of variational and ensemble-variational data assimilation. *Quarterly Journal of the Royal Meteorological Society*, 143, 607–633. <https://doi.org/10.1002/qj.2982>.
- Bengtsson, L., Andrae, U., Aspöf, T., Batrak, Y., Calvo, J., deRooy, W. and Ødegard Kølitzow, M. (2017) The HARMONIE-AROME model configuration in the ALADIN-HIRLAM NWP system. *Monthly Weather Review*, 145, 1919–1935. <https://doi.org/10.1175/MWR-D-16-0417.1>.
- Benjamin, S.G., Dévényi, D., Weygandt, S.S., Brundage, K.J., Brown, J.M., Grell, G.A. and Manikin, G.S. (2004) An hourly assimilation/forecast cycle: the RUC. *Monthly Weather Review*, 132, 495–518. [https://doi.org/10.1175/1520-0493\(2004\)132<0495:AHACTR>2.0.CO;2](https://doi.org/10.1175/1520-0493(2004)132<0495:AHACTR>2.0.CO;2).
- Benjamin, S.G., Weygandt, S.S., Brown, J.M., Hu, M., Alexander, C.R., Smirnova, T.G. and Manikin, G.S. (2016) A North American hourly assimilation and model forecast cycle: the Rapid Refresh. *Monthly Weather Review*, 144, 1669–1694. <https://doi.org/10.1175/MWR-D-15-0242.1>.
- Bennit, G.V. and Jupp, A. (2012) Operational assimilation of GPS Zenith Total Delay observations into the Met Office numerical weather prediction models. *Monthly Weather Review*, 140, 2706–2719. <https://doi.org/10.1175/MWR-D-11-00156.1>.
- Berre, L. (2000) Estimation of synoptic and mesoscale forecast-error covariances in a limited-area model. *Monthly Weather Review*, 128, 644–667. [https://doi.org/10.1175/1520-0493\(2000\)128<0644:EOSAMF>2.0.CO;2](https://doi.org/10.1175/1520-0493(2000)128<0644:EOSAMF>2.0.CO;2).
- Berre, L., Varella, H. and Desroziers, G. (2015) Modelling of flow-dependent ensemble-based background-error correlations using a wavelet formulation in 4D-Var at Météo-France. *Quarterly Journal of the Royal Meteorological Society*, 141, 2803–2812. <https://doi.org/10.1002/qj.2565>.
- Bick, T., Simmer, C., Trömel, S., Wapler, K., Hendricks Franssen, H.-J., Stephan, K. and Potthast, R. (2016) Assimilation of 3D radar reflectivities with an ensemble Kalman filter on the convective scale. *Quarterly Journal of the Royal Meteorological Society*, 142, 1490–1504. <https://doi.org/10.1002/qj.2751>.
- Bishop, C.H. (2016) The GIGG-EnKF: Ensemble Kalman filtering for highly skewed non-negative uncertainty distributions. *Quarterly Journal of the Royal Meteorological Society*, 142, 1395–1412. <https://doi.org/10.1002/qj.2742>.
- Bishop, C.H., Etherton, B.J. and Majumdar, S.J. (2001) Adaptive sampling with the ensemble transform Kalman filter, part I: Theoretical aspects. *Monthly Weather Review*, 129, 420–436. [https://doi.org/10.1175/1520-0493\(2001\)129<0420:ASWTFET>2.0.CO;2](https://doi.org/10.1175/1520-0493(2001)129<0420:ASWTFET>2.0.CO;2).
- Bloom, S.C., Takacs, L.L., Da Silva, A.M. and Ledvina, D. (1996) Data assimilation using incremental analysis updates. *Monthly Weather Review*, 124, 1256–1271. [https://doi.org/10.1175/1520-0493\(1996\)124<1256:DAUIAU>2.0.CO;2](https://doi.org/10.1175/1520-0493(1996)124<1256:DAUIAU>2.0.CO;2).
- Bojarova, J., Gustafsson, N., Johansson, A. and Vignes, O. (2010) The ETKF rescaling scheme in HIRLAM. *Tellus*, 63A, 385–401. <https://doi.org/10.1111/j.1600-0870.2011.00513.x>.
- Böläni, G. (2006) Development of a variational data assimilation system for a limited-area model at the Hungarian Meteorological Service. *Quarterly Journal of the Hungarian Meteorological Service*, 110, 309–327.
- Böläni, G., Berre, L. and Adamcsek, E. (2015) Comparison of static mesoscale background-error covariances estimated by three different ensemble data assimilation techniques. *Quarterly Journal of the Royal Meteorological Society*, 141, 413–425. <https://doi.org/10.1002/qj.2361>.
- Bormann, N. and Bauer, P. (2010) Estimates of spatial and interchannel observation error characteristics for current sounder radiances for numerical weather prediction. I: methods and application to ATOVS data. *Quarterly Journal of the Royal Meteorological Society*, 136, 1036–1050. <https://doi.org/10.1002/qj.616>.
- Bormann, N., Geer, A.J. and Bauer, P. (2011) Estimates of observation-error characteristics in clear and cloudy regions for microwave imager radiances from numerical weather prediction. *Quarterly Journal of the Royal Meteorological Society*, 137, 2014–2023. <https://doi.org/10.1002/qj.833>.
- Bormann, N., Bonavita, M., Dragani, R., Eresmaa, R., Matricardi, M. and McNally, A.P. (2016) Enhancing the impact of IASI observations through an updated observation-error covariance matrix. *Quarterly Journal of the Royal Meteorological Society*, 142, 1767–1780. <https://doi.org/10.1002/qj.2774>.
- Bott, A. (1989) A positive definite advection scheme obtained by nonlinear renormalization of the advection fluxes. *Monthly Weather Review*, 117, 1006–1015. [https://doi.org/10.1175/1520-0493\(1989\)117<1006:APDASO>2.0.CO;2](https://doi.org/10.1175/1520-0493(1989)117<1006:APDASO>2.0.CO;2).
- Bouttier, F., Vié, B., Nuissier, O. and Raynaud, L. (2012) Impact of stochastic physics in a convection-permitting ensemble. *Monthly Weather Review*, 140, 3706–3721. <https://doi.org/10.1175/MWR-D-12-00031.1>.
- Brousseau, P., Berre, L., Bouttier, F. and Desroziers, G. (2011) Background-error covariances for a convective-scale data-assimilation system: AROME-France 3D-Var. *Quarterly Journal of the Royal Meteorological Society*, 137, 409–422. <https://doi.org/10.1002/qj.750>.
- Brousseau, P., Desroziers, G., Bouttier, F. and Chapnik, B. (2014) A posteriori diagnostics of the impact of observations on the AROME-France convective-scale data assimilation system. *Quarterly Journal of the Royal Meteorological Society*, 140, 982–994. <https://doi.org/10.1002/qj.282210>.
- Brousseau, P., Seity, Y., Ricard, D. and Léger, J. (2016) Improvement of the forecast of convective activity from the AROME-France system. *Quarterly Journal of the Royal Meteorological Society*, 142, 2231–2243. <https://doi.org/10.1002/qj.2822>.
- Brožková, R., Klaric, D., Ivatek-Sahdan, S., Geleyn, J.-F., Cassé, V., Šíroká, M. and Seidl, H. (2001). *DFI blending: an alternative tool for preparation of the initial conditions for LAM*. Geneva: WMO. SAC/JSC WGNE Report No. 31.
- Brožková, R., Derková, M., Belluš, M. and Farda, A. (2006) Atmospheric forcing by ALADIN/MFSTEP and MFSTEP oriented tunings. *Ocean Science Discussions*, 3, 319–342. <https://doi.org/10.5194/os-2-113-2006>.
- de Bruijn, E.I.F., de Haan, S., Bosveld, F.C., Wichers Schreur, B. and Holtslag, A.A.M. (2016) Observing boundary-layer winds from hot-air balloon flights. *Weather and Forecasting*, 31, 1451–1463. <https://doi.org/10.1175/WAF-D-0028.1>.
- Buehner, M. (2005) Ensemble-derived stationary and flow-dependent background-error covariances: evaluation in a quasi-operational NWP setting. *Quarterly Journal of the Royal Meteorological Society*, 131, 1013–1044. <https://doi.org/10.1256/qj.04.15>.
- Buehner, M. and Shlyayeva, A. (2015) Scale-dependent background-error covariance localisation. *Tellus A*, 67, 28027. <https://doi.org/10.3402/tellusa.v67.28027>.
- Buehner, M., Morneau, J. and Charette, C. (2013) Four-dimensional ensemble-variational data assimilation for global deterministic weather prediction. *Nonlinear Processes in Geophysics*, 20, 669–682. <https://doi.org/10.5194/npg-20-669-2013>.
- Buizza, R. (1994) *Impact of a Simple Vertical Diffusion Scheme and of the Optimisation Time Interval on Optimal Unstable Structures*. Technical Memorandum 192. Reading, England: ECMWF.
- Buizza, R., Miller, M. and Palmer, T.N. (1999) Stochastic representation of model uncertainties in the ECMWF ensemble prediction system. *Quarterly Journal of the Royal Meteorological Society*, 125, 2887–2908. <https://doi.org/10.1002/qj.49712556006>.
- Campbell, W.F., Satterfield, E.A., Ruston, B. and Baker, N.L. (2016) Accounting for correlated observation error in a dual formulation 4D-variational data assimilation system. *Monthly Weather Review*, 145, 1019–1032. <https://doi.org/10.1175/MWR-D-16-0240.1>.
- Caumont, O., Ducrocq, V., Delrieu, G., Gosset, M., Pinty, J.-P., Parent du Châtelet, J. and Scialom, G. (2006) A radar simulator for high-resolution non-hydrostatic models. *Journal of Atmospheric and Oceanic Technology*, 23, 1049–1067. <https://doi.org/10.1175/JTECH1905.1>.
- Caumont, O., Ducrocq, V., Wattrelot, E., Jaubert, G. and Pradier-Vabre, S. (2010) 1D+3DVar assimilation of radar reflectivity data: a proof of concept. *Tellus*, 62A, 173–187. <https://doi.org/10.1111/j.1600-0870.2009.00430.x>.
- Clark, P.A., Harcourt, S.A., Macpherson, B., Mathison, C.T., Cusack, S. and Naylor, M. (2008) Prediction of visibility and aerosol within the operational Met Office Unified Model. Part I: model formulation and variational assimilation. *Quarterly Journal of the Royal Meteorological Society*, 134, 1801–1816. <https://doi.org/10.1002/qj.318>.
- Clayton, A.M., Lorenc, A.C. and Barker, D.M. (2013) Operational implementation of a hybrid ensemble/4D-Var global data assimilation system at the

- Met Office. *Quarterly Journal of the Royal Meteorological Society*, 139, 1445–1461. <https://doi.org/10.1002/qj.2054>.
- Cordoba, M., Dance, S.L., Kelly, G.A., Nichols, N.K. and Waller, J.A. (2017) Diagnosing atmospheric motion vector observation errors in an operational high-resolution data assimilation system. *Quarterly Journal of the Royal Meteorological Society*, 143, 333–341. <https://doi.org/10.1002/qj.2925>.
- Courtier, P., Thépaut, J.-N. and Hollingsworth, A. (1994) A strategy for operational implementation of 4D-Var using an incremental approach. *Quarterly Journal of the Royal Meteorological Society*, 120, 1367–1387. <https://doi.org/10.1002/qj.49712051912>.
- Dahlgren, P. and Gustafsson, N. (2012) Assimilating host model information into a limited area model. *Tellus A*, 64, 15836. <https://doi.org/10.3402/tellusa.v64i0.15836>.
- Daley, R. (1992) The lagged innovation covariance: a performance diagnostic for atmospheric data assimilation. *Monthly Weather Review*, 120, 178–196.
- Derber, J. and Bouttier, F. (1999) A reformulation of the background-error covariance in the ECMWF global data assimilation system. *Tellus*, 51A, 195–221. <https://doi.org/10.1034/j.1600-0870.1999.t01-2-00003.x>.
- Derber, J. and Rosati, A. (1989) A global oceanic data assimilation system. *Journal of Physical Oceanography*, 19, 1333–1347. [https://doi.org/10.1175/1520-0485\(1989\)019<1333:AGODAS>2.0.CO;2](https://doi.org/10.1175/1520-0485(1989)019<1333:AGODAS>2.0.CO;2).
- Derková, M. and Belluš, M. (2007) Various applications of the blending by digital filter technique in the ALADIN numerical weather prediction system. *Meteorologický Časopis*, 10, 27–36.
- Desroziers, G., Berre, L., Chapnik, B. and Poli, P. (2005) Diagnosis of observation-, background- and analysis-error statistics in observation space. *Quarterly Journal of the Royal Meteorological Society*, 131, 3385–3396. <https://doi.org/10.1256/qj.05.108>.
- Desroziers, G., Camino, J.-T. and Berre, L. (2014) 4D-EnVar: link with 4D state formulation of variational assimilation and different possible implementations. *Quarterly Journal of the Royal Meteorological Society*, 140, 2097–2110. <https://doi.org/10.1002/qj.2325>.
- Desroziers, G., Arbogast, E. and Berre, L. (2016) Improving spatial localization in 4D-EnVar. *Quarterly Journal of the Royal Meteorological Society*, 142, 3171–3185. <https://doi.org/10.1256/qj.05.115>.
- Dharssi, I., Bovis, K.J., Macpherson, B. and Jones, C.P. (2011) Operational assimilation of ASCAT surface soil wetness at the Met Office. *Hydrology and Earth System Sciences*, 15, 2729–2746. <https://doi.org/10.5194/hess-15-2729-2011>.
- Dharssi, I., Steinle, P. and Candy, B. (2012). *Towards a Kalman Filter-based land surface data assimilation scheme for ACCESS*. Melbourne: CAWCR. Technical Report No. 54.
- Drusch, M. (2007) Initializing numerical weather prediction models with satellite-derived surface soil moisture: data assimilation experiments with ECMWF's Integrated Forecast System and the TMI soil moisture data set. *Journal of Geophysical Research*, 112, D03102. <https://doi.org/10.1029/2006JD007478>.
- Ek, M.B., Mitchell, K.E., Lin, Y., Rogers, E., Grunmann, P., Koren, V. and Tarp-ley, J.D. (2003) Implementation of Noah land surface model advances in the National Centers for Environmental Prediction operational mesoscale Eta model. *Journal of Geophysical Research*, 108, 8851. <https://doi.org/10.1029/2002JD003296>.
- Eliassen, A. (1954). *Provisional report on calculation of spatial covariance and autocorrelation of the pressure field*. Oslo: Institute of Weather and Climate Research, Academy of Science. Report No. 5.
- Evensen, G. (1994) Sequential data assimilation with a nonlinear quasi-geostrophic model using Monte Carlo methods to forecast error statistics. *Journal of Geophysical Research*, 99, 10143–10162. <https://doi.org/10.1029/94JC00572>.
- Fabry, F. and Sun, J. (2010) For how long should what data be assimilated for the mesoscale forecasting of convection and why? Part I: on the propagation of initial condition errors and their implications for data assimilation. *Monthly Weather Review*, 138, 242–255. <https://doi.org/10.1175/2009MWR2883.1>.
- Fischer, C., Montmerle, T., Berre, L., Auger, L. and Ștefănescu, S.E. (2005) An overview of the variational assimilation in the ALADIN/France numerical weather-prediction system. *Quarterly Journal of the Royal Meteorological Society*, 131, 3477–3492. <https://doi.org/10.1256/qj.05.115>.
- Gao, J., Smith, T., Stensrud, D., Fu, C., Calhoun, K., Manross, K. and Xue, M. (2013) A real-time weather-adaptive 3DVAR analysis system for severe weather detections and warnings. *Weather and Forecasting*, 28, 727–745. <https://doi.org/10.1175/WAF-D-12-00093.1>.
- Gaspari, G. and Cohn, S.E. (1999) Construction of correlation functions in two and three dimensions. *Quarterly Journal of the Royal Meteorological Society*, 125, 723–757. <https://doi.org/10.1002/qj.49712555417>.
- Gauthier, P. and Thépaut, J.-N. (2001) Impact of the digital filter as a weak constraint in the pre-operational 4DVAR assimilation system of Météo-France. *Monthly Weather Review*, 129, 2089–2102. [https://doi.org/10.1175/1520-0493\(2001\)129<2089:IOTDFA>2.0.CO;2](https://doi.org/10.1175/1520-0493(2001)129<2089:IOTDFA>2.0.CO;2).
- Gebhardt, C., Theis, S.E., Paulat, M. and Ben Bouallegue, Z. (2011) Uncertainties in COSMO-DE precipitation forecasts introduced by model perturbations and variation of lateral boundaries. *Atmospheric Research*, 100, 168–177. <https://doi.org/10.1016/j.atmosres.2010.12.008>.
- Geer, A.J. and Bauer, P. (2011) Observation errors in all-sky data assimilation. *Quarterly Journal of the Royal Meteorological Society*, 137, 2014–2037. <https://doi.org/10.1002/qj.833>.
- Giard, D. and Bazile, E. (2000) Implementation of a new assimilation scheme for soil and surface variables in a global NWP model. *Monthly Weather Review*, 128, 997–1015. [https://doi.org/10.1175/1520-0493\(2000\)128<0997:IOANAS>2.0.CO;2](https://doi.org/10.1175/1520-0493(2000)128<0997:IOANAS>2.0.CO;2).
- Greybush, S.J., Kalnay, E., Miyoshi, T., Ide, K. and Hunt, B.R. (2011) Balance and ensemble Kalman filter localization techniques. *Monthly Weather Review*, 139, 511–522. <https://doi.org/10.1175/2010MWR3328.1>.
- Guidard, V. and Fischer, C. (2008) Introducing the coupling information in a limited-area variational assimilation. *Quarterly Journal of the Royal Meteorological Society*, 134, 723–735. <https://doi.org/10.1002/qj.215>.
- Guidard, V., Fischer, C., Nuret, M. and Džiedžic, A. (2006) Evaluation of the ALADIN 3D-VAR with observations of the MAP campaign. *Meteorology and Atmospheric Physics*, 92, 161–173. <https://doi.org/10.1007/s00703-005-0156-5>.
- Guidard, V., Fourrié, N., Brousseau, P. and Rabier, F. (2011) Impact of IASI assimilation at global and convective scales and challenges for the assimilation of cloudy scenes. *Quarterly Journal of the Royal Meteorological Society*, 137, 1975–1987. <https://doi.org/10.1002/qj.928>.
- Gustafsson, N. and Bojarova, J. (2014) Four-dimensional ensemble variational (4D-En-Var) data assimilation for the High Resolution Limited Area Model (HIRLAM). *Nonlinear Processes in Geophysics*, 21, 745–762. <https://doi.org/10.5194/npg-21-745-2014>.
- Gustafsson, N., Berre, L., Hörnquist, S., Huang, X.-Y., Lindskog, M., Navascués, B. and Thorsteinsson, S. (2001) Three-dimensional variational data assimilation for a limited-area model. Part I: general formulation and the background-error constraint. *Tellus*, 53A, 425–446. <https://doi.org/10.3402/tellusa.v53i4.12198>.
- Gustafsson, N., Huang, X.-Y., Yang, X., Mogensen, K., Lindskog, M., Vignes, O. and Thorsteinsson, S. (2012) Four-dimensional variational data assimilation for a limited-area model. *Tellus*, 64A, 14985. <https://doi.org/10.3402/tellusa.v64i0.14985>.
- de Haan, S. (2011) High-resolution wind and temperature observations from aircraft tracked by Mode-S air traffic control radar. *Journal of Geophysical Research*, 116, D10111. <https://doi.org/10.1029/2010JD015264>.
- de Haan, S. (2015) Estimates of Mode-S EHS aircraft derived wind observation errors using triple collocation. *Atmospheric Measurement Techniques*, 9, 4141–4150. <https://doi.org/10.5194/amt-8-12633-2015>.
- de Haan, S. and Stoffelen, A. (2012) Assimilation of high-resolution Mode-S wind and temperature observations in a regional NWP model for nowcasting applications. *Weather and Forecasting*, 27, 918–937. <https://doi.org/10.1175/WAF-D-11-00088.1>.
- Hamil, T.M., Whitaker, J.S. and Snyder, C. (2001) Distance-dependent filtering of background error covariance estimates in an ensemble Kalman filter. *Monthly Weather Review*, 129, 2776–2790. [https://doi.org/10.1175/1520-0493\(2001\)129<2776:DDFOBE>2.0.CO;2](https://doi.org/10.1175/1520-0493(2001)129<2776:DDFOBE>2.0.CO;2).
- Hara, T., Kawano, K., Aranami, K., Kitamura, Y., Sakamoto, M., Kusabiraki, H. and Ishida, J. (2012). *Development of the Physics Library and its application to ASUCA*. CAS/JSC WGNE report. Available at: http://www.wcrp-climate.org/WGNE/BlueBook/2012/individual-articles/05_Hara_Tabito_physicslib_asuca.pdf.
- Harnisch, F., Weissmann, M. and Perriñez, A. (2016) Error model for the assimilation of cloud-affected infrared satellite observations in an ensemble data assimilation system. *Quarterly Journal of the Royal Meteorological Society*, 142, 1797–1808. <https://doi.org/10.1002/qj.2776>.
- Hess, H. (2001) Assimilation of screen-level observations by variational soil moisture analysis. *Meteorology and Atmospheric Physics*, 77, 145–154. <https://doi.org/10.1007/s007030170023>.

- Hodyss, D. (2011) Ensemble state estimation for nonlinear systems using polynomial expansions in the innovation. *Monthly Weather Review*, 139, 3571–3588. <https://doi.org/10.1175/2011MWR3558.1>.
- Hohenegger, C. and Schär, C. (2007) Atmospheric predictability at synoptic versus cloud-resolving scales. *Bulletin of the American Meteorological Society*, 88, 1783–1793. <https://doi.org/10.1175/BAMS-88-11-1783>.
- Hollingsworth, A. and Lönnberg, P. (1986) The statistical structure of short-range forecast errors as determined from radiosonde data, Part 1: the wind field. *Tellus*, 38A, 111–136. <https://doi.org/10.3402/tellusa.v38i2.11707>.
- Honda, Y., Nishijima, M., Koizumi, K., Ohta, Y., Tamiya, K., Kawabata, T. and Tsuyuki, T. (2005) A pre-operational variational data assimilation system for a non-hydrostatic model at the Japan Meteorological Agency: formulation and preliminary results. *Quarterly Journal of the Royal Meteorological Society*, 131, 3465–3475. <https://doi.org/10.1256/qj.05.132>.
- Houtekamer, P.L., Lefaire, L., Derome, J., Ritchie, H. and Mitchell, H.L. (1996) A system simulation approach to ensemble prediction. *Monthly Weather Review*, 124, 1225–1242. [https://doi.org/10.1175/1520-0493\(1996\)124<1225:ASSATE>2.0.CO;2](https://doi.org/10.1175/1520-0493(1996)124<1225:ASSATE>2.0.CO;2).
- Hu, M., Xue, M. and Brewster, K. (2006) 3DVAR and cloud analysis with WSR-88D level-II data for the prediction of the Fort Worth, Texas, tornadic thunderstorms. Part I: cloud analysis and its impact. *Monthly Weather Review*, 134, 675–698. <https://doi.org/10.1175/MWR3093.1>.
- Hu, M., Benjamin, S.G., Ladwig, T.T., Dowell, D.C., Weygandt, S.S., Alexander, C.R. and Whitaker, J.S. (2017) GSI three-dimensional ensemble-variational hybrid data assimilation using a global ensemble for the regional Rapid Refresh model. *Monthly Weather Review*, 145, 4205–4225. <https://doi.org/10.1175/MWR-D-16-0418.1>.
- Hunt, B.R., Kostelich, E.J. and Szunyogh, I. (2007) Efficient data assimilation for spatiotemporal chaos: a local ensemble transform Kalman filter. *Physica D*, 230, 112–126. <https://doi.org/10.1016/j.physd.2006.11.008>.
- Huuskonen, A., Saltikoff, E. and Holleman, I. (2014) The operational weather radar network in Europe. *Bulletin of the American Meteorological Society*, 95(6), 897–907. <https://doi.org/https://doi.org/10.1175/BAMS-D-12-00216.1>.
- Iacono, M.J., Delamere, J.S., Mlawer, E.J., Shephard, M.W., Clough, S.A. and Collins, W.D. (2008) Radiative forcing by long-lived greenhouse gases: calculations with the AER radiative transfer models. *Journal of Geophysical Research*, 113, D13103. <https://doi.org/10.1029/2008JD009944>.
- Ikuta, Y. (2016a). Impact of appropriate consideration of observation time in the meso-scale hybrid 4D-Var system. In: *Sixth WMO Workshop on the Impact of Various Observing Systems on NWP*, 10–13 May, 2016a, Shanghai, China.
- Ikuta, Y. (2016b). Data assimilation with adjoint model including three-ice bulk cloud microphysics. In: *5th Annual International Symposium on Data Assimilation*, 18–22 July, 2006, Reading, UK.
- Ikuta, Y. (2016c). Impact of flow-dependent assimilation using adjoint model including three-ice microphysics scheme. In: *4th International Workshop on Non-hydrostatic Models*, 30 November–2 December, 2016, Hakone, Japan.
- Ikuta, Y. (2016d) Data assimilation using GPM/DPR at JMA. *CAS/JSC WGNE Research Activities in Atmospheric and Oceanic Modelling*, 46, 01.11–01.12.
- Ingleby, N.B., Lorenc, A.C., Ngan, K., Rawlins, F. and Jackson, D.R. (2013) Improved variational analyses using a nonlinear humidity control variable. *Quarterly Journal of the Royal Meteorological Society*, 139, 1875–1887. <https://doi.org/10.1002/qj.2073>.
- Ishida, J., Muroi, C. and Aikawa, Y. (2009) Development of a new dynamical core for the nonhydrostatic model. *CAS/JSC WGNE Research Activities in Atmospheric and Oceanic Modelling*, 39, 0509–0510. Available at: http://www.wcrp-climate.org/WGNE/BlueBook/2009/individual-articles/05_Ishida_Junichi_WGNE_ishida_muroi_aikawa_asuca.pdf.
- Ishida, J., Muroi, C., Kawano, K. and Kitamura, Y. (2010) Development of a new nonhydrostatic model. *CAS/JSC WGNE Research Activities in Atmospheric and Oceanic Modelling*, 40, 0511–0512.
- Jacques, D. and Zawadzki, I. (2014) The impacts of representing the correlation of errors in radar data assimilation. Part I: experiments with simulated background and observation estimates. *Monthly Weather Review*, 142, 3998–4016. <https://doi.org/10.1175/MWR-D-14-00104.1>.
- Jacques, D. and Zawadzki, I. (2015) The impacts of representing the correlation of errors in radar data assimilation. Part II: model output as background estimates. *Monthly Weather Review*, 143, 2637–2656. <https://doi.org/10.1175/MWR-D-14-00243.1>.
- Janisková, M., Thépaut, J.-N. and Geleyn, J.-F. (1997) Simplified and regular physical parameterizations for incremental four-dimensional variational assimilation. *Monthly Weather Review*, 127, 26–45. [https://doi.org/10.1175/1520-0493\(1999\)127<0026:SARPPF>2.0.CO;2](https://doi.org/10.1175/1520-0493(1999)127<0026:SARPPF>2.0.CO;2).
- Janjić, Z.I. (2001). *Non-singular implementation of the Mellor–Yamada level 2.5 scheme in the NCEP meso model*. Camp Springs, MD: NCEP. NCEP Office Note 437.
- Janjić, Z.I. (2003) A non-hydrostatic model based on a new approach. *Meteorology and Atmospheric Physics*, 82, 271–285. <https://doi.org/10.1007/s00703-001-0587-6>.
- Janjić, Z.I. and Gall, R. (2012) *Scientific Documentation of the NCEP Non-hydrostatic Multiscale Model on the B Grid (NMMB). Part I Dynamics*. Technical Note NCAR/TN-489+STR. Boulder, CO: NCAR.
- Janjić, T., Nerger, L., Albertella, A., Schroeter, J. and Skachko, S. (2011) On domain localization in ensemble based Kalman filter algorithms. *Monthly Weather Review*, 139, 2046–2060. <https://doi.org/10.1175/2011MWR3552.1>.
- Janjić, T., McLaughlin, D., Cohn, S.E. and Verlaan, M. (2014) Conservation of mass and preservation of positivity with ensemble-type Kalman filter algorithms. *Monthly Weather Review*, 142, 755–773. <https://doi.org/10.1175/MWR-D-13-00056.1>.
- Janjić, T., Bormann, N., Bocquet, M., Carton, J.A., Cohn, S.E., Dance, S.L. and Weston, P. (2017) On the representation error in data assimilation. *Quarterly Journal of the Royal Meteorological Society*. <https://doi.org/10.1002/qj.3130>.
- Jiang, Y., Xu, Q., Zhang, P., Nai, K. and Liu, L. (2013) Using WSR-88D polarimetric data to identify bird-contaminated Doppler velocity. *Advances in Meteorology*, 2013, 769275. <https://doi.org/10.1155/2013/769275>.
- JMA (2016) *Joint WMO Technical Progress Report on the Global Data Processing and Forecasting System and Numerical Weather Prediction*. Tokyo: Japan Meteorological Agency. Available at: http://www.jma.go.jp/jma/jma-eng/jma-center/nwp/report/2015_Japan.pdf.
- Jones, C.D. and Macpherson, B. (1997) A latent-heat nudging scheme for the assimilation of precipitation data into an operational mesoscale model. *Meteorological Applications*, 4, 269–277. <https://doi.org/10.1017/S1350482797000522>.
- Jones, T.A., Knopfmeier, K., Wheatley, D., Creager, G., Minnis, P. and Palikonda, R. (2016) Storm-scale data assimilation and ensemble forecasting with the NSSL Experimental Warn-on-Forecast System. PartII: combined radar and satellite data experiments. *Weather and Forecasting*, 31, 297–327. <https://doi.org/10.1175/WAF-D-15-0107.1>.
- Jung, Y., Xue, M. and Zhang, G. (2010) Simulations of polarimetric radar signatures of a supercell storm using a two-moment bulk microphysics scheme. *Journal of Applied Meteorology and Climatology*, 49, 146–163. <https://doi.org/10.1175/2009JAMC2178.1>.
- Keil, C., Heinlein, F. and Craig, G.C. (2014) The convective adjustment time-scale as indicator of predictability of convective precipitation. *Quarterly Journal of the Royal Meteorological Society*, 140, 480–490. <https://doi.org/10.1002/qj.2143>.
- Keptert, J.D. (2009) Covariance localisation and balance in an ensemble Kalman filter. *Quarterly Journal of the Royal Meteorological Society*, 135, 1157–1176. <https://doi.org/10.1002/qj.443>.
- Kleist, D.T. and Ide, K. (2015) An OSSE-based evaluation of hybrid variational-ensemble data assimilation for the NCEP GFS. Part I: system description and 3D-hybrid results. *Monthly Weather Review*, 143, 433–451. <https://doi.org/10.1175/MWR-D-13-00350.1>.
- Kostka, P.M., Weissmann, M., Buras, R., Mayer, B. and Stiller, O. (2014) Observation operator for visible and near-infrared satellite reflectances. *Journal of Atmospheric and Oceanic Technology*, 31, 1216–1233. <https://doi.org/10.1175/JTECH-D-13-00116.1>.
- Lange, H. and Janjić, T. (2016) Assimilation of Mode-S EHS aircraft observations in COSMO-KENDA. *Monthly Weather Review*, 144, 1697–1711. <https://doi.org/10.1175/MWR-D-15-0112.1>.
- LeDimet, F.-X. and Talagrand, O. (1986) Variational algorithms for analysis and assimilation of meteorological observations. Theoretical aspects. *Tellus*, 38A, 97–110. <https://doi.org/10.3402/tellusa.v38i2.11706>.
- van Leeuwen, P.J. (2009) Particle filtering in geophysical systems. *Monthly Weather Review*, 137, 4089–4114. <https://doi.org/10.1175/2009MWR2835.1>.
- Li, H., Kalnay, E. and Miyoshi, T. (2009) Simultaneous estimation of covariance inflation and correlation errors within an ensemble Kalman filter. *Quarterly Journal of the Royal Meteorological Society*, 135, 523–533. <https://doi.org/10.1002/qj.371>.
- Lilly, D.K. (1990) Numerical prediction of thunderstorms – has its time come? *Quarterly Journal of the Royal Meteorological Society*, 116, 779–798. <https://doi.org/10.1256/qj.02.170>.

- Lindskog, M., Salonen, K., Järvinen, H. and Michelson, D.B. (2004) Doppler radar wind data assimilation with HIRLAM 3DVAR. *Monthly Weather Review*, 132, 1081–1092. [https://doi.org/10.1175/1520-0493\(2004\)132<1081:DRWDAW>2.0.CO;2](https://doi.org/10.1175/1520-0493(2004)132<1081:DRWDAW>2.0.CO;2).
- Liu, C., Xiao, Q. and Wang, B. (2008) An ensemble-based four-dimensional variational data assimilation scheme. Part I: technical formulation and preliminary test. *Monthly Weather Review*, 136, 3363–3373. <https://doi.org/10.1175/2008MWR2312.1>.
- Liu, S., Xu, Q. and Zhang, P. (2005) Identifying Doppler velocity contamination caused by migrating birds Part II: Bayes identification and probability tests. *Journal of Atmospheric and Oceanic Technology*, 22, 1114–1121. <https://doi.org/10.1175/JTECH1758.1>.
- Liu, S., DiMego, G., Guan, S., Kumar, V.K., Keyser, D., Xu, Q. and Ator, J. (2016) WSR-88D radar data processing at NCEP. *Weather and Forecasting*, 31, 2047–2055. <https://doi.org/10.1175/WAF-D-16-0003.1>.
- Liu, S., Carley, J.R., Wu, W., Rogers, E., He, J., Ferrier, B.S. and Derber, J. (2017). WSR-88D radar data and NLDN lightning data assimilation at NCEP. *21st Conference on Integrated Observing and Assimilation Systems for Atmosphere, Ocean and Land Surface*, Seattle, WA and Boston, MA: American Meteorological Society.
- Liu, Z.Q. and Rabier, F. (2003) The potential of high density observations for numerical weather prediction: A study with simulated observations. *Quarterly Journal of the Royal Meteorological Society*, 129, 3013–3035. <https://doi.org/10.1256/qj.02.170>.
- Lorenc, A.C. (1981) A global three-dimensional multivariate statistical interpolation scheme. *Monthly Weather Review*, 109, 701–721. [https://doi.org/10.1175/1520-0493\(1981\)109<0701:AGTDM>2.0.CO;2](https://doi.org/10.1175/1520-0493(1981)109<0701:AGTDM>2.0.CO;2).
- Lorenc, A.C. (2003) The potential of the ensemble Kalman Filter for NWP – a comparison with 4D-Var. *Quarterly Journal of the Royal Meteorological Society*, 129, 3183–3203. <https://doi.org/10.1256/qj.02.132>.
- Lorenc, A.C. (2013) Recommended nomenclature for EnVar data assimilation methods. *CAS/JSC WGNE Research Activities in Atmospheric and Oceanic Modelling*, 43, 0107–0108. Available at: http://www.wcrp-climate.org/WGNE/BlueBook/2013/individual-articles/01_Lorenc_Andrew_EnVar_nomenclature.pdf.
- Lorenc, A.C., Ballard, S.P., Bell, R.S., Ingleby, N.B., Andrews, P.L.F., Barker, D.M. and Saunders, F.W. (2000) The Met. Office global three-dimensional variational data assimilation scheme. *Quarterly Journal of the Royal Meteorological Society*, 126, 2991–3012. <https://doi.org/10.1002/qj.49712657002>.
- Lynch, P., Giard, D. and Ivanovici, V. (1997) Improving the efficiency of a digital filtering scheme for diabatic initialization. *Monthly Weather Review*, 125, 1976–1982. [https://doi.org/10.1175/1520-0493\(1997\)125<1976:ITEOAD>2.0.CO;2](https://doi.org/10.1175/1520-0493(1997)125<1976:ITEOAD>2.0.CO;2).
- Macpherson, B. (2001) Operational experience with assimilation of rainfall data in the Met Office mesoscale model. *Meteorology and Atmospheric Physics*, 76, 3–8. <https://doi.org/10.1007/s007030170035>.
- Macpherson, S.R., Deblonde, G., Aparicio, J.M. and Casati, B. (2008) Impact of NOAA ground-based GPS observations on the Canadian regional analysis and forecast system. *Monthly Weather Review*, 136, 2727–2746. <https://doi.org/10.1175/2007MWR2263.1>.
- Madaus, L.E. and Mass, C.F. (2016) Evaluating smartphone pressure observations for mesoscale analyses and forecasts. *Weather and Forecasting*, 32, 511–531. <https://doi.org/10.1175/WAF-D-16-0135.1>.
- Masson, V., Le Moigne, P., Martin, E., Faroux, S., Alias, A., Alkama, R. and Voldoire, A. (2013) The SURFEX v7.2 land and ocean surface platform for coupled or offline simulation of earth surface variables and fluxes. *Geoscientific Model Development Discussions*, 5, 3771–3851. <https://doi.org/10.5194/gmd-6-929-2013>.
- Ménard, R. (2016) Error covariance estimation methods based on analysis residuals: theoretical foundation and convergence properties derived from simplified observation networks. *Quarterly Journal of the Royal Meteorological Society*, 142, 257–273. <https://doi.org/10.1002/qj.2650>.
- Ménétrier, B., Montmerle, T., Michel, Y. and Berre, L. (2015) Linear filtering of sample covariances for ensemble-based data assimilation. Part II: application to a convective-scale NWP model. *Monthly Weather Review*, 143, 1644–1664. <https://doi.org/10.1175/MWR-D-14-00157.1>.
- Michel, Y., Auligné, T. and Montmerle, T. (2011) Heterogeneous convective-scale background error covariances with the inclusion of hydrometeor variables. *Monthly Weather Review*, 139, 2994–3015. <https://doi.org/10.1175/2011MWR3632.1>.
- Mile, M., Bölöni, G., Randriamampianina, R., Steib, R. and Kucukkaraca, E. (2015) Overview of mesoscale data assimilation developments at the Hungarian Meteorological Service. *Quarterly Journal of the Hungarian Meteorological Service*, 119, 213–237.
- Mlawer, E.J., Taubman, S.J., Brown, P.D., Iacono, M.J. and Clough, S.A. (1997) Radiative transfer for inhomogeneous atmospheres: RRTM, a validated correlated-k model for the longwave. *Journal of Geophysical Research*, 102, 16663–16682. <https://doi.org/10.1029/97JD00237>.
- Montmerle, T. (2016) *Statement of Guidance for High-resolution Numerical Weather Prediction (NWP)*. Geneva: WMO. Available at: <http://www.wmo.int/pages/prog/www/OSY/SOG/SoG-HighRes-NWP.pdf>.
- Montmerle, T. and Berre, L. (2010) Diagnosis and formulation of heterogeneous background error covariances at the mesoscale. *Quarterly Journal of the Royal Meteorological Society*, 136, 1408–1420. <https://doi.org/10.1002/qj.655>.
- Montmerle, T. and Faccani, C. (2009) Mesoscale assimilation of radial velocities from Doppler radars in a preoperational framework. *Monthly Weather Review*, 137, 1939–1953. <https://doi.org/10.1175/2008MWR2725.1>.
- Montmerle, T., Rabier, F. and Berre, L. (2007) Relative impact of polar-orbiting and geostationary satellite radiances in the Aladin/France numerical weather prediction system. *Quarterly Journal of the Royal Meteorological Society*, 133, 655–671. <https://doi.org/10.1002/qj.34>.
- Müller, M., Homleid, M., Ivarsson, K.-I., Køltzow, M.A.O., Lindskog, M., Midtbo, K.H. and Vignes, O. (2017) AROME-MetCoOp: a Nordic convective-scale operational weather prediction model. *Weather and Forecasting*, 32, 609–627. <https://doi.org/10.1175/WAF-D-16-0099.1>.
- Pagé, C., Fillion, L. and Zwack, P. (2007) Diagnosing summertime mesoscale vertical motion: implications for atmospheric data assimilation. *Monthly Weather Review*, 135, 2076–2094. <https://doi.org/10.1175/MWR3371.1>.
- Parrish, D.F. and Derber, J.C. (1992) The National Meteorological Center's spectral statistical-interpolation analysis system. *Monthly Weather Review*, 120, 1747–1763. [https://doi.org/10.1175/1520-0493\(1992\)120<1747:TNMCSS>2.0.CO;2](https://doi.org/10.1175/1520-0493(1992)120<1747:TNMCSS>2.0.CO;2).
- Periáñez, A., Reich, H. and Potthast, R. (2014) Optimal localization for ensemble Kalman filter systems. *Journal of the Meteorological Society of Japan*, 92, 585–597. <https://doi.org/10.2151/jmsj.2014-605>.
- Piccolo, C. and Cullen, M.J.P. (2011) Adaptive mesh method in the Met Office variational data assimilation system. *Quarterly Journal of the Royal Meteorological Society*, 137, 631–640. <https://doi.org/10.1002/qj.801>.
- Piccolo, C. and Cullen, M.J.P. (2012) A new implementation of the adaptive mesh transform in the Met Office 3D-Var system. *Quarterly Journal of the Royal Meteorological Society*, 138, 1560–1570. <https://doi.org/10.1002/qj.1880>.
- Rabier, F., Järvinen, H., Klinker, E., Mahfouf, J.-F. and Simmons, A. (2000) The ECMWF operational implementation of four-dimensional variational assimilation. I: experimental results with simplified physics. *Quarterly Journal of the Royal Meteorological Society*, 126, 1143–1170. <https://doi.org/10.1002/qj.49712656415>.
- Rainwater, S., Bishop, C.H. and Campbell, W.F. (2015) The benefits of correlated observation errors for small scales. *Quarterly Journal of the Royal Meteorological Society*, 141, 3439–3445. <https://doi.org/10.1002/qj.2582>.
- Raschendorfer, M. (2001) The new turbulence parameterisation of LM. *COSMO Newsletter*, 1, 89–97.
- Rawlins, F., Ballard, S.P., Bovis, K.J., Clayton, A.M., Li, D.M., Inverarity, G.W. and Payne, T.J. (2007) The Met Office global four-dimensional data assimilation system. *Quarterly Journal of the Royal Meteorological Society*, 133, 347–362. <https://doi.org/10.1002/qj.32>.
- Renshaw, R.J. and Francis, P. (2011) Variational assimilation of cloud fraction in the operational Met Office Unified Model. *Quarterly Journal of the Royal Meteorological Society*, 137, 1963–1974. <https://doi.org/10.1002/qj.980>.
- Ridal, M. and Dahlbom, M. (2017) Assimilation of multinational radar data in a mesoscale model: a proof of concept. *Journal of Applied Meteorology and Climatology*, 56, 1739–1751. <https://doi.org/10.1175/JAMC-D-16-0247.1>.
- Ritter, B. and Geleyn, J.-F. (1992) A comprehensive radiation scheme for numerical weather prediction models with potential applications in climate simulations. *Monthly Weather Review*, 120, 303–325. [https://doi.org/10.1175/1520-0493\(1992\)120<0303:ACRSFN>2.0.CO;2](https://doi.org/10.1175/1520-0493(1992)120<0303:ACRSFN>2.0.CO;2).
- Rhodin, A., Lange, H., Potthast, R. and Janjić, T. (2013) *Documentation of the DWD Data Assimilation System*. Offenbach: Deutscher Wetterdienst.
- Roberts, N.M. and Lean, H.W. (2008) Scale-selective verification of rainfall accumulations from high-resolution forecasts of convective events. *Monthly Weather Review*, 136, 78–97. <https://doi.org/10.1175/2007MWR2123.1>.

- Rogers, E., Carley, J., Ferrier, B., Aligo, E., Gayno, G., Janjić, Z. and DiMego, G. (2017). Available at: http://wmc.meteoinfo.ru/bluebook/uploads/2017/docs/05_Rogers_Eric_mesoscale_modeling.pdf.
- de Rosnay, P., Drusch, M., Vasiljevic, D., Balsamo, G., Albergel, C. and Isaksen, L. (2012) A simplified extended Kalman filter for the global operational soil moisture analysis at ECMWF. *Quarterly Journal of the Royal Meteorological Society*, 139, 1199–1213. <https://doi.org/10.1002/qj.2023>.
- Saito, K., Fujita, T., Yamada, Y., Ishida, J., Kumagai, Y., Aranami, K. and Yamazaki, Y. (2006) The operational JMA non-hydrostatic mesoscale model. *Monthly Weather Review*, 134, 1266–1298. <https://doi.org/10.1175/MWR3120.1>.
- Saito, K., Ishida, J., Aranami, K., Hara, T., Segawa, T., Narita, M. and Honda, Y. (2007) Non-hydrostatic atmospheric models and operational development at JMA. *Journal of the Meteorological Society of Japan*, 85B, 271–304. <https://doi.org/10.2151/jmsj.85B.271>.
- Salonen, K., Järvinen, H., Haase, G., Niemelä, S. and Eresmaa, R. (2009) Doppler radar radial winds in HIRLAM. Part II: optimizing the super-observation processing. *Tellus*, 61A, 288–295. <https://doi.org/10.1111/j.1600-0870.2008.00381.x>.
- Scheck, L., Frerebeau, P., Buras-Schnell, R. and Mayer, B. (2016) A fast radiative transfer method for the simulation of visible satellite imagery. *Journal of Quantitative Spectroscopy and Radiative Transfer*, 175, 54–67. <https://doi.org/10.1016/j.jqsrt.2016.02.008>.
- Schomburg, A., Schraff, C. and Potthast, R. (2015) A concept for the assimilation of satellite cloud information in an Ensemble Kalman filter: single-observation experiments. *Quarterly Journal of the Royal Meteorological Society*, 141, 893–908. <https://doi.org/10.1002/qj.2407>.
- Schraff, C., Reich, H., Rhodin, A., Schomburg, A., Stephan, K., Perriñez, A. and Potthast, R. (2016) Kilometre-scale ensemble data assimilation for the COSMO model (KENDA). *Quarterly Journal of the Royal Meteorological Society*, 142, 1453–1472. <https://doi.org/10.1002/qj.2748>.
- Seity, Y., Brousseau, P., Malardel, S., Hello, G., Bénard, P., Bouttier, F. and Masson, V. (2011) The AROME-France convective-scale operational model. *Monthly Weather Review*, 139, 976–991. <https://doi.org/10.1175/2010MWR3425.1>.
- Simmer, C., Adrian, G., Jones, S., Wirth, V., Göber, M., Hohenegger, C. and Vormann, A. (2016) HERZ – The German Hans-Ertel Centre for Weather Research. *Bulletin of the American Meteorological Society*, 97, 1057–1068. <https://doi.org/10.1175/BAMS-D-13-00227.1>.
- Simonin, D., Ballard, S.P. and Li, Z. (2014) Doppler radar radial wind assimilation using an hourly cycling 3D-Var with a 1.5 km resolution version of the Met Office Unified Model for nowcasting. *Quarterly Journal of the Royal Meteorological Society*, 140, 2298–2314. <https://doi.org/10.1002/qj.2298>.
- Široká, M., Boloni, G., Brozkova, R., Dziedzic, A., Fischer, C., Geleyn, J.-F. and Soci, C. (2001) *Innovative Developments for a 3DVAR Analysis in a Limited-area Model: Scale Selection and Blended Cycling TD, 1–53*. Geneva, Switzerland: World Meteorological Organization.
- Široká, M., Fischer, C., Cassé, V., Brozkova, R. and Geleyn, J.-F. (2003) The definition of mesoscale selective forecast-error covariances for a limited-area variational analysis. *Meteorology and Atmospheric Physics*, 82, 227–244. <https://doi.org/10.1007/s00703-001-0588-5>.
- Soci, C., Fischer, C. and Horányi, A. (2006) Sensitivity of high-resolution forecasts using the adjoint technique at the 10 km scale. *Monthly Weather Review*, 134, 772–790. <https://doi.org/10.1175/MWR3091.1>.
- Sommer, M. and Weissmann, M. (2016) Ensemble-based approximation of observation impact using an observation-based verification metric. *Tellus A*, 68, 27885. <https://doi.org/10.3402/tellusa.v68.27885>.
- Stensrud, D.J., Wicker, L.J., Kelleher, K.E., Xue, M., Foster, M.P., Schaefer, J.T. and Tuell, J.P. (2009) Convective-scale warn-on-forecast system: a vision for 2020. *Bulletin of the American Meteorological Society*, 90, 1487–1499. <https://doi.org/10.1175/2009BAMS2795.1>.
- Stephan, K., Klink, S. and Schraff, C. (2008) Assimilation of radar-derived rain rates into the convective-scale model COSMO-DE at DWD. *Quarterly Journal of the Royal Meteorological Society*, 134, 1315–1326. <https://doi.org/10.1002/qj.269>.
- Stewart, L.M., Dance, S.L., Nichols, N.K., Eyre, J.R. and Cameron, J. (2014) Estimating interchannel observation-error correlations for IASI radiance data in the Met Office system. *Quarterly Journal of the Royal Meteorological Society*, 140, 1236–1244. <https://doi.org/10.1002/qj.2211>.
- Strajnar, B. (2012) Validation of mode-s meteorological routine air report aircraft observations. *Journal of Geophysical Research*, 117, D23110. <https://doi.org/10.1029/2012JD018315>.
- Strajnar, B. (2015). *Four-dimensional data assimilation of aircraft observations of the atmosphere in complex terrain*. Doctoral thesis, Ljubljana University, Slovenia.
- Strajnar, B., Žagar, N. and Berre, L. (2015) Impact of new aircraft observations Mode-S MRAR in a mesoscale NWP model. *Journal of Geophysical Research Atmospheres*, 120, 3920–3938. <https://doi.org/10.1002/2014JD022654>.
- Sun, J. and Wang, H. (2013) Radar data assimilation with WRF 4D-Var. Part II: comparison with 3D-Var for a squall line over the US Great Plains. *Monthly Weather Review*, 141, 2245–2264. <https://doi.org/10.1175/MWR-D-12-00169.1>.
- Szintai, B., Szücs, M., Randriamampianina, R. and Kullmann, L. (2015) Application of the AROME non-hydrostatic model at the Hungarian Meteorological Service: Physical parameterizations and ensemble forecasting. *Idojaras*, 119, 241–266.
- Tang, L., Zhang, J., Langston, C., Krause, J., Howard, K. and Lakeshmana, V. (2014) A physically based precipitation/non-precipitation radar echo classifier using polarimetric and environmental data in a real-time national system. *Weather and Forecasting*, 29, 1106–1119. <https://doi.org/10.1175/WAF-D-13-00072.1>.
- Tang, Y., Lean, H.W. and Bornemann, J. (2013) The benefits of the Met Office variable resolution NWP model for forecasting convection. *Meteorological Applications*, 20, 417–426. <https://doi.org/10.1002/met.1300>.
- Tiedtke, M. (1989) A comprehensive mass flux scheme for cumulus parameterization in large-scale models. *Monthly Weather Review*, 117, 1779–1800. [https://doi.org/10.1175/1520-0493\(1989\)117<1779:ACMFSF>2.0.CO;2](https://doi.org/10.1175/1520-0493(1989)117<1779:ACMFSF>2.0.CO;2).
- Waller, J.A., Dance, S.L. and Nichols, N.K. (2016a) Theoretical insight into diagnosing observation-error correlations using observation-minus-background and observation-minus-analysis statistics. *Quarterly Journal of the Royal Meteorological Society*, 142, 418–431. <https://doi.org/10.1002/qj.2661>.
- Waller, J.A., Simonin, D., Dance, S.L., Nichols, N.K. and Ballard, S.P. (2016b) Diagnosing observation-error correlations for Doppler radar radial winds in the Met Office UKV model using observation-minus-background and observation-minus-analysis statistics. *Monthly Weather Review*, 144, 3533–3551. <https://doi.org/10.1175/MWR-D-15-0340.1>.
- Waller, J.A., Ballard, S.P., Dance, S.L., Kelly, G., Nichols, N.K. and Simonin, D. (2016c) Diagnosing horizontal and inter-channel observation-error correlations for SEVIRI observations using observation-minus-background and observation-minus-analysis statistics. *Remote Sensing*, 8, 581. <https://doi.org/10.3390/rs8070581>.
- Wang, H., Sun, J., Fan, S. and Huang, X.-Y. (2013a) Indirect assimilation of radar reflectivity with WRF 3D-Var and its impact on prediction of four summertime convective events. *Journal of Applied Meteorology and Climatology*, 52, 889–902. <https://doi.org/10.1175/JAMC-D-12-0120.1>.
- Wang, H., Sun, J., Zhang, X., Huang, X.-Y. and Auligné, T. (2013b) Radar data assimilation with WRF 4D-Var. Part I: system development and preliminary testing. *Monthly Weather Review*, 141, 2224–2244. <https://doi.org/10.1175/MWR-D-12-00168.1>.
- Wang, H., Huang, X.-Y., Xu, D. and Liu, J. (2014) A scale-dependent blending scheme for WRFDA: impact on regional weather forecasting. *Geoscientific Model Development*, 7, 1819–1828. <https://doi.org/10.5194/gmd-7-1819-2014>.
- Wang, X., Snyder, C. and Hamill, T.M. (2007) On the theoretical equivalence of differently proposed ensemble 3D-Var hybrid analysis schemes. *Monthly Weather Review*, 135, 222–227. <https://doi.org/10.1175/MWR3282.1>.
- Wattrelot, E. (2016). *Radar assimilation at higher density in the operational AROME model at 1.3 km horizontal resolution*, Combined Newsletter of the HIRLAM and ALADIN Consortia, No. 6, pp. 53–63. Retrieved from <http://www.cnrm-game-meteo.fr/aladin/IMG/pdf/nl6.pdf>.
- Wattrelot, E., Montmerle, T. and Guerrero, C.G. (2012). Evolution of the assimilation of radar data in the AROME model at convective scale. In: *Proceedings of the Seventh European Conference on Radar in Meteorology and Hydrology*, 24–29 June, 2012, Toulouse, France. Available at: http://www.meteo.fr/cic/meetings/2012/ERAD/extended_abs/NWP_401_ext_abs.pdf.
- Wattrelot, E., Caumont, O. and Mahfouf, J.-F. (2014) Operational implementation of the 1D+3D-Var assimilation method of radar reflectivity data in the AROME model. *Monthly Weather Review*, 142, 1852–1873. <https://doi.org/10.1175/MWR-D-13-00230.1>.

- Wattrelot, E., Montmerle, T. and Mahfouf, J.-F. (2016). Higher density radar assimilation in the operational AROME model at 1.3 km horizontal resolution. In: *6th Workshop on the Impact of Various Observing Systems on NWP*, 10–13 May, 2016. Available at: http://www.wmo.int/pages/prog/www/WIGOS-WIS/reports/6NWP_Shanghai2016/WMO6-Impact-workshop_Shanghai-May2016.html.
- Weissmann, M., Göber, M., Hohenegger, C., Janjić, T., Keller, J., Ohlwein, C. and Deneke, H. (2014) The Hans-Ertel Centre for Weather Research – Research objectives and highlights from its first three years. *Meteorologische Zeitschrift*, 23, 193–208. <https://doi.org/10.1127/0941-2948/2014/0558>.
- Weston, P.P., Bell, W. and Eyre, J.R. (2014) Accounting for correlated error in the assimilation of high-resolution sounder data. *Quarterly Journal of the Royal Meteorological Society*, 140, 2420–2429. <https://doi.org/10.1002/qj.2306>.
- Wheatley, D.M., Knopfmeier, K.H., Jones, T.A. and Creager, G.J. (2015) Storm-scale data assimilation and ensemble forecasting with the NSSL Experimental Warn-on-Forecast System. Part I: radar data experiments. *Weather and Forecasting*, 30, 1795–1816. <https://doi.org/10.1175/WAF-D-15-0043.1>.
- Whitaker, J.S. and Hamill, T.M. (2012) Evaluating methods to account for system errors in ensemble data assimilation. *Monthly Weather Review*, 140, 3078–3089. <https://doi.org/10.1175/MWR-D-11-00276.1>.
- Whitaker, J.S., Compo, G.P., Wei, X. and Hamill, T.M. (2004) Reanalysis without radiosondes using ensemble data assimilation. *Monthly Weather Review*, 132, 1190–1200. [https://doi.org/10.1175/1520-0493\(2004\)132<1190:RWRUED>2.0.CO;2](https://doi.org/10.1175/1520-0493(2004)132<1190:RWRUED>2.0.CO;2).
- Whitaker, J.S., Hamill, T.M., Wei, X., Song, Y. and Toth, Z. (2008) Ensemble data assimilation with the NCEP global forecast system. *Monthly Weather Review*, 136, 463–482. <https://doi.org/10.1175/2007MWR2018.1>.
- Wicker, L.J. and Skamarock, W.C. (2002) Time splitting methods for elastic models using forward time schemes. *Monthly Weather Review*, 130, 2088–2097. [https://doi.org/10.1175/1520-0493\(2002\)130<2088:TSMFEM>2.0.CO;2](https://doi.org/10.1175/1520-0493(2002)130<2088:TSMFEM>2.0.CO;2).
- Wu, W.-S., Parrish, D.F., Rogers, E. and Lin, Y. (2017) Regional ensemble-variational data assimilation using global ensemble forecasts. *Weather and Forecasting*, 32, 83–96. <https://doi.org/10.1175/WAF-D-16-0045.1>.
- Xie, Y., Koch, S., McGinley, J., Albers, S., Bieringer, P.E., Wolfson, M. and Chan, M. (2011) A space-time multiscale analysis system: a sequential variational analysis approach. *Monthly Weather Review*, 139, 1224–1240. <https://doi.org/10.1175/2010MWR3338.1>.
- Xu, Q., Nai, K., Wei, L., Zhang, P., Liu, S. and Parrish, D. (2011) A VAD-based de-aliasing method for radar velocity data quality control. *Journal of Atmospheric and Oceanic Technology*, 28, 50–62. <https://doi.org/10.1175/2010JTECHA1444.1>.
- Xu, Q., Wei, L., Gao, J., Zhao, Q., Nai, K. and Liu, S. (2016) Multistep variational data assimilation: important issues and a spectral approach. *Tellus A*, 68, 31110. <https://doi.org/10.3402/tellusa.v68.31110>.
- Yang, X. (2005) Analysis blending using spatial filter in grid-point model coupling. *HIRLAM Newsletter*, 49, 3–11.
- Zängl, G., Reinert, D., Ripodas, P. and Baldauf, M. (2015) The ICON (ICOsahe-dral Non-hydrostatic) modelling framework of DWD and MPI-M: description of the non-hydrostatic dynamical core. *Quarterly Journal of the Royal Meteorological Society*, 141, 563–579. <https://doi.org/10.1002/qj.2378>.
- Zeng, Y. and Janjić, T. (2016) Study of conservation laws with the Local Ensemble Transform Kalman Filter. *Quarterly Journal of the Royal Meteorological Society*, 142, 2359–2372. <https://doi.org/10.1002/qj.2829>.
- Zeng, Y., Blahak, U. and Jerger, D. (2016) An efficient modular volume-scanning radar forward operator for NWP models: description and coupling to the COSMO model. *Quarterly Journal of the Royal Meteorological Society*, 142, 3234–3256. <https://doi.org/10.1002/qj.2904>.
- Zhang, F., Snyder, C. and Sun, J. (2004) Impacts of initial estimate and observation availability on convective-scale data assimilation with an ensemble Kalman filter. *Monthly Weather Review*, 132, 1238–1253. [https://doi.org/10.1175/1520-0493\(2004\)132<1238:IOIEAO>2.0.CO;2](https://doi.org/10.1175/1520-0493(2004)132<1238:IOIEAO>2.0.CO;2).
- Zhang, J., Howard, K. and Gourley, J.J. (2005a) Constructing three-dimensional multiple-radar reflectivity mosaics: examples of convective storms and stratiform rain echoes. *Journal of Atmospheric and Oceanic Technology*, 22, 30–42. <https://doi.org/10.1175/JTECH-1689.1>.
- Zhang, P., Liu, S. and Xu, Q. (2005b) Identifying Doppler velocity contamination caused by migrating birds Part I: feature extraction and quantification. *Journal of Atmospheric and Oceanic Technology*, 22, 1105–1113. <https://doi.org/10.1175/JTECH1757.1>.
- Zupanski, M. (2005) Maximum likelihood ensemble filter: theoretical aspects. *Monthly Weather Review*, 133, 1710–1726. <https://doi.org/10.1175/MWR2946.1>.

How to cite this article: Gustafsson N, Janjić T, Schraff C, et al. Survey of data assimilation methods for convective-scale numerical weather prediction at operational centres. *Q J R Meteorol Soc.* 2018;144:1218–1256. <https://doi.org/10.1002/qj.3179>